

Design, Implementation, Control, and
User Evaluations of ASSISTON-ARM
Self-Aligning
Upper-Extremity Exoskeleton

by
Mustafa Yalçın

Submitted to the Graduate School of Sabancı University
in partial fulfillment of the requirements for the degree of
Doctor of Philosophy

Sabancı University
January, 2020

DESIGN, IMPLEMENTATION, CONTROL, AND
USER EVALUATIONS OF ASSISTON-ARM
SELF-ALIGNING
UPPER-EXTREMITY EXOSKELETON

APPROVED BY:

Prof. Dr. Volkan Patođlu
(Thesis Advisor)



.....

Prof. Dr. Erhan Budak



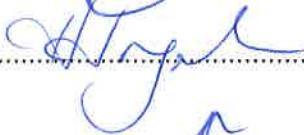
.....

Assoc. Prof. Dr. Gll Kızıldaş Őendur



.....

Assist. Prof. Dr. Hande ArgunŐah Bayram



.....

Assist. Prof. Dr. Elif Hocaođlu Őetinsoy



.....

DATE OF APPROVAL:

09/12/2019
.....

Mustafa Yalçın, 2020 ©
All Rights Reserved

ABSTRACT

DESIGN, IMPLEMENTATION, CONTROL, AND USER EVALUATIONS OF ASSISTON-ARM SELF-ALIGNING UPPER-EXTREMITY EXOSKELETON

Mustafa Yalçın

Mechatronics, Doctor of Philosophy, 2019

Thesis Supervisor: Prof. Dr. Volkan Patoglu

Keywords: Rehabilitation Robotics, Force Controlled Exoskeleton, Physical Human-Robot Interaction (pHRI), Impedance Control, Self-Alignment Mechanisms

Physical rehabilitation therapy is indispensable for treating neurological disabilities. The use of robotic devices for rehabilitation holds high promise, since these devices can bear the physical burden of rehabilitation exercises during intense therapy sessions, while therapists are employed as decision makers. Robot-assisted rehabilitation devices are advantageous as they can be applied to patients with all levels of impairment, allow for easy tuning of the duration and intensity of therapies and enable customized, interactive treatment protocols. Moreover, since robotic devices are particularly good at repetitive tasks, rehabilitation robots can decrease the physical burden on therapists and enable a single therapist to supervise multiple patients simultaneously; hence, help to lower cost of therapies. While the intensity and quality of manually delivered therapies depend on the skill and fatigue level of therapists, high-intensity robotic therapies can always be delivered with high accuracy. Thanks to their integrated sensors, robotic devices can gather measurements throughout therapies, enable quantitative tracking of patient progress and development of evidence-based personalized rehabilitation programs.

In this dissertation, we present the design, control, characterization and user evaluations of ASSISTON-ARM, a powered, self-aligning exoskeleton for robot-assisted upper-extremity rehabilitation.

ASSISTON-ARM is designed as a passive back-driveable impedance-type robot such that patients/therapists can move the device transparently, without much interference of the device dynamics on natural movements. Thanks to its novel kinematics and mechanically transparent design, ASSISTON-ARM can passively self-align its joint axes to provide an ideal match between human joint axes and

the exoskeleton axes, guaranteeing ergonomic movements and comfort throughout physical therapies.

The self-aligning property of ASSISTON-ARM not only increases the usable range of motion for robot-assisted upper-extremity exercises to cover almost the whole human arm workspace, but also enables the delivery of glenohumeral mobilization (scapular elevation/depression and protraction/retraction) and scapular stabilization exercises, extending the type of therapies that can be administered using upper-extremity exoskeletons. Furthermore, the self-alignment property of ASSISTON-ARM significantly shortens the setup time required to attach a patient to the exoskeleton.

As an impedance-type device with high passive back-driveability, ASSISTON-ARM can be force controlled without the need of force sensors; hence, high fidelity interaction control performance can be achieved with open-loop impedance control. This control architecture not only simplifies implementation, but also enhances safety (coupled stability robustness), since open-loop force control does not suffer from the fundamental bandwidth and stability limitations of force-feedback.

Experimental characterizations and user studies with healthy volunteers confirm the transparency, range of motion, and control performance of ASSISTON-ARM.

ÖZET

KENDİNDEN HİZALAMALI ÜST EKSTREMİTE DIŞ İSKELETİ ASSISTON-ARM'IN TASARIMI, UYGULAMASI, KONTROLÜ VE KULLANICI DEĞERLENDİRMELERİ

Mustafa Yalçın

Mekatronik Mühendisliği, Doktora Tezi, 2019

Tez Danışmanı: Prof. Dr. Volkan Patoglu

Anahtar kelimeler: Rehabilitasyon Robotları, Kuvvet Geri-Beslemeli Dış-İskeletler, Fiziksel İnsan-Robot Etkileşimi, Empedans Kontrolü, Kendinden Hizalamalı Mekanizmalar.

Fizik tedavi ve rehabilitasyon, nörolojik sakatlıkların tedavisinde vazgeçilmez bir tedavi yöntemidir. Rehabilitasyon amaçlı kullanılan robotik cihazlar, yoğun tedavi seanslarında terapistlerin fiziksel yükünü hafifletebilmektedirler. Robot destekli rehabilitasyon cihazları her seviyedeki hastalara uygulanabilmeleri, tedavi yoğunluğunun ve süresinin kolay ayarlanabilmesine izin vermeleri, kişileştirilmiş ve interaktif tedavi protokollerini gerçekleştirmeleri nedeniyle avantajlıdır. Ayrıca, robotik cihazlar tek bir terapistin aynı anda birden fazla hastayı tedavi etmesine olanak sağlamakta; bundan dolayı her hastaya bir ya da daha fazla terapistin eşlik etmesi gereken manuel tedaviye kıyasla tedavi masraflarının azaltılmasına yardımcı olmaktadır. Bunun yanında, uygulanan robotik tedavilerin nitelik ve yoğunluğu, terapistin hünerine ve yorgunluğuna bağlı olmayıp, yüksek yoğunluklu robotik tedaviler her zaman yüksek hassasiyetle verilebilmektedir. Robotik cihazlar, yapılarındaki sensörleri sayesinde, tedavi süresince ölçüm yaparak hastaların gelişimini nicel olarak takip edebilmekte ve kanıta dayalı kişileştirilmiş rehabilitasyon programlarının geliştirilmesine olanak sağlamaktadırlar.

Bu çalışmada, robot destekli üst-ekstremitte rehabilitasyonu için tahrikli ve kendinden hizalamalı bir dış iskelet olarak geliştirilen ASSISTON-ARM'ın tasarımı, kontrolü, karakterizasyonu ve kullanıcı değerlendirmeleri sunulmuştur.

Pasif geri-sürülebilir empedans tipi bir robot olarak tasarlanan ASSISTON-ARM, hastalar ve terapistler tarafından cihazın dinamiği hissedilmeden kolayca hareket ettirebilmekte ve bu sayede egzersizlerin doğal bir şekilde gerçekleştirilmesine imkan vermektedir. Özgün kinematik yapısı ve mekanik şeffaflığı sayesinde pasif bir

şekilde kendinden hizalamayı gerçekleştirebilen ASSISTON-ARM, dış-iskelet ile insan eklemleri arasında ideal eşleşmeyi sağlamakta, böylece fiziksel tedavi süresince ergonomiyi ve konforu garanti etmektedir.

Kendinden hizalama özelliği sayesinde ASSISTON-ARM, hem üst-ekstremité robot destekli egzersizlerinin kullanılabilir hareket alanını artırarak insan çalışma alanını kapsamakta, hem de glenohumeral öteleme hareketleri (skapulaya ait elevasyon/depresyon ve öne doğru uzanma/geri çekme) ile skapular stabilizasyon egzersizlerinin kullanıcılara uygulanmasını sağlayarak, üst-ekstremité dış iskeletleri tarafından uygulanabilen terapi çeşitliliğini arttırabilmektedir. Ayrıca, ASSISTON-ARM'ın kendinden hizalama özelliği robotun hastalara bağlanması için gereken süreyi önemli ölçüde azaltmaktadır.

Yüksek geri-sürülebilirliğe sahip empedans tipi bir cihaz olarak tasarlanan ASSISTON-ARM ile kuvvet sensörlerine gerek duyulmadan kuvvet kontrolü yapılabilmekte, açık-döngü empedans kontrolü ile yüksek fiziksel etkileşim kontrol performansı elde edilebilmektedir. Bu kontrol mimarisi yalnızca uygulamayı kolaylaştırmakla kalmakla kalmayıp, ayrıca açık-döngü kuvvet kontrolcüsünün kuvvet geri beslemesine ait olan temel bant genişliği ve kararlılık kısıtlarına tabi olmamasından dolayı, bağlaşıklık kararlılık gürbüz bir şekilde garanti edilebilmektedir.

Deneyssel karakterizasyon ve sağlıklı gönüllüler ile yapılan kullanıcı çalışmaları, ASSISTON-ARM'ın kolay kullanımını, çalışma alanı ve kontrol performansını teyit etmiştir.

Acknowledgements

It is a great pleasure to extend my gratitude to my thesis advisor Prof. Dr. Volkan Patoglu for his precious guidance and support. I am greatly indebted to him for his supervision and excellent advises throughout my Master and Doctorate study. I would gratefully thank Prof. Dr. Erhan Budak, Assoc. Prof. Dr. Güllü Kızıltaş Şendur, Assist. Prof. Dr. Elif Hocaoglu Çetinsoy and Assist. Prof. Dr. Hande Argunsah Bayram for their feedback and spending their valuable time to serve as my jurors.

I am heartily thankful to my friends and colleagues Mehmet Alper Ergin, Dr. Gökay Çoruhlu, Oğuzhan Yılmaz for their support and invaluable help. I owe my deepest gratitude to them for support throughout my doctorate studies and sharing precious experiences as colleagues. Many thanks to my friends, Dr. Hammad Munawar, Dr. Vahid Tavakol, Umut Çalışkan, Zeynep Özge Orhan, Ali Khalilian Motamed, Ali Yaşar, Cansu Öztürk for making the laboratory enjoyable and memorable and other colleagues from the Department of Mechatronics supported me in my research work. Thanks to Mükerrerem İlker Sevgen, he is like a big brother for me, for his precious support throughout my research and for sharing his experience and technical knowledge as well as enjoyable times together.

I would like to thank Sibel Aksu Yıldırım and Muhammed Kılınç (Hacettepe University, School of Physical Therapy and Rehabilitation) for their feedbacks during the initial design of ASSISTON-ARM. I also would like to thank Zeynep Güven and Nuray Alaca (Acibadem University, Department

of Physical Medicine and Rehabilitation) and Hande Argunşah Bayram and Begüm Yalçın (Acibadem University, Department of Medical Engineering) for their assistance during the user studies with ASSISTON-ARM.

I would like to acknowledge the financial support provided by The Scientific and Technological Research Council of Turkey (TÜBİTAK) through my PhD education under 2211-A (Genel Yurt İçi Doktora Burs Programı) BİDEB scholarship.

Contents

1	Introduction	1
1.1	Contributions	4
1.2	Organization	6
2	Related Work	8
2.1	Physical Rehabilitation of Human Shoulder	8
2.2	Exoskeletons for Upper-Extremity Rehabilitation	10
2.3	Proposed Exoskeleton: ASSISTON-ARM	15
3	Kinematic Type Selection of ASSISTON-ARM	19
3.1	Kinematics of Human Shoulder Complex	19
3.2	Kinematics of Human Elbow	21
3.3	Kinematic Type Selection of ASSISTON-ARM	21
4	Kinematic Analysis of ASSISTON-ARM	25
4.1	Configuration Level Kinematics of 3RRP Mechanism	26
4.2	Motion Level Kinematics of 3RRP Mechanism	30
4.3	Configuration Level Kinematics of ASSISTON-ARM	33
4.4	Motion Level Kinematics of ASSISTON-ARM	34
4.5	Dynamics of ASSISTON-ARM	38
4.6	Singularities of ASSISTON-ARM	39
4.7	Workspace of ASSISTON-ARM	43
4.8	Passive Gravity Compensation of ASSISTON-ARM	47
5	Implementation of ASSISTON-ARM	53
5.1	Actuation and Power Transmission	53

5.2	Power Electronics and Instrumentation	59
5.3	Passive Gravity Compensation	61
6	Characterization of ASSISTON-ARM	66
6.1	Manipulability of 3RRP Mechanism	66
6.2	Performance Characterization of ASSISTON-ARM	69
7	Interaction Control And Operation Modes of ASSISTON-ARM	74
7.1	Interaction Control of ASSISTON-ARM	74
7.1.1	Isometric Mode	84
7.1.2	Isotonic Mode	84
7.1.3	Isokinetic Mode	85
7.2	Path Following Control of ASSISTON-ARM	86
7.2.1	Record and Play	86
7.2.2	Assist-As-Needed	89
8	User Studies with ASSISTON-ARM	92
8.1	Participants	92
8.2	Experimental Setup	92
8.3	Experimental Procedure	93
8.4	Performance Measurement	95
8.5	Results and Discussion	96
8.5.1	Range of Motion	96
8.5.2	Repeatability	99
8.5.3	Smoothness	103
8.5.4	Quantitative Evaluation	106
9	Conclusion and Future Works	108

9.1	Design Improvements for ASSISTON-ARM	108
9.2	Future Works	117

List of Figures

3.1	Joints at the shoulder complex	19
3.2	Movements of human shoulder complex	20
3.3	Schematic representation of the kinematics of ASSISTON-ARM	22
4.1	Schematic representation of the kinematics of ASSISTON-ARM	26
4.2	Schematic representation of kinematics of 3RRP mechanism .	27
4.3	Singularity analysis of 3RRP mechanism through interval ana- lysis	40
4.4	Translational reachable workspace of ASSISTON-ARM at the shoulder complex	45
4.5	Top, side, and front view of the reachable workspace of ASSISTON- ARM at its end-effector	46
4.6	Several gravity compensation mechanisms	49
4.7	Schematics of gravity compensator used with ASSISTON-ARM	50
5.1	Representation of capstan transmission method	57
5.2	Solid model of 3RRP with two layered capstan transmission .	58
5.3	Solid model of internal/external joint with two motored cap- stan transmission	59
5.4	Solid model of ASSISTON-ARM	59
5.5	Transmission details of ASSISTON-ARM	60
5.6	Front view of realized exoskeleton	62
5.7	Solid model of parallelogram based gravity compensation mech- anism	63
5.8	Workspace of parallelogram based the gravity compensation mechanism and center of mass of ASSISTON-ARM	64

5.9	Performance characteristics of parallelogram based gravity compensation mechanism with respect to elbow joint motions . . .	64
5.10	A prototype of ASSISTON-ARM	65
6.1	Manipulability measure of 3RRP mechanism at $\theta = 0^\circ$	68
6.2	Manipulability of 3RRP mechanism for at various orientations of its end-effector	69
7.1	Reference and experimentally measured trajectories during the joint space impedance control of the first revolute joint . .	77
7.2	Block diagram for open loop impedance control	78
7.3	Reference and experimentally measured trajectories during the task space impedance control of the rotational DoF of the 3RRP mechanism	79
7.4	Reference and experimentally measured trajectories during the task space impedance control of the translational DoF of the 3RRP mechanism	80
7.5	Reference and experimentally measured trajectories during the joint space impedance control of the internal/external rotation	81
7.6	Reference and experimentally measured trajectories during the joint space impedance control of the elbow joint	82
7.7	Rendering virtual stiffness of 5 N/mm under open-loop impedance control	83
7.8	A virtual tunnel around the path during a Record-and-Play exercise	88
8.1	ASSISTON-ARM prototype used during the human subject experiments	93

8.2	Data recorded during flexion/extension movements in the sagittal plane during patient active trials	96
8.3	Data recorded during abduction/adduction movements in the horizontal plane during patient active trials	97
8.4	Translations of the humerus head in the sagittal plane of a volunteer during flexion/extension of the shoulder complex during a patient active trial	98
8.5	Translations of the humerus head in the sagittal plane of five volunteers during flexion/extension of the shoulder complex during patient active trials	99
8.6	Data recorded during flexion/extension movements in the sagittal plane during patient passive trials	100
8.7	Data recorded during abduction/adduction movements in the frontal plane during patient passive trials	100
8.8	Translations of the humerus head in the sagittal plane of five volunteers during flexion/extension of the shoulder complex during patient passive trials	101
8.9	Translations of the humerus head in the frontal plane of four volunteers during abduction/adduction of the shoulder complex during patient passive trials	102
8.10	Dimensionless jerk metric analysis of user active and passive shoulder flexion movements	105
8.11	User active and user passive shoulder flexion movement together with a generated disturbed movement path	106
9.1	Implementation of remote center of rotation mechanism at upper arm module	110

9.2	Configuration of ASSISTON-ARM for right/left arm use	111
9.3	CAD details and schematics of RCoR mechanism	112
9.4	Representation of the gravity compensation mechanism op- tions for ASSISTON-ARM	115
9.5	ASSISTON-ARM with a healthy volunteer shown at various arm poses	116
9.6	Schematic representation of simplified kinematics of ASSISTON- ARM used for singularity analysis	138
9.7	Representation of tilting angles β and γ , after introducing them in order to extent usable range of motion without sin- gularities, when $\theta = 92^\circ$ and determinant of J_u is equal to zero	139

List of Tables

4.1	Range of motion of the human shoulder and ASSISTON-ARM	44
6.1	Actuation characteristics of ASSISTON-ARM	71
6.2	Experimental characterization results for the prototype of 3RRP mechanism	71
6.3	Experimental back-driveability characterization results of re- alized assembly	72

LIST OF SYMBOLS AND ABBREVIATIONS

ADL	Activities of Daily Living
DoF	Degrees of Freedom
GH	Glenohumeral
SH	Scapulohumeral
RoM	Range of Motion
SC	Sternoclavicular
AC	Acromioclavicular
ST	Scapulothoracic
RMS	Root-Mean-Square
AAN	Assist-As-Needed
IRB	Institutional Review Board
RCoR	Remote Center of Rotation
$SO(3)$	Special Orthogonal group of order 3
\textcircled{N}	Newtonian reference frame
\textcircled{P}	Body after first joint
\textcircled{R}	Base Body of $3\underline{R}RP$
\textcircled{U}	Upper arm Body
\textcircled{L}	Body after shoulder internal/external rotation
\textcircled{H}	Lower arm Body
$3\underline{R}RP$	Planar parallel 3 DoF mechanism for shoulder module
α_1	Rotation angle of first joint with respect to \vec{n}_3
y_s	End-effector position of $3\underline{R}RP$ on the direction of \vec{r}_2
z_s	End-effector position of $3\underline{R}RP$ on the direction of \vec{r}_3
θ	End-effector rotation angle of $3\underline{R}RP$ around the axis of \vec{r}_1
α_2	Rotation angle of internal/external joint around the axis of $-\vec{u}_3$

α_3	Rotation angle of elbow joint around the axis of \vec{l}_2
q_1, q_2, q_3	Rotation angles of disks of $\underline{3RRP}$ around the axis of \vec{r}_1
\textcircled{Q}	First disk Body of $\underline{3RRP}$
\textcircled{V}	Second disk Body of $\underline{3RRP}$
\textcircled{T}	Third disk Body of $\underline{3RRP}$
$\dot{X}_{\underline{3RRP}}$	Task space velocity variable of $\underline{3RRP}$
$J_{\underline{3RRP}}$	Jacobian matrix of $\underline{3RRP}$
$\dot{q}_{\underline{3RRP}}$	Joint space velocity variable of $\underline{3RRP}$
x_w, y_w, z_w	End-effector positions of ASSISTON-ARM
φ	End-effector unit quaternion vector of ASSISTON-ARM
J_v, J_w	Linear and angular kinematic Jacobian of ASSISTON-ARM
J_k	Intermediate kinematic Jacobian of ASSISTON-ARM
F_x, F_y, F_z	External forces on ASSISTON-ARM
T_x, T_y, T_z	External torques on ASSISTON-ARM
τ_i	Joint torques of ASSISTON-ARM (i=1,...,6)
$M(q)$	Mass matrix defined in $\mathbb{R}^{6 \times 6}$
$C(q, \dot{q})$	Coriolis and centrifugal matrix defined in $\epsilon\mathbb{R}^{6 \times 6}$
$G(q)$	Gravity matrix defined in $\epsilon\mathbb{R}^{6 \times 1}$
τ_{ext}	External torque/force effecting on system
q, \dot{q}, \ddot{q}	Joint variables, velocities and accelerations of ASSISTON-ARM
J_{ii}	6x6 minor kinematic Jacobian of ASSISTON-ARM
α, β	Joint angles of spring based gravity compensator mechanism
x_1, x_2, k_1, k_2	Zero-length spring deflections and constants
V_g	Gravitational potential energy of overall system
V_s	Potential energy stored in zero-length springs
V_t	Total mechanical potential energy of the system

\mathbf{g}	Gravitational acceleration
\hat{J}	Normalized Jacobian of 3RRP for manipulability analysis
S_J	Maximum torque capabilities of 3RRP
S_T	Maximum desired torque/force at the end-effector of 3RRP
u	Manipulability measure
Z_d	Desired impedance
F_d	Reference force/torque
τ_d	Desired motor torques at the joint space
τ_{ff}	Active feed-forward gravity compensation torques
τ_g	Joint torques eliminated by passive gravity compensator
τ	Motor torques at joint space
$(\hat{\cdot})$	Estimates of the actual system parameters
ϵ_v	Lower threshold limit velocity for generating AAN control
F^{\parallel}	Assistance force along tangential direction of the path
ρ	Maximum amount of assistance
v	Measured velocity of the user
δ	Steepness value for the sigmoid curve of AAN control
$\textcircled{\text{B}} \textcircled{\text{C}} \textcircled{\text{D}} \textcircled{\text{F}}$	Bodies of RCoR mechanism
$\gamma_1, \gamma_2, \gamma_3$	Link lengths of RCoR mechanism
γ_4	Radius of rotation of RCoR mechanism
μ_{nj}	Dimensionless squared jerk metric

Chapter I

1 Introduction

Neurological injuries, such as stroke, are the leading cause of long term disabilities. Among 15 million people that suffer from a stroke each year, about 5 million patients are left permanently disabled [1]. These disabilities not only place a high burden on the welfare of patients, but also negatively impact the contribution of these individuals to the society. Despite recent medical developments, the number of stroke incidents continues to increase, due to the ageing of population.

Physical rehabilitation therapy is indispensable for treating neurological disabilities. Therapies are more effective when they are repetitive [2], intense [3], task specific [4], and long term [5]. Repetitive and high intensity therapies place physical burden on therapists, reducing the effectiveness of therapies while increasing their cost. The use of robotic devices for rehabilitation holds high promise, since these devices can bear the physical burden of rehabilitation exercises during intense therapy sessions, while therapists are employed as decision makers.

Robot-assisted rehabilitation devices are advantageous as they can be applied to patients with all levels of impairment, allow for easy tuning of the duration and intensity of therapies and enable customized, interactive treatment protocols. Moreover, since robotic devices are particularly good

at repetitive tasks, rehabilitation robots can decrease the physical burden on therapists and enable a single therapist to supervise multiple patients simultaneously; hence, help to lower cost of therapies [6]. Besides, while the intensity and quality of manually delivered therapies depend on the skill and fatigue level of therapists, high-intensity robotic therapies can always be delivered with high accuracy. Furthermore, thanks to their integrated sensors, robotic devices can gather measurements throughout therapies, enable quantitative tracking of patient progress and development of evidence-based personalized rehabilitation programs. Clinical trials with robot-assisted rehabilitation indicate that this form of therapy is effective for motor recovery and possesses high potential for improving functional independence of patients [7–13].

Active rehabilitation devices, utilized to treat upper-limb impairment, can be loosely categorized as end-effector type robots [14–17] and exoskeletons [18–24].

End-effector type rehabilitation robots feature a single point of interaction (an end-effector) with a patient and the joint motions of these devices do not correspond to human movements. Therefore, without external restraints applied to constrain patients, joint specific therapies cannot be delivered by such devices. Similarly, measurements cannot be taken at the individual joint level. Moreover, compensatory movements of the patient cannot be detected or actively compensated using end-effector type devices. On the other hand, end-effector type robots typically possess simple kinematic structure and may be implemented at lower costs.

End-effector type rehabilitation robots can be further categorized as fixed based and mobile. MIT-Manus [14], ARM Guide [25], MIME [26] and Gen-

tle/S [17, 27] are examples of fixed based end-effector type rehabilitation devices aimed for clinical use. In contrast, MOTORE [15] and ASSISTON-Mobile [16] are light-weight mobile platforms mainly aimed for home-based robotic therapies.

Exoskeletons are attached to human limbs at multiple interaction points and movements of these devices correspond to human joints, in contrast to the end-effector type robots. As a result, exoskeletons are capable of applying controlled torques to individually targeted joints and measuring movements of these specific joints decoupled from movements of other joints. On the other hand, exoskeletons possess more complex kinematic structure compared to end-effector type robots; hence, are typically more costly to implement. Exoskeletons designed for rehabilitation are generally fixed-base devices aimed for clinical use.

Being able to target individual movements of human joints is the main advantage of exoskeleton type rehabilitation robots. An imperative criteria for the design of exoskeletons is to ensure the correspondence of human joint axes with the robot axes. Misalignment can occur since human joints are not simple revolute joints, the exact positions of the human joint axes cannot be determined externally without using special imaging techniques, and placement of human limbs on the exoskeleton may change from one therapy session to another [28, 29].

Misalignment of joint axes results in parasitic forces to be applied to patients around the attachment points and at the joints, causing discomfort, pain, and even long term injury under repetitive use. Most importantly, axis misalignment may promote compensatory movements of patients which can inhibit potential recovery and decrease the real life use of the limb [30].

1.1 Contributions

This dissertation presents the design, control, characterization and user evaluations of ASSISTON-ARM, a novel, powered, self-aligning exoskeleton for robot-assisted upper-extremity rehabilitation.

i) ASSISTON-ARM can passively follow and actively deliver both rotational and translational movements of shoulder and elbow while ensuring ergonomics. ASSISTON-ARM can deliver glenohumeral mobilization (scapular elevation/depression and protraction/retraction) and scapular stabilization exercises, rehabilitation protocols and exercises related to physical rehabilitation of human arm. As an active exoskeleton, it can restrict undesired compensatory movements, assist or resist targeted joint movements, and provide measurements.

ii) ASSISTON-ARM is a self-aligning exoskeleton, which aligns its joint axes with human axes, passively. This property not only guarantees ergonomics and comfort, but also extends the range of the exercises can be delivered during rehabilitation processes. This self-aligning feature significantly shortens the setup time required to attach a patient to the exoskeleton.

iii) Kinematics of ASSISTON-ARM maximizes singularity-free workspace of the device such that almost all of the human workspace required for activities of daily living (ADL) is covered.

iv) ASSISTON-ARM minimally interferes with the natural movements of patients, thanks to its mechanically transparent and passively back-driveable features. Passive back-driveability allows therapist to use ASSISTON-ARM as a measurement device for diagnosis. The passive back-driveability of the device together with its passive gravity compensation mechanism also ensures safety of patients even under power losses.

v) Mechanically transparency of the device is highly beneficial during the interaction control. The transparency of the system allows for a precise model of the device dynamics, which helps model based controllers to be implemented with high fidelity, without large parasitic effects due to unmodelled device dynamics. Since interaction controllers of ASSISTON-ARM can be implemented without the need for force sensors, high-fidelity force control and precise impedance control can be achieved at high control bandwidths. Transparency helps to simplify control architecture implementation, and enhances safety (coupled stability robustness), as open-loop force control does not suffer from the fundamental stability limitations of force-feedback.

vi) ASSISTON-ARM features interaction controllers and path-based assistance control approaches to deliver a wide range of physical rehabilitation protocols. The operation modes ensure that ASSISTON-ARM can be utilized from acute to chronic phase of the stroke. ASSISTON-ARM can be used to improve muscle strength, flexibility and endurance and help motor recovery of patients.

vii) ASSISTON-ARM is equipped with various operation modes. For instance *isotonic*, *isometric* and *isokinetic* exercises can be delivered with ASSISTON-ARM, utilizing a stiff impedance controller. *Record and Play* mode allows therapist to save the desired synchronization and coordination among joints and delivers the desired motion to the patient at a desired pace under path control. *Assist-as-Needed* mode can be applied with ASSISTON-ARM under path control where the level of assistance can be adjusted online during the exercise. These exercises enable delivery of the repetitive tasks without repeating the same movement and increase the number of exercises that can be administered during a therapy session.

viii) The effectiveness of ASSISTON-ARM has been tested with series of experiments with healthy human subjects. These experiments indicate that users find the device safe and easy-to-use and therapists are satisfied with the workspace of the device. Furthermore, therapists evaluate the self-aligning property as an indispensable feature for achieving the desired RoM, while the passive back-driveability is perceived as an important safety feature.

1.2 Organization

The rest of the dissertation is organized as follows:

Chapter 2 gives a detailed and comparative literature review of upper-extremity exoskeletons after a review about physical rehabilitation of shoulder. At the end of Chapter 2, ASSISTON-ARM is introduced.

Chapter 3 details kinematic type selection of ASSISTON-ARM. The correspondence among human shoulder movements and movements of the exoskeleton is also given in this chapter.

In Chapter 4, the kinematic structure of ASSISTON-ARM is reviewed, and the configuration and motion level kinematics of 3RRP, a mechanism that serves as the main shoulder module, is explained in detail. Overall configuration and motion level kinematics of the exoskeleton are also presented. Singularity analysis of the redundant system is presented and workspace of mechanism is analyzed. Chapter 4 concludes with the kinematic type selection and the kinematic analysis of the passive gravity compensation mechanism.

Implementation details of the system are described in Chapter 5. The actuation and power transmission of the system are presented for each joint and the power electronics is described. This chapter is concluded with the imple-

mentation details of the spring-based passive gravity compensation mechanism.

Chapter 6 presents the experimental characterization of ASSISTON-ARM. Manipulability of 3RRP mechanism is computed to verify the uniform kinematic performance of this mechanism within its workspace. The workspace, torque/force exerting capability and back-driveability of each joint of ASSISTON-ARM are also experimentally verified.

Chapter 7 presents the interaction control and operation modes of ASSISTON-ARM. This chapter details the rationale behind open-loop impedance control of the device and characterizes control performance of the system. Various operation modes, such as isometric, isotonic, isokinetic modes under impedance control, and Record-and-Play and Assist-as-Needed modes under path following control are discussed.

In Chapter 8, human subject experiments to evaluate the ergonomics, range of motion and useability of ASSISTON-ARM are presented.

Chapter 9 concludes the dissertation. Further improvements of the system to increase comfort and safety are discussed. Ongoing works and future research directions for the system are presented.

Chapter II

2 Related Work

This section discusses the important aspects related to the physical rehabilitation of human shoulder and reviews exoskeletons designed for upper-extremity rehabilitation.

2.1 Physical Rehabilitation of Human Shoulder

Human shoulder complex possesses two translational degrees of freedom (DoF) coupled to three rotational DoF [31,32]. In addition to the decoupled translational movements of the center of glenohumeral (GH) joint, movements of the shoulder girdle are tightly coupled with the elevational rotation of the humerus [33]. This coupling is known as the scapulohumeral (SH) rhythm. As a consequence of shoulder rotations, the tip of the humerus translates in the sagittal and frontal planes due to SH rhythm.

Stroke and upper limb paralysis may cause various impairments in the upper extremity. Inferior GH joint displacement, commonly referred to as shoulder subluxation, is one of the most common musculoskeletal problems caused by the gravitational pull on the humerus and stretching of the capsule of the shoulder joint once the shoulder muscles are weakened by paralysis [34]. Shoulder subluxation is one of the possible causes of shoulder pain following

a stroke [35]. Moreover, it restricts the passive and active range of motion (RoM) and can hinder recovery of upper limb function. Consistent evidences in literature indicate that subluxation is correlated with poor upper limb function [36] and reflex sympathetic dystrophy [37]. As a result, prevention or counteraction of shoulder subluxation is important for upper extremity rehabilitation after stroke.

Scapular dyskinesia is another condition that refers to abnormalities in the SH rhythm. Since abnormality of SH rhythm results in secondary effects on the function of the shoulder joint, restoring a stable scapular base through scapular stabilization exercises is essential to rehabilitating shoulder and returning to functional activities. Similarly, GH mobilization exercises are required for re-gaining RoM of the joint. Most stroke patients cannot perform shoulder girdle movements by themselves; hence, it is imperative that these movements are properly assisted during physical therapies until the patient can actively stabilize and orient his/her upper limb during activities of daily living.

Another aspect is related to gaining upper extremity function after stroke via recovery or compensation. Re-integration of the impaired arm into ADL critically depends on the type of functional gains, while improvement in functional performance can be achieved through compensatory adaptations as well as from recovery of normative movement and muscle activation patterns. [30] provide evidence that adoption of compensatory strategies early in treatment can inhibit potential recovery. This study also shows that increased arm use at home is strongly predicted by increased recovery and only weakly predicted by increased function via compensation. In particular, even though patients may achieve high clinical scores using compensation strate-

gies, they tend not to integrate these unnatural and energetically ineffective strategies in their daily lives. Hence, resorting to compensation strategies early in treatment decrease the amount of real-world limb use. On the other hand, gains that are due to recovery of normative movement and muscle activation patterns result in increased use of the limb which promote further functional gains.

All of the above clinical treatment guidelines suggest that to deliver effective rehabilitation therapies to human shoulder complex, an exoskeleton should be capable of actively locating the humerus head to counteract shoulder subluxation, should be able to provide assistance to patients during scapular stabilization and GH mobilization exercises such that they can restore their natural SH rhythm and actively stabilize and orient their upper limbs during ADL. Most importantly, an effective shoulder exoskeleton is expected to promote recovery, not compensation. End-effector type devices and exoskeletons that do not allow natural movements of shoulder girdle necessitate compensatory movements, which can detrimentally affect further functional gains that are achievable by the upper limb.

2.2 Exoskeletons for Upper-Extremity Rehabilitation

Exoskeletons for upper-extremity rehabilitation can be loosely categorized into three, with respect to their ability to align with human shoulder complex and to assist movements of the shoulder girdle.

The first group includes the exoskeletons whose kinematics model the human shoulder complex as an ideal spherical joint. For instance, the mobile exoskeleton developed by [38] features 2 actuated rotational DoF at the shoulder complex, BOTAS [22] and SAM [39] have 3 actuated rotational DoF

located at the shoulder complex, while [40] utilize a spherical 4R mechanism at the shoulder complex such that kinematic singularities can be avoided through redundant actuation. Similarly, CADEN-7 [20] and L-exos [41] are cable-driven exoskeletons that rely on spherical shoulder kinematics. Exoskeletons that belong to the first group cannot accommodate for the inherent translations of the human shoulder complex; hence, do not allow for natural movements that include GH mobilization and SH rhythm.

The second group of exoskeletons relies on more realistic kinematic models of the human shoulder complex and possesses kinematics that can *partially* allow for or assist the movements of the shoulder joint complex. These exoskeletons either feature passive joints at the shoulder girdle to enable alignment, or approximate the shoulder kinematics to follow simplified curves. These exoskeletons cannot actively assist all movements of shoulder complex.

SH rhythm has been included into the kinematic design of the passive exoskeleton presented in [42] through two passive revolute joints located near the scapula thoracic joint. ESA exoskeleton [43] introduces two passive revolute joints and a passive prismatic joint to allow for the movements of the shoulder complex. MGA exoskeleton [44] approximates the movements of the shoulder complex with circular paths and utilizes an active revolute joint in series with spherical rotations to enable scapular rotation.

Passive anti-gravity arm orthosis WREX [45], its enhanced version T-WREX [46], and pneumatically powered Pneu-WREX [47] share the same underlying kinematics, where the translations of the shoulder complex is modelled as a single rotation of the scapula. RUPERT [48] also relies on simplified shoulder kinematics and features one pneumatic muscle.

In recent years, there has also been some interest in low DoF exoskeletons. For instance, passive gravity compensation of the arm for industrial applications is targeted via passive exoskeletons that feature passive joints for alignment of shoulder joint axes [49, 50].

ARMin I [51] is a semi-exoskeleton solution with three active and two passive DoF at the shoulder complex, such that it can actively deliver shoulder flexion/extension, horizontal flexion/extension and internal/external rotations, while passively allowing for shoulder abduction/adduction movements. ARMin II [19, 52] has introduced a novel linkage mechanism to passively allow for elevation/depression movements of the humerus head, drastically decreasing the ergonomic problems of ARMin I. On the other hand, the additional passive DoF through the linkage mechanism has significantly increased the kinematic complexity of the robot. In ARMin III [53], the passive linkage mechanism has been removed from the system and the new kinematics rely on a circular approximation of shoulder movements and a manual adjustment mechanism. While ARMin III simplifies the kinematic structure of ARMin II, this is achieved at the expense of deteriorated ergonomics. By approximating the movements of center of GH joint by a circular path, the movements of the device no longer properly correspond with human joint movements even after individualized adjustments for each patient. ARMin IV [54] and later versions of ARMin inherit their underlying kinematics from ARMin III.

In order to comply with the SH rhythm, both Dampace [55] and Limbact [56] include two DoF self-alignment mechanisms that increase their ergonomics. Even though these exoskeletons allow for GH mobilization, the translational movements of shoulder complex are not actuated; hence, they cannot assist shoulder during GH stabilization and mobilization exercises.

ShouldeRO [57] uses a poly-articulated structure with Bowden-cable transmission to implement an alignment-free two DoF exoskeleton for the shoulder. ShouldeRO cannot assist patients while performing movements of the shoulder girdle. Similarly, ALEx [23] is a cable-driven light-weight exoskeleton that features a novel remote center of rotation mechanism at its shoulder joint. ALEx possesses four actuated rotational DoF; hence, approximates GH movements via circular paths, and cannot actively deliver translational movements of human shoulder complex.

Finally, IntelliArm [58] utilizes $PP\underline{RRR}$ ¹ serial kinematics with two passive and one active DoF for the alignment of the center of GH joint with the exoskeleton rotation axes. IntelliArm can assist elevation/depression movements of the shoulder girdle, but cannot provide assistance for the protraction/retraction movements.

The third group includes exoskeletons that allow for all movements of the shoulder complex and can actively deliver all GH mobilization exercises. MEDARM [59] features \underline{RRRR} serial kinematics with an actuated two DoF shoulder girdle mechanism to assist both elevation/depression and protraction/retraction movements. This exoskeleton possesses a rather complex kinematic structure. An exoskeleton with \underline{RPRPRR} serial kinematic chain is proposed in [60] that also allows for tracking and assisting of all shoulder girdle movements of the human shoulder. However, this design still suffers from joint misalignment problem, since the girdle movements is based on the approximation that the center of the GH follows a circular path at the sternoclavicular joint.

¹In this representation R refers to a revolute, P refers to a prismatic joint, and Pa refers to a parallelogram mechanism. Underlined joints are actuated and measured, while overlined joints are measured.

Harmony [24,61] possesses *RPaRRR* kinematics with two active DoF at the shoulder girdle, in addition to three active shoulder rotations. Harmony allows for and can deliver GH mobilization exercises, as it relies on a remote center of rotation mechanism implemented via four-bar parallelogram linkages to actuate shoulder protraction/retraction and an active revolute joint for shoulder elevation/depression movements. However, ergonomic shoulder movements of Harmony necessitate the rotation axes of acromioclavicular and sternoclavicular joints to be located and link lengths of the exoskeleton to be manually adjusted to ensure good correspondence of human joint axes with robot axes.

Proper alignment of exoskeleton axes with human joint axes is indispensable in order to deliver effective rehabilitation therapies, especially for the high DoF human shoulder complex. The exact motion of the shoulder complex shows wide variation among patients, as this motion strongly depends on the age of the patient, size and orientation of underlying bones, the shape of articulated surfaces and the constraints imposed by ligaments, capsules and tendons of the individual. For instance, clinical studies indicate that the mean ratio of scapular plane rotations contributing to SH rhythm is 1:2.4 for adults, while it is 1:1.3 for children [62]. Exoskeletons such as Armin III [53] and Harmony [61] rely on manual adjustments of link lengths to approximately match human joint rotation axes; however, adjusting robot joint axes to closely match the human axes is a tedious process that may take up an important portion of the precious therapy session. Mechanisms that have self-alignment feature, as introduced in [21, 23, 55, 56, 63], eliminate the need for manual adjustments and can ensure ergonomic movements throughout therapies.

2.3 Proposed Exoskeleton: ASSISTON-ARM

ASSISTON-ARM is a *self-aligning* powered exoskeleton for robot-assisted upper-extremity rehabilitation. ASSISTON-ARM has been designed and implemented as an impedance-type device, since the passive self-alignment of joint axes necessitates the exoskeleton to follow movements of human limb with very low resistance, while actuation of all movements of the shoulder complex require robust and high fidelity interaction control.

Robots can be categorized as admittance-type or impedance-type devices, depending on whether they behave like velocity or force sources, respectively. The type of a robot is determined by its structural design, actuation and power transmission characteristics [64]. As an impedance-type device, ASSISTON-ARM receives force commands and applies forces to its user in response to measured positions. The rationale behind implementing ASSISTON-ARM as an impedance-type device follows from the following arguments on interaction control.

All controllers are fundamentally band-limited due to roll-off in actuators, amplifiers, and sensors. Hence, at high-frequencies, the closed-loop impedance transfer function of the controlled system always matches the open-loop impedance of the robot. Given that inertial forces dominate at high-frequencies, the impedance transfer function appears as the apparent end-effector inertia, that is, the effective inertia located after the inherent compliance of the system. It has been well-established within the frequency domain passivity framework that, force control cannot hide this inertia at any frequency, while simultaneously maintaining the absolute stability of the controlled system [65–67]. Along these lines, the inertia after the inherent compliance of the system can only be reduced through mechanical

design of a robot and not by force feedback, if coupled stability guarantees are enforced [68]. While force feedback can be used to compensate for parasitic effects, such as friction and stiction, within the closed-loop control bandwidth of the system [66,67], the unavoidable non-collocation between the force sensor and the actuators imposes inherent limitations on controller gains to ensure coupled stability [65]. Hence, to simultaneously guarantee coupled stability and good interaction control performance, closed-loop force control must rely on carefully tuned controller gains and a mechanical design with low apparent inertia.

ASSISTON-ARM utilizes the alternative solution, as commonly preferred in the design of haptic interfaces. In particular, ASSISTON-ARM relies on its mechanical design to minimize friction, stiction and backlash like parasitic effects, while also keeping the apparent inertia of the exoskeleton as low as possible. Along these lines, the design of ASSISTON-ARM features a planar parallel mechanism actuated by capstan-driven direct drive motors, which, not only minimizes parasitic effects but also acts as a mechanical torque sumner to achieve high torque outputs. The parallel mechanism increases the device stiffness, while helping reduce the moving mass and reflected inertia of the exoskeleton. Coupled to a spring based passive gravity compensation mechanism, ASSISTON-ARM achieves high mechanical transparency. Consequently, ASSISTON-ARM does not necessitate closed loop force control to achieve high back-driveability. ASSISTON-ARM's transparent design enables high-fidelity interaction controllers to be implemented without being bound by the coupled stability limitations of force-feedback; interaction control of ASSISTON-ARM can be implemented through open-loop control of motor torques at high bandwidths.

As a result of its novel self-aligning kinematics, low apparent inertia, and impedance-type power transmission, ASSISTON-ARM possesses several important properties.

i) ASSISTON-ARM can both actively and passively follow and assist translational movements of the center of glenohumeral joint. Consequently, in addition to all shoulder rotations and reaching exercises, it can deliver glenohumeral mobilization (scapular elevation/depression and protraction/retraction) and scapular stabilization exercises, extending the type of therapies that can be administered using upper-arm exoskeletons. As an active exoskeleton, it can restrict undesired compensatory movements, assist targeted joint movements, and provide such measurements.

ii) Passively aligning its joint axes, ASSISTON-ARM can provide an ideal match between human joint axes and the exoskeleton axes, guaranteeing ergonomics and comfort throughout therapies, and extending the usable range of motion for upper extremity movement. Furthermore, this self-aligning feature significantly shortens the setup time required to attach a patient to the exoskeleton. Kinematics of ASSISTON-ARM maximizes singularity-free workspace of the device such that almost all of the human workspace required for ADL is covered.

iii) ASSISTON-ARM is mechanically transparent and passively back-driveable; thus, it minimally interferes with the natural movements of patients. Passive back-driveability allows therapist to use ASSISTON-ARM as a measurement device for diagnosis. The passive back-driveability of the device also ensures safety of patients even under power losses.

iv) Mechanical transparency and passive back-driveability of ASSISTON-ARM beneficially affect the interaction control performance of the system. In

particular, the transparency of the system allows for a precise model of the device dynamics to be identified and model based controllers to be implemented with high fidelity, without large parasitic effects due to unmodelled device dynamics. Since interaction controllers of ASSISTON-ARM can be implemented without the need for force sensors, high-fidelity force control and precise impedance control can be achieved at high control bandwidths. This control architecture not only simplifies implementation, but also enhances safety (coupled stability robustness), as open-loop force control does not suffer from the fundamental stability limitations of force-feedback.

Chapter III

3 Kinematic Type Selection of ASSISTON-ARM

A good understanding of human joint kinematics is imperative for the kinematic type selection of exoskeletons to ensure ergonomics and comfort. In this section information about kinematics of human arm and kinematic type selection for ASSISTON-ARM is given.

3.1 Kinematics of Human Shoulder Complex

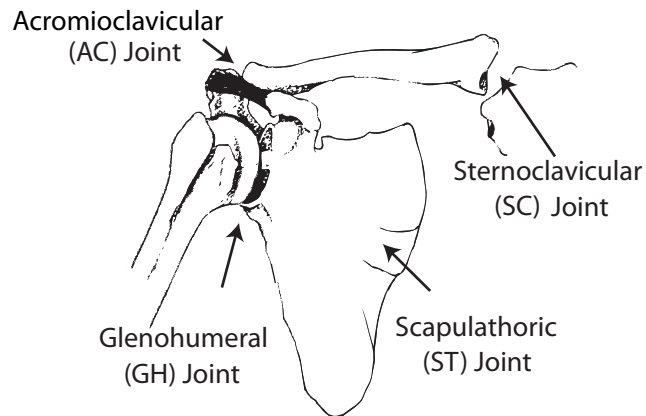


Figure 3.1: Joints at the shoulder complex

Human shoulder complex, depicted in Figure 3.1, consists of different joints including shoulder and shoulder girdle. Shoulder complex has the ability to move both in a translational and rotational manner. The sternoclavicular (SC) and the acromioclavicular (AC) joints at the shoulder girdle each

have 3 DoF, while the scapulothoracic (ST) joint possesses 5 DoF. However, the overall movement of the shoulder girdle is constrained and the movements of these joints cause the center of GH joint to shift [69].

In the literature, it has been shown that shoulder girdle is mainly responsible for 2 DoF translational movements of elevation/depression and protraction/retraction of shoulder [70]. Given the 3 rotational DoF of the shoulder socket itself, the shoulder complex can be modeled as a 5 DoF kinematic chain [31, 32, 42], with three rotations (shoulder flexion/extension, internal/external rotation and horizontal abduction/adduction) and two translations (scapular protraction/retraction and elevation/depression), as depicted in Figure 3.2.

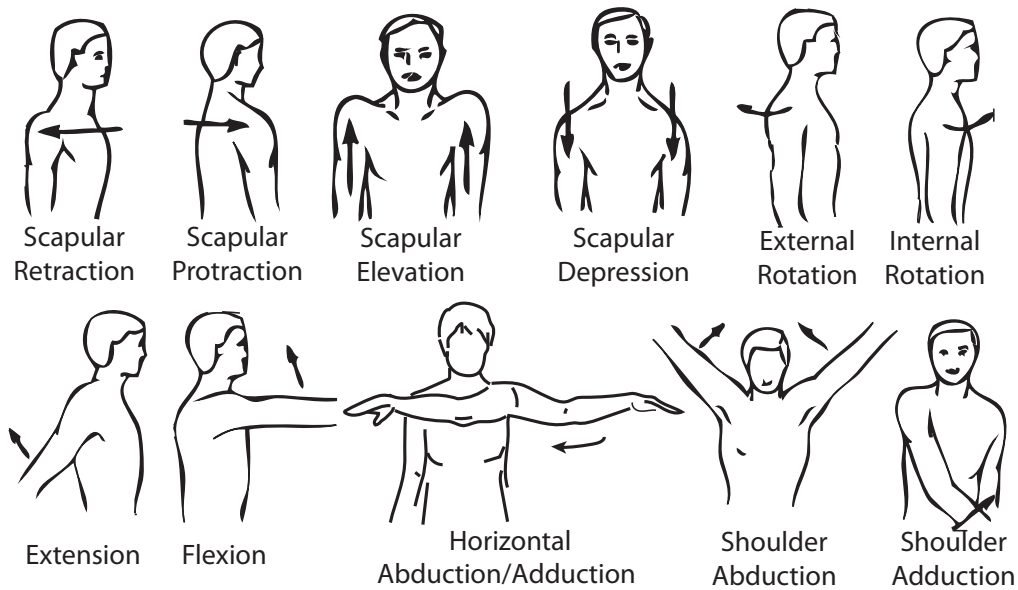


Figure 3.2: Movements of human shoulder complex

The center of GH joint can be controlled independently from the shoulder rotations. Furthermore, there also exists a strong coupling between the shoulder rotations and the translations of the center of GH joint, called the Scapu-

loHumeral (SH) rhythm [33], as the movement of humerus causes scapula to move.

It has been reported in the literature that when the human arm is fully flexed or abducted (corresponding to a 180° rotation), the humerus is rotated only by an amount of 120° , while the scapular motion accounts for the remaining 60° rotation [71]. This ratio differs for every individual, since the exact motion of the humerus head shows wide variation among humans. For instance, the mean ratio is about 1:2.4 for healthy adults, while the mean ratio drastically changes to 1:1.3 for children [62].

The internal/external rotation of upper arm has a similar function as the pronation/supination rotation of the forearm and can be faithfully modeled as a simple 1 DoF revolute joint, the axis of which stands on the center line of the humerus [72].

3.2 Kinematics of Human Elbow

Human elbow also possesses coupled translations with its rotation. These translations are due to the quasi-conic double frustum of the mobile rotation axis [73]. However, the translations of the rotation axis of the elbow joint are very small and elbow movements can be faithfully modelled as a single DoF revolute joint [43, 44, 47, 53, 56, 58].

3.3 Kinematic Type Selection of ASSISTON-ARM

In order to obtain an ideal match between a human and an exoskeleton, it is imperative that the exoskeleton can faithfully replicate the movements of human joints. To achieve this goal, ASSISTON-ARM consists of a shoulder

module that passively tracks the shoulder movements and assists them as needed. Figure 3.3 presents a schematic representation of the kinematics of ASSISTON-ARM.

The shoulder module of ASSISTON-ARM is responsible for faithfully reproducing shoulder motions during rehabilitation exercises. The shoulder module possesses a 6 DoF hybrid $\underline{R}\overline{P} - 3\underline{R}R\underline{P} - \underline{R}$ kinematic structure.

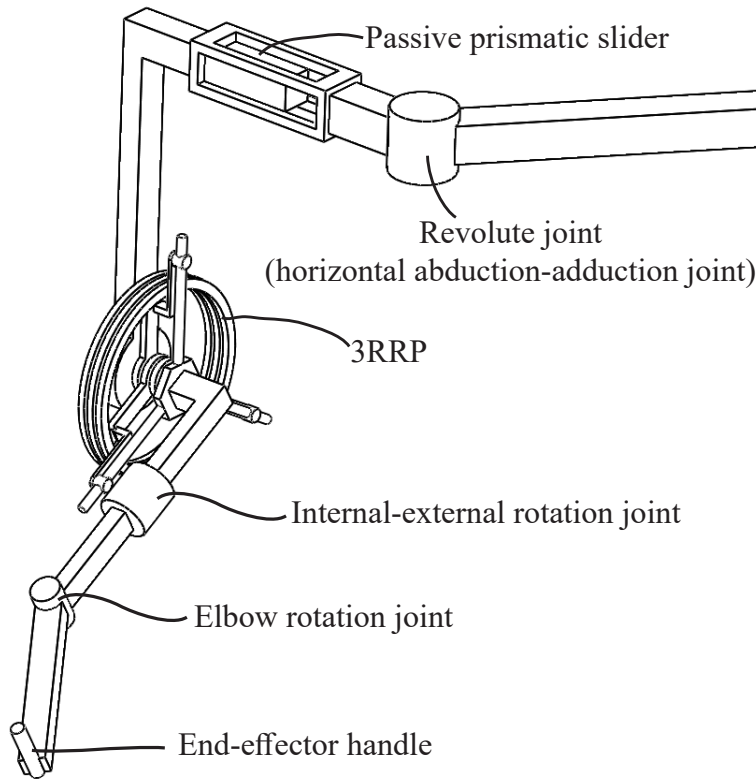


Figure 3.3: Schematic representation of ASSISTON-ARM

First revolute joint is an actuated joint located at top of the mechanism and is responsible for horizontal abduction/adduction movements of the shoulder. A passive slider is located after this revolute joint, forming $\underline{R}\overline{P}$ series kinematic chain for the first section of the shoulder module. The

passive prismatic joint is required to ensure an ideal match of the shoulder module to various human shoulder sizes. Furthermore, this passive prismatic joint helps prevent singularities and ensures better alignment of joint axes during shoulder movements when the humerus moves in the frontal plane.

The ability of ASSISTON-ARM to faithfully reproduce shoulder movements is largely due to its self-aligning joint, implemented as a $3\underline{R}$ RP mechanism that is rigidly connected to one end of the passive prismatic joint. $3\underline{R}$ RP is a parallel mechanism that possesses 3 DoF in a plane. Through three actuators grounded to its frame, $3\underline{R}$ RP mechanism adds 2 translational and one rotational DoF that can be controlled independently; hence, $3\underline{R}$ RP mechanism can assist SH rhythm and deliver GH joint mobilization movements. In coordination with the first revolute joint, kinematics of ASSISTON-ARM can also faithfully produce shoulder abduction/adduction movements.

$3\underline{R}$ RP mechanism has a symmetric structure and provides a large, circular, singularity free workspace. Due to its parallel kinematics, $3\underline{R}$ RP mechanism not only features high bandwidth and stiffness, but also serves as a mechanical summer for the end-effector rotations. Hence, relatively small actuators can be used to impose large torques and forces at the end-effector of this mechanism, while keeping the moving mass and reflected inertia of the system low.

The last part of the shoulder module is for shoulder internal/external rotation and consists of a remote center of rotation mechanism, currently implemented using a curved rail. This structure allows patient's arm to conveniently go through the joint and can provide internal/external rotation of shoulder, faithfully tracking and reproducing the required RoM.

The underlying kinematics of the elbow module of ASSISTON-ARM is

implemented as a single DoF revolute joint, since small changes in the axis of rotation of the elbow can be neglected without causing ergonomics limitations, as the connection straps of the exoskeleton inherently feature sufficient compliance to allow for such small movements.

Chapter IV

4 Kinematic Analysis of ASSISTON-ARM

ASSISTON-ARM features a hybrid kinematic chain which can be represented as $\underline{R}\overline{P} - 3\underline{R}R\underline{P} - \underline{R} - \underline{R}$. As a result, ASSISTON-ARM can be modeled as a 7 DoF mechanism.

Figure 4.1 depicts a schematic representation of ASSISTON-ARM together with relevant variables used during its kinematic analysis. Let N represent the Newtonian reference frame attached to the ground. Let Point A be located at the axis of rotation of the horizontal abduction-adduction joint, Point E be located at the elbow joint, and Point Z be located at the end-effector of ASSISTON-ARM. Point G on N is taken as the origin. Body P has gone through a simple rotation about the direction \vec{n}_3 with an amount of α_1 . Body R translates with respect to Body P along the direction \vec{p}_1 with an amount of d_1 . The base of $3\underline{R}R\underline{P}$ parallel mechanism is rigidly attached to Body R , while its end-effector is rigidly attached to Body U . Due to the motion of $3\underline{R}R\underline{P}$ mechanism, Body U translates on the $\vec{r}_2 - \vec{r}_3$ plane with the configuration variables y_s and z_s and rotates about \vec{r}_1 with an amount of θ , with respect to Body R . Body L goes through a simple rotation with respect to Body U about the direction \vec{u}_3 with an amount of α_2 . Lastly, the lower arm part of the exoskeleton, Body H , goes through a simple rotation with respect to Body L about the direction \vec{l}_1 with an amount of α_3 .

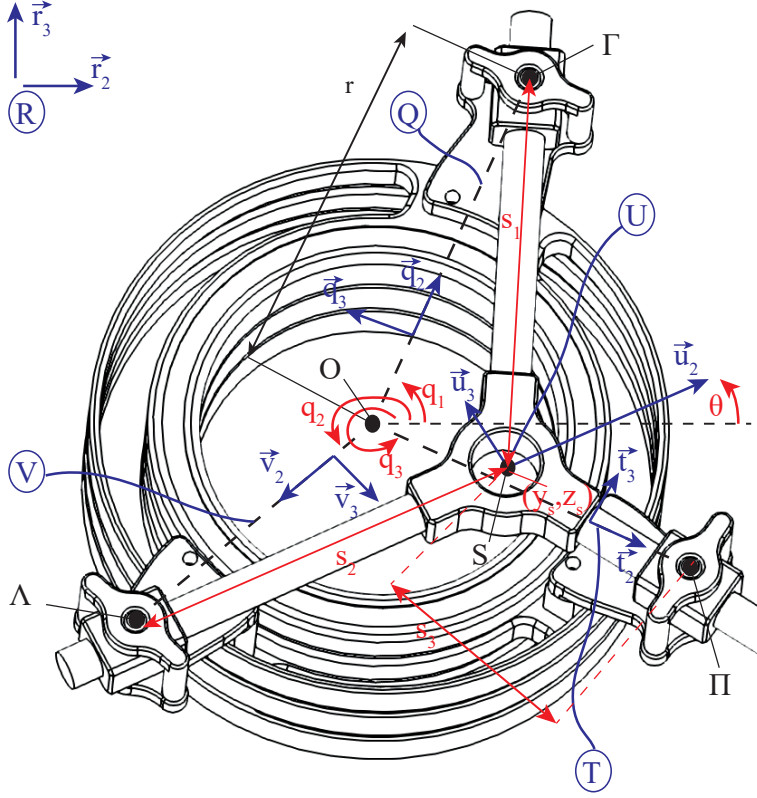


Figure 4.2: Schematic representation of kinematics of 3RRP mechanism

respect to base frame Body R about the axis \vec{r}_1 with angles q_1 , q_2 and q_3 , respectively. These angles are actuated via motors that turn the disks of the 3RRP mechanism. Symmetric end-effector, Body U is connected to arm bodies at Points Γ , Λ and Π via collocated prismatic and revolute joints. Let Point O be fixed on Body R , located at the center of the disks and S represent the point at the middle of the end-effector Body U of 3RRP mechanism. Let the translations of Body U with respect to Body R along directions \vec{r}_2 and \vec{r}_3 be given as y_s and z_s , respectively. Furthermore, Body U rotates about the axis \vec{r}_1 with an amount of θ .

The fixed distance between the pairs of points $O\Gamma$, $O\Pi$ and $O\Lambda$ is defined

as r . Variable distances between the pairs of points ΓS , ΠS and ΛS are indicated as s_1 , s_2 and s_3 , respectively. In the kinematic calculations, the variable distances depicted above are assumed to be always positive as shown, while angles are taken as positive if counter-clockwise.

At the initial configuration (homing position) \vec{r}_2 of Body R and \vec{u}_2 of end-effector Body U overlap with each other, and the angle θ is zero. Also the end-effector of 3RRP mechanism is at $y_s = 0$, $z_s = 0$, while arm vectors \vec{q}_2 , \vec{v}_2 and \vec{t}_2 have rotated around \vec{r}_1 axis about $\pi/3$, π and $-\pi/3$ with respect to \vec{r}_2 , at the homing position.

Below we first present the configuration and motion level kinematics of 3RRP mechanism, followed by the overall kinematics of ASSISTON-ARM.

Forward kinematics at the configuration level calculates the end-effector configuration when the joint angles are provided as inputs.

The end-effector of a symmetric 3RRP mechanism is known to be located at *the first Fermat point* (or the isogonic center) of the triangle defined by the revolute joints located on the disks of the mechanism, since the angle between the prismatic joints of a symmetric end-effector is set to 120° . In particular, the first Fermat point is a special point within the triangle that minimizes the sum of distances to the vertices of the triangle. There exists several other interesting physical interpretations of the first Fermat point as reviewed in [74].

The centuries old geometric problem of locating the first Fermat point of the triangle has been proposed by Fermat in 1643. An elegant geometric solution that does not involve vector algebra or calculus has been provided by Torricelli (1608–1647) and published by his student Viviani in 1659 [75]. Recently, closed form analytical solutions to the forward and inverse con-

figuration level kinematics of 3RRP mechanism have also been established in [76] and our earlier work [21, 77] using vector algebra.

In particular, given the joint angles q_1 , q_2 and q_3 , the configuration level forward kinematics (the end-effector variables y_s , z_s and θ) of 3RRP mechanism can be calculated in a closed form as

$$y_s = -\frac{M}{\sqrt{3}(K^2 + L^2)} \quad (1)$$

$$z_s = c_{22} - \frac{K}{L}c_{21} - \frac{KM}{\sqrt{3}L(K^2 + L^2)} \quad (2)$$

$$\theta = \text{atan2}(K, L) \quad (3)$$

where

$$\begin{aligned} K &= c_{12} + c_{32} + \sqrt{3}c_{31} - 2c_{22} - \sqrt{3}c_{11} \\ L &= c_{11} + c_{31} + \sqrt{3}c_{12} - 2c_{21} - \sqrt{3}c_{32} \\ M &= L(L - \sqrt{3}K)c_{12} - L(K + \sqrt{3}L)c_{11} \\ &\quad - (L - \sqrt{3}K)(Lc_{22} - Kc_{21}) \end{aligned}$$

with

$$\begin{aligned} c_{11} &= r \cos(q_1) & c_{12} &= r \sin(q_1) \\ c_{21} &= r \cos(q_2) & c_{22} &= r \sin(q_2) \\ c_{31} &= r \cos(q_3) & c_{32} &= r \sin(q_3) \end{aligned}$$

Configuration level inverse kinematics calculates the joint angles given the end-effector pose of the mechanism. In particular, given y_s , z_s and θ , the

actuator angles q_1 , q_2 and q_3 can be calculated as

$$q_1 = \text{atan2}(M_1, L_1) \quad (4)$$

$$q_2 = \text{atan2}(M_2, L_2) \quad (5)$$

$$q_3 = \text{atan2}(M_3, L_3) \quad (6)$$

where

$$\begin{aligned} M_1 &= K_1 \cos(\theta + \frac{\pi}{3}) - \sqrt{r^2 - K_1^2} \sin(\theta + \frac{\pi}{3}) \\ L_1 &= -K_1 \sin(\theta + \frac{\pi}{3}) - \sqrt{r^2 - K_1^2} \cos(\theta + \frac{\pi}{3}) \\ M_2 &= K_2 \cos(\theta + \pi) - \sqrt{r^2 - K_2^2} \sin(\theta + \pi) \\ L_2 &= -K_2 \sin(\theta + \pi) - \sqrt{r^2 - K_2^2} \cos(\theta + \pi) \\ M_3 &= K_3 \cos(\theta - \frac{\pi}{3}) - \sqrt{r^2 - K_3^2} \sin(\theta - \frac{\pi}{3}) \\ L_3 &= -K_3 \sin(\theta - \frac{\pi}{3}) - \sqrt{r^2 - K_3^2} \cos(\theta - \frac{\pi}{3}) \\ K_1 &= y_s \sin(\theta + \frac{\pi}{3}) - z_s \cos(\theta + \frac{\pi}{3}) \\ K_2 &= y_s \sin(\theta + \pi) - z_s \cos(\theta + \pi) \\ K_3 &= y_s \sin(\theta - \frac{\pi}{3}) - z_s \cos(\theta - \frac{\pi}{3}) \end{aligned}$$

In both the configuration level forward and inverse kinematic solutions, the intermediate variables s_1 , s_2 and s_3 can also be solved for in a closed form, using simple trigonometric relations.

4.2 Motion Level Kinematics of 3RRP Mechanism

Motion level kinematics determines the relationship between the actuator velocities and the end-effector (linear and angular) velocities. For the planar

parallel mechanism, the time derivative of the configuration level kinematic equations can be utilized to solve for its motion level kinematics, since all rotations are simple planar ones. In particular, the relationship between the end-effector velocities \dot{y}_s , \dot{z}_s and $\dot{\theta}$ and the actuator angular velocities \dot{q}_1 , \dot{q}_2 , \dot{q}_3 , represented by the kinematic Jacobian of $3\underline{R}RP$ mechanism, can be calculated as

$$\dot{X}_{3\underline{R}RP} = J_{3\underline{R}RP} \dot{q}_{3\underline{R}RP} \quad (7)$$

where $\dot{X}_{3\underline{R}RP} = [\dot{y}_s \ \dot{z}_s \ \dot{\theta}]^T$ and $\dot{q}_{3\underline{R}RP} = [\dot{q}_1 \ \dot{q}_2 \ \dot{q}_3]^T$ with $J_{3\underline{R}RP_{ij}}$ ($i, j=1, 2, 3$) are as given at the top of next page.

$$\begin{aligned}
J_{\underline{3RRP}_{11}} &= -r[(s_3 - s_2) \cos q_1 + 2(s_2 + s_3) \cos (q_1 - 2\theta) + \sqrt{3}(s_2 + s_3) \sin q_1 \\
&\quad + \sqrt{3}s_3 \sin (q_1 - 2\theta)]/2\sqrt{3}(s_1 + s_2 + s_3) \\
J_{\underline{3RRP}_{12}} &= -\sqrt{3}r[\sqrt{3}(s_1 + s_3) \sin q_2 - \sqrt{3}(s_1 + s_3) \sin (q_2 - 2\theta) + (s_1 - s_3) \cos q_2 \\
&\quad + (s_1 - s_3) \cos (q_2 - 2\theta)]/6(s_1 + s_2 + s_3) \\
J_{\underline{3RRP}_{13}} &= -\sqrt{3}r[(s_2 - s_1) \cos q_3 - (2s_2 + s_1) \cos (q_3 - 2\theta) + \sqrt{3}(s_1 + s_2) \sin q_3 \\
&\quad + \sqrt{3}s_1 \sin (q_3 - 2\theta)]/6(s_1 + s_2 + s_3) \\
J_{\underline{3RRP}_{21}} &= \sqrt{3}r[\sqrt{3}(s_2 + s_3) \cos q_1 + (s_2 - s_3) \sin q_1 + (2s_2 + s_3) \sin (q_1 - 2\theta) \\
&\quad - \sqrt{3}s_3 \cos (q_1 - 2\theta)]/6(s_1 + s_2 + s_3) \\
J_{\underline{3RRP}_{22}} &= \sqrt{3}r[\sqrt{3}(s_1 + s_3) \cos q_2 + \sqrt{3}(s_1 + s_3) \cos (q_2 - 2\theta) + (s_3 - s_1) \sin q_2 \\
&\quad + (s_1 - s_3) \sin (q_2 - 2\theta)]/6(s_1 + s_2 + s_3) \\
J_{\underline{3RRP}_{23}} &= -\sqrt{3}r[\sqrt{3}s_1 \cos (q_3 - 2\theta) - \sqrt{3}(s_1 + s_2) \cos q_3 + (s_2 - s_1) \sin q_3 \\
&\quad + (s_1 + 2s_2) \sin (q_3 - 2\theta)]/6(s_1 + s_2 + s_3) \\
J_{\underline{3RRP}_{31}} &= \frac{r \cos (\theta - q_1 + \frac{\pi}{3})}{s_1 + s_2 + s_3} \\
J_{\underline{3RRP}_{32}} &= \frac{-r \cos (q_2 - \theta)}{s_1 + s_2 + s_3} \\
J_{\underline{3RRP}_{33}} &= \frac{r \cos (q_3 - \theta + \frac{\pi}{3})}{s_1 + s_2 + s_3} \tag{8}
\end{aligned}$$

Motion level inverse kinematics of $\underline{3RRP}$ mechanism can be calculated through the inverse of the kinematic Jacobian, since no singularities exists within the circular workspace of $\underline{3RRP}$ mechanism.

4.3 Configuration Level Kinematics of ASSISTON-ARM

Given the closed form kinematic solution of 3RRP mechanism, the hybrid kinematics of the exoskeleton can be calculated using a serial connection of $\underline{R}, \overline{P}, 3RRP, \underline{R}, \underline{R}$ joints. In particular, the position of the end-effector of ASSISTON-ARM can be expressed as

$$\vec{r}^{GO} + \vec{r}^{OS} + \vec{r}^{SE} + \vec{r}^{EZ} = x_w \vec{n}_1 + y_w \vec{n}_2 + z_w \vec{n}_3 \quad (9)$$

where x_w , y_w and z_w represent the position coordinates of ASSISTON-ARM handle with respect to the Newtonian frame. Note that, given the forward kinematics of 3RRP, \vec{r}^{OS} in Eqn. (9) can be expressed as

$$\vec{r}^{OS} = y_s \vec{r}_2 + z_s \vec{r}_3 \quad (10)$$

where y_s and z_s indicate the end-effector positions of 3RRP mechanism with respect to Point O on Body R . In particular, the end-effector position can be calculated in a closed form as

$$\begin{aligned} x_w = & k_2 + y_s \sin \alpha_1 + k_6 + k_7 \sin \alpha_1 \cos \theta \\ & - \cos \alpha_1 (k_5 - k_3 - d_1) - k_8 (\sin \alpha_3 \cos \alpha_1 \cos \alpha_2 \\ & + \sin \alpha_1 (\cos \alpha_3 \cos \theta - \sin \alpha_2 \sin \alpha_3 \sin \theta)) \end{aligned} \quad (11)$$

$$\begin{aligned} y_w = & y_s \cos \alpha_1 + (k_6 + k_7) \cos \alpha_1 \cos \theta + \sin \alpha_1 (k_3 \\ & + d_1 - k_5) + k_8 (\sin \alpha_1 \sin \alpha_3 \cos \alpha_2 \\ & + \cos \alpha_1 (\cos \alpha_3 \cos \theta + \sin \alpha_2 \sin \alpha_3 \sin \theta)) \end{aligned} \quad (12)$$

$$\begin{aligned} z_w = & k_1 + z_s - k_4 + (k_6 + k_7) \sin \theta \\ & + k_8 (\sin \theta \cos \alpha_3 + \sin \alpha_2 \sin \alpha_3 \cos \theta) \end{aligned} \quad (13)$$

where k_i ($i=1,\dots,8$) denote the link lengths. The end-effector position (y_s, z_s) and orientation θ of 3RRP mechanism can be utilized to express configuration level forward kinematics of ASSISTON-ARM in terms of actuated joint angles and other measured joint variables.

The end-effector orientation of ASSISTON-ARM with respect to Newtonian frame can be represented with a unit quaternion $\varphi = \varphi_0 + \varphi_1\mathbf{i} + \varphi_2\mathbf{j} + \varphi_3\mathbf{k}$, where

$$\begin{aligned}\varphi_0 &= \cos \frac{\alpha_3}{2} \cos \frac{\theta}{2} \cos \left(\frac{\alpha_1 + \alpha_2}{2} \right) - \sin \frac{\alpha_3}{2} \sin \frac{\theta}{2} \cos \left(\frac{\alpha_2 - \alpha_1}{2} \right) \\ \varphi_1 &= \cos \frac{\alpha_3}{2} \sin \frac{\theta}{2} \cos \left(\frac{\alpha_2 - \alpha_1}{2} \right) + \sin \frac{\alpha_3}{2} \cos \frac{\theta}{2} \cos \left(\frac{\alpha_1 + \alpha_2}{2} \right) \\ \varphi_2 &= \cos \frac{\alpha_3}{2} \sin \frac{\theta}{2} \sin \left(\frac{\alpha_2 - \alpha_1}{2} \right) - \sin \frac{\alpha_3}{2} \cos \frac{\theta}{2} \sin \left(\frac{\alpha_1 + \alpha_2}{2} \right) \\ \varphi_3 &= \cos \frac{\alpha_3}{2} \cos \frac{\theta}{2} \sin \left(\frac{\alpha_1 + \alpha_2}{2} \right) + \sin \frac{\alpha_3}{2} \sin \frac{\theta}{2} \sin \left(\frac{\alpha_2 - \alpha_1}{2} \right)\end{aligned}\quad (14)$$

The configuration level inverse kinematics of ASSISTON-ARM does not assume a closed form solution. However, the equations characterizing the inverse kinematics can be decoupled and simplified as in [21], when the displacement d_1 of the passive slider is measured. An efficient numerical solution can be computed for the configuration level inverse kinematics by implementing an algorithm based on feedback stabilization that relies on the kinematic Jacobian of the system [78].

4.4 Motion Level Kinematics of ASSISTON-ARM

Motion level kinematics that map the joint velocities to end-effector velocities of ASSISTON-ARM can be determined by differentiating Eqn. (9) and calculating the angular velocity of the end-effector of the system.

Let the kinematic Jacobian of ASSISTON-ARM be expressed with respect to the end-effector motions of the 3RRP mechanism as

$$\begin{bmatrix} \dot{x}_w \\ \dot{y}_w \\ \dot{z}_w \\ {}^N\vec{w}^H \cdot \vec{n}_1 \\ {}^N\vec{w}^H \cdot \vec{n}_2 \\ {}^N\vec{w}^H \cdot \vec{n}_3 \end{bmatrix} = \begin{bmatrix} J_v \\ J_w \end{bmatrix} \begin{bmatrix} \dot{\alpha}_1 \\ \dot{y}_s \\ \dot{z}_s \\ \dot{\theta} \\ \dot{\alpha}_2 \\ \dot{\alpha}_3 \\ \dot{d}_1 \end{bmatrix} \quad (15)$$

where J_v and J_w denote linear and angular velocity components of the 6×7 kinematic Jacobian, respectively. Note that, in order to calculate motion level kinematics of the system, the displacement and the velocity of the passive prismatic joint are assumed to be measured.

The angular velocity part of the kinematic Jacobian J_w that represents relationship between the angular velocities of end-effector and the joint velocities is given as

$$J_w = \begin{bmatrix} 0 & 0 & 0 & \cos \alpha_1 & \sin \alpha_1 \cos \theta & \sin \alpha_1 \sin \theta & 0 \\ 0 & 0 & 0 & \sin \alpha_1 & \cos \alpha_1 \cos \theta & -\sin \theta \cos \alpha_1 & 0 \\ 1 & 0 & 0 & 0 & \sin \theta & \cos \theta & 0 \end{bmatrix} \quad (16)$$

The linear velocity part of the kinematic Jacobian J_v is calculated by taking the time derivatives of end-effector position vector given in Eqns. (11)–(13). The linear velocity part of the kinematic Jacobian J_v of ASSISTON-ARM can be derived as:

$$J_v = \begin{bmatrix} J_{v11} & J_{v12} & J_{v13} & J_{v14} & J_{v15} & J_{v16} & J_{v17} \\ J_{v21} & J_{v22} & J_{v23} & J_{v24} & J_{v25} & J_{v26} & J_{v27} \\ J_{v31} & J_{v32} & J_{v33} & J_{v34} & J_{v35} & J_{v36} & J_{v37} \end{bmatrix} \quad (17)$$

where

$$\begin{aligned} J_{v11} = & (k_5 - d_1 - k_3) \sin \alpha_1 + k_8 (\sin \alpha_2 \cos \alpha_1 \\ & + \sin \alpha_1 \sin \theta \cos \alpha_2) (\sin \alpha_3 \sin \theta - \sin \alpha_2 \cos \alpha_3 \cos \theta) \\ & - y_s \cos \alpha_1 - (k_6 + k_7) \cos \alpha_1 \cos \theta \\ & - k_8 \cos \alpha_2 \cos \theta (\cos \alpha_1 \cos \alpha_2 \cos \alpha_3 \\ & - \sin \alpha_1 (\sin \alpha_3 \cos \theta + \sin \alpha_2 \sin \theta \cos \alpha_3)) \end{aligned}$$

$$J_{v12} = -\sin \alpha_1$$

$$J_{v13} = 0$$

$$\begin{aligned} J_{v14} = & \sin \alpha_1 ((k_6 + k_7) \sin \theta + k_8 (\sin \theta \cos \alpha_3 \\ & + \sin \alpha_2 \sin \alpha_3 \cos \theta)) \end{aligned}$$

$$J_{v15} = k_8 \sin \alpha_3 (\sin \alpha_2 \cos \alpha_1 + \sin \alpha_1 \sin \theta \cos \alpha_2)$$

$$\begin{aligned} J_{v16} = & -k_8 (\cos \alpha_1 \cos \alpha_2 \cos \alpha_3 - \sin \alpha_1) (\sin \alpha_3 \cos \theta \\ & + \sin \alpha_2 \sin \theta \cos \alpha_3) \end{aligned}$$

$$J_{v17} = -d_1 \sin \alpha_1$$

$$\begin{aligned}
J_{v21} &= (d_1 + k_3 - k_5) \cos \alpha_1 + k_8(\sin \alpha_1 \sin \alpha_2 \\
&\quad - \sin \theta \cos \alpha_1 \cos \alpha_2)(\sin \alpha_3 \sin \theta - \sin \alpha_2 \cos \alpha_3 \cos \theta) \\
&\quad y_s \sin \alpha_1 - (k_6 + k_7) \sin \alpha_1 \cos \theta \\
&\quad - k_8 \cos \alpha_2 \cos \theta(\sin \alpha_1 \cos \alpha_2 \cos \alpha_3 + \cos \alpha_1(\sin \alpha_3 \cos \theta \\
&\quad + \sin \alpha_2 \sin \theta \cos \alpha_3)) \\
J_{v22} &= \cos \alpha_1 \\
J_{v23} &= 0 \\
J_{v24} &= -\cos \alpha_1((k_6 + k_7) \sin \theta + k_8 \sin \theta \cos \alpha_3) \\
&\quad + k_8 \sin \alpha_2 \sin \alpha_3 \cos \theta \\
J_{v25} &= k_8 \sin \alpha_3(\sin \alpha_1 \sin \alpha_2 - \sin \theta \cos \alpha_1 \cos \alpha_2) \\
J_{v26} &= -k_8(\sin \alpha_3 \cos \alpha_2 \cos \alpha_3 \\
&\quad + \cos \alpha_1)(\sin \alpha_3 \cos \theta + \sin \alpha_2 \sin \theta \cos \alpha_3) \\
J_{v27} &= -d_1 \cos \alpha_1 \\
J_{v31} &= 0 \\
J_{v32} &= 0 \\
J_{v33} &= 1 \\
J_{v34} &= (k_6 + k_7) \cos \theta + k_8 \cos \alpha_3 \cos \theta - k_8 \sin \alpha_2 \sin \alpha_3 \sin \theta \\
J_{v35} &= k_8 \sin \alpha_3 \cos \alpha_2 \cos \theta \\
J_{v36} &= -k_8(\sin \alpha_3 \sin \theta - \sin \alpha_2 \cos \alpha_3 \cos \theta) \\
J_{v37} &= 0
\end{aligned}$$

Given that the mapping between the joint velocities and the end-effector velocities of 3RRP is already defined in J_{3RRP} , the kinematic Jacobian J_k

based on the joint velocities of ASSISTON-ARM can be derived as

$$\begin{bmatrix} \dot{x}_w \\ \dot{y}_w \\ \dot{z}_w \\ {}^N\vec{w}^H \cdot \vec{n}_1 \\ {}^N\vec{w}^H \cdot \vec{n}_2 \\ {}^N\vec{w}^H \cdot \vec{n}_3 \end{bmatrix} = \begin{bmatrix} J_v \\ J_w \end{bmatrix} J_k \begin{bmatrix} \dot{\alpha}_1 \\ \dot{q}_1 \\ \dot{q}_2 \\ \dot{q}_3 \\ \dot{\alpha}_2 \\ \dot{\alpha}_3 \\ \dot{d}_1 \end{bmatrix}$$

$$\begin{bmatrix} \dot{x}_w \\ \dot{y}_w \\ \dot{z}_w \\ {}^N\vec{w}^H \cdot \vec{n}_1 \\ {}^N\vec{w}^H \cdot \vec{n}_2 \\ {}^N\vec{w}^H \cdot \vec{n}_3 \end{bmatrix} = \begin{bmatrix} J_v \\ J_w \end{bmatrix} \begin{bmatrix} 1 & 0_{1 \times 3} & 0_{1 \times 3} \\ 0_{3 \times 1} & \underline{J}_{3RRP} & 0_{3 \times 3} \\ 0_{3 \times 1} & 0_{3 \times 3} & \mathbf{I}_{3 \times 3} \end{bmatrix} \begin{bmatrix} \dot{\alpha}_1 \\ \dot{q}_1 \\ \dot{q}_2 \\ \dot{q}_3 \\ \dot{\alpha}_2 \\ \dot{\alpha}_3 \\ \dot{d}_1 \end{bmatrix} \quad (18)$$

4.5 Dynamics of ASSISTON-ARM

After the configuration and the motion level kinematics have been derived, the dynamic model of ASSISTON-ARM has been computed symbolically utilizing Autolev [79]. To model the system using Kane's method, the acceleration level kinematics equations are calculated via symbolic differentiation of the motion level kinematics with respect to time. The inertial properties

and center of mass of all bodies are extracted from the solid models of components. External forces F_x, F_y, F_z and torques T_x, T_y, T_z are considered at the multiple interaction points of exoskeleton with the human user. Actuator torques τ_i ($i=1,\dots,6$) that drive joints are also added to the calculations.

Overall dynamic equation for the robot can be defined as

$$M(q)\ddot{q} + C(q, \dot{q})\dot{q} + G(q) = \tau_{ext} + \tau_i \quad (19)$$

where $M(q)$ is mass matrix defined in $\mathbb{R}^{6 \times 6}$, $C(q, \dot{q}) \in \mathbb{R}^{6 \times 6}$ is the Coriolis and centrifugal matrix, $G(q) \in \mathbb{R}^{6 \times 1}$ is representing gravitational effect on moving parts. τ_{ext} are external forces, namely $\tau_{ext} = [F_x, F_y, F_z, T_x, T_y, T_z]^T$, and τ_i is the control torques. $q \in \mathbb{R}^{6 \times 1}$ is joint variables.

The resulting symbolic equations of motions are used for feed-forward dynamic compensation and model based control of ASSISTON-ARM. Due to their very large size, these symbolic dynamics equations are not presented.

4.6 Singularities of ASSISTON-ARM

The underlying kinematics of ASSISTON-ARM comprises of a hybrid kinematic chain that includes a $3\underline{R}$ RP planar parallel mechanism. The $3\underline{R}$ RP mechanism is singularity free within its workspace when the end-effector position is limited to stay inside the virtual circle created by collocated revolute and prismatic joints [76, 80]. Figure 4.3 presents the results of a numerical singularity of the $3\underline{R}$ RP mechanism analysis, conducted using the complete branch-and-prune based interval analysis method proposed in [81]. The blue region indicates singularity free reachable workspace, verifying the lack of singularities.

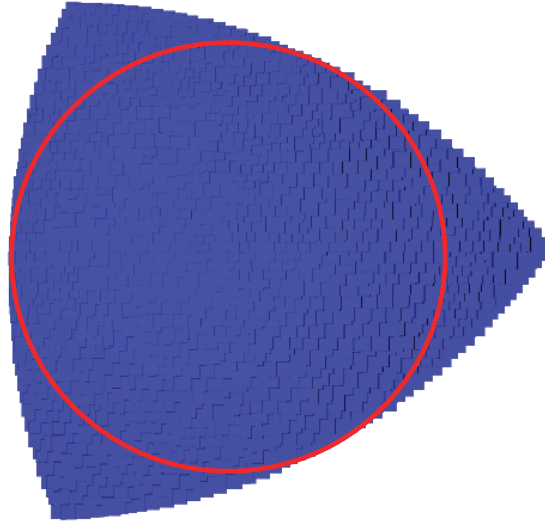


Figure 4.3: Singularity analysis of 3RRP mechanism through interval analysis proposed in [81]. Red circle indicates the boundary of the dexterous workspace while blue region indicates singularity free reachable workspace.

Given that the 3RRP mechanism is singularity free, the simplified kinematics presented in Appendix I Figure 9.6 can be used to study the singularities of ASSISTON-ARM, which features redundant kinematics with one passive and six actuated joints. The degree of redundancy for ASSISTON-ARM is one and the 6×7 kinematic Jacobian J_k of the device is presented in Section 4.4. It is well established that the probability of the manipulator to get into a singularity decreases as the degree of redundancy increases. Singularities of redundant robots may be determined by studying configurations that set the manipulability measure $|JJ^T|$ to zero. However, a symbolic solution to this equation is typically very cumbersome. An alternative singularity analysis approach exists thanks to Cauchy-Binet formula: A redundant robot is singular in the performance of an m -dimensional task if and only if all its $m \times m$ submatrices (also called minors) are singular at the same configuration [82]. In particular, to study the singularities of ASSISTON-ARM for 6

dimensional spatial movements at its handle, $\binom{7}{1}$ 6x6 minors of the kinematic Jacobians need to be studied, each minor corresponding to a kinematic Jacobian with a locked joint of ASSISTON-ARM. Intersection set of all singular configurations of these 6x6 minors determines singular configurations of the redundant system, that is, redundant robot has singularities if and only if the same singular configuration shows up in all of its 6×6 minors [82–84]. Along these lines, to study singularities of ASSISTON-ARM, we compute the determinants all minors as follows:

- i. If $\alpha_1 = \text{constant}$, then

$$\det(J_i) = -\sin(\alpha_2).$$

- ii. If $d_1 = \text{constant}$, then

$$\det(J_{ii}) = \sin(\alpha_2)(y_s - (k_6 + k_7) \sin(\theta)).$$

- iii. If $y_s = \text{constant}$ then

$$\det(J_{iii}) = (k_6 + k_7) \sin(\theta) \cos(\alpha_2) \cos(\theta) - \sin(\alpha_2)(k_5 - k_3 - d_1).$$

- iv. If $z_s = \text{constant}$, then

$$\begin{aligned} \det(J_{iv}) = & -\sin(\theta)(\sin(\alpha_1)(k_1 \cos(\alpha_2) - k_8 \sin(\alpha_2) \sin(\alpha_3))(\cos(\alpha_1) \cos(\alpha_2) - \\ & \sin(\alpha_1) \sin(\alpha_2) \cos(\theta)) + \cos(\alpha_1)(\cos(\alpha_1) \cos(\alpha_2) - \sin(\alpha_1) \sin(\alpha_2) \cos(\theta))((k_6 + \\ & k_7) \sin(\theta) + k_1 \sin(\alpha_2) \cos(\theta) + k_8(\sin(\theta) \cos(\alpha_3) + \sin(\alpha_3) \cos(\alpha_2) \cos(\theta))) - \\ & k_8(\sin(\alpha_3) \cos(\theta) + \sin(\theta) \cos(\alpha_2) \cos(\alpha_3)) - (\sin(\alpha_1) \cos(\alpha_2) + \\ & \sin(\alpha_2) \cos(\alpha_1) \cos(\theta)) \cos(\alpha_1)(k_1 \cos(\alpha_2) - k_8 \sin(\alpha_2) \sin(\alpha_3)) - \sin(\alpha_1)((k_6 + \\ & k_7) \sin(\theta) + k_1 \sin(\alpha_2) \cos(\theta) + k_8(\sin(\theta) \cos(\alpha_3) + \sin(\alpha_3) \cos(\alpha_2) \cos(\theta))). \end{aligned}$$

- v. If $\theta = \text{constant}$, then

$$\det(J_v) = \sin(\theta) \cos(\alpha_2).$$

vi. If $\alpha_2 = \text{constant}$, then

$$\det(J_{vi}) = \cos(\theta) \sin(\alpha_2).$$

vii. If $\alpha_3 = \text{constant}$, then

$$\det(J_{vii}) = -\sin(\theta).$$

These determinants reveal that there exist no common configurations when all 7 determinants are singular simultaneously; hence, ASSISTON-ARM is singularity free for all spatial movements seen from its handle.

The study of $\det(J_{ii})$ further reveals the necessity of the passive slider to avoid singular configurations. In particular, if there exists no passive slider at the second joint, then there exists a singular configuration when the elbow joint is located along the perpendicular line that passes through the center of 3RRP mechanism, that is $y_s = (k_6 + k_7) \sin(\theta)$. In this configuration, it is not possible for the system to assume velocity components perpendicular to the plane of the 3RRP mechanism (without the passive slider). Another such singularity occurs, when the axes of rotation of the elbow joint and 3RRP mechanisms align. Addition of passive slider helps avoid both of these singularities.

Note that, while the spatial movements at the handle of ASSISTON-ARM are singularity free, the orientation kinematics of the shoulder rotations still suffer from gimbal locks, since such singularities are unavoidable when only three rotational joints are used to cover $\text{SO}(3)$. For ASSISTON-ARM, the gimbal lock takes place when the axis of rotation of the shoulder abduction/adduction joint (the first revolute joint) becomes parallel to the axis of

rotation of the internal/external joint (the revolute joint between Body U and Body L). In particular, these singularities take place at two configurations; when the upper arm Body U is configured at vertically up or down. At these configurations, the orientation Jacobian at the shoulder becomes rank deficient.

While these kinematic singularities are inherent for the underlying kinematics, they can be relocated to more favorable configurations within the workspace of the device, through introduction of oblique connections between the rotating bodies. Appendix I presents details of relocating singularities through properly designed oblique rigid connections.

4.7 Workspace of ASSISTON-ARM

Human arm possesses a wide range of translations and rotations. RoM spanned by human shoulder joints, as reported in [85], are presented in Table 4.1, together with RoM of ASSISTON-ARM for the corresponding movements. Apart from some structural limitations due to the self-collisions of links, ASSISTON-ARM can cover the majority of RoM of human shoulder complex. ASSISTON-ARM can cover up to 90° of elbow flexion, while human elbow joint is known to flex up to 146° during ADL [86,87].

Figure 4.4 depicts a point cloud that represents the reachable workspace of ASSISTON-ARM at the shoulder complex. This point cloud is also computed numerically through the forward kinematics of the device with the joint limits.

Table 4.1: Range of motion of the human shoulder and ASSISTON-ARM

Joint Plane	Frontal		Sagittal		Horizontal		Scapular	
	Abduction	Adduction	Flexion	Extension	Abduction	Adduction	Elevation/Depression	Protraction/Retraction
Human	Amplitude	180°	180°	50°	30°	140°	30/50mm	25/25mm
	Range	210°	230°		170°		80 mm	50 mm
ASSISTON-ARM	Amplitude	170°	170°	50°	30°	140°	Elevation/Depression 120/120 mm	Protraction/Retraction 120/120mm
	Range	200°	220°		170°		240 mm	240 mm

It can be observed from Figure 4.4 that ASSISTON-ARM can effectively locate its rotation axes at a relatively large volume around the shoulder complex; hence, can faithfully track and assist the movements of the humerus head even during GH mobilization exercises. Note that, coupled with the self-alignment property of ASSISTON-ARM, the large workspace of shoulder module is useful both for the alignment of human joint axes with the device axes and for accommodating large variations in the arm lengths of patients, significantly shortening the setup time required to attach a patient to the exoskeleton.

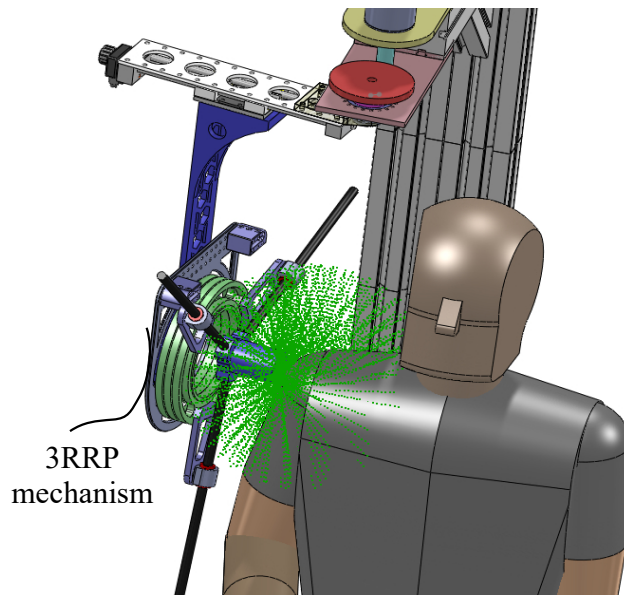


Figure 4.4: Translational reachable workspace of ASSISTON-ARM at the shoulder complex

Figure 4.5 presents the boundary of the reachable workspace of ASSISTON-ARM. This boundary is computed numerically through the forward kinematics of the device, considering all the joint limits. The reachable workspace of the exoskeleton looks approximately like a spherical shell, with an un-

reachable spherical volume around the center of the workspace. Inspecting the resulting reachable workspace, one can verify that ASSISTON-ARM can cover almost the whole RoM of human arm. An unreachable volume around the user is preferable to avoid collisions. The size of the unreachable volume can easily be adjusted by changing the joint limits of the shoulder internal/external rotation and the elbow rotation.



Figure 4.5: Top, side, and front view of the reachable workspace of ASSISTON-ARM at its end-effector

4.8 Passive Gravity Compensation of ASSISTON-ARM

As an impedance-type device, passive backdrivability of ASSISTON-ARM is indispensable to achieve high performance for interaction control. To achieve mechanical transparency, passive compensation of the gravitational forces is essential, in addition to the proper selection of power transmission and actuation. For this purpose ASSISTON-ARM utilizes a spring based passive gravity compensation mechanism.

Static gravity balancing can be obtained either by (i) facilitating a fixed inertia by adding counterweights or (ii) keeping potential energy constant by adding auxiliary spring to the overall mechanism [88,89]. Since the counterweight approach increases the overall inertia of the system, spring based passive gravity mechanisms are more commonly employed. Spring based passive gravity compensation mechanisms are preferred in many designs, as they reduce the burden of gravitational forces on the actuators and do so without introducing additional inertia.

One of the first passive gravity compensation mechanisms has been introduced in [90] with a single spring attached to a single DoF arm. [91] showed that passive balancing of gravitational forces can be performed using several techniques, including adding counterweights, utilizing linkage or cam mechanism, and using spring suspension methods. It has been proven that fewer number of springs can be used in compensation mechanisms, if zero-length springs are employed [92]. Along these lines, studies [88,89,92–95] present gravity compensation mechanisms with zero-length springs.

Passive gravity compensation mechanisms have also been utilized for physical rehabilitation, by assisting patients through elimination of arm weight [46,92,96–98].

ASSISTON-ARM is a 7 DoF mechanism whose center of mass moves spatially. Full compensation of gravity for ASSISTON-ARM necessitates a complex design, since passive gravity balancing of an n DoF manipulator can be obtained by using at least n zero-length springs [99], or using $2(n - 1)$ conventional springs and $4(n - 1)$ links [100]. Luckily, the effect of shoulder internal/external rotation and elbow rotation are relatively small on the movement of the center of gravity of ASSISTON-ARM. Along these lines, the gravity compensation mechanism of ASSISTON-ARM is designed to work in a plane that is parallel to the working plane of 3RRP mechanism. This way, the gravitational forces on the self-aligning mechanism can be compensated passively with a spring based compensator, while the gravitational forces due to the internal/external and the elbow rotations are compensated actively through the actuators. For safety, these joint may also be equipped with brakes that engage when the device power is cut off.

In order to obtain constant potential energy, the design of compensator mechanism and the selection of springs should be decided simultaneously. Furthermore, the compensation mechanism must cover the workspace of the movement of the gravity center of ASSISTON-ARM, and collisions between the exoskeleton and gravity compensation mechanism should be avoided within the workspace.

Several kinematic designs considered for the gravity compensation are presented in Figure 4.6 [101]. Among the candidates of zero-length spring based gravity compensation mechanisms, the gravity compensator in Figure 4.6(a) [91] is not suited for ASSISTON-ARM, since this mechanism needs to go through a singular configuration to track the movement of the gravity center of ASSISTON-ARM. The gravity compensator in Figure 4.6(b) [89] also

suffers from a limited workspace that is inappropriate for ASSISTON-ARM. If workspace of these mechanisms are extended by increasing their link lengths, then the gravity compensation mechanisms collide with the other structural elements of the exoskeleton. Hence, the gravity compensator presented in Figure 4.6(c) [100] is selected. This compensator can cover the workspace of the center of mass of ASSISTON-ARM, while keeping the potential energy of the system constant.

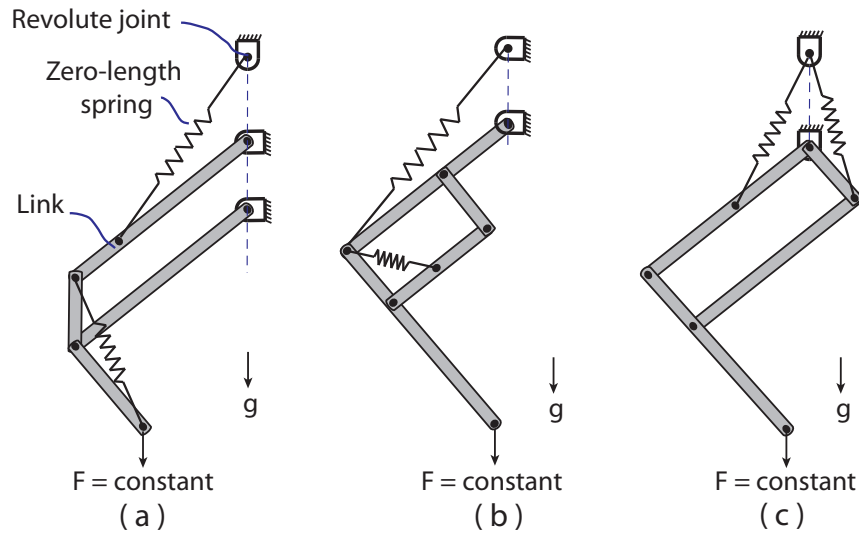


Figure 4.6: Kinematics of several spring based gravity compensation mechanisms as presented in (a) [91], (b) [89], and c) [100]

A schematic representation of the gravity compensation mechanism used in ASSISTON-ARM is depicted in Figure 4.7. In Figure 4.7, A , O , P , R , S , Q and Z denote the revolute joints of the system. Springs are attached between Points A – Q and Points A – P . Points O and A are fixed on ground link of the gravity compensator. Symbol h defines the distance between Points O and A . Points O , P , R and S define an auxiliary parallelogram and the moving arm of ASSISTON-ARM is attached to this mechanism at Point Z , where the

are approximated as point masses located at their corresponding center of masses; m_i ($i=1,\dots,4$) represent mass of links, while m_e represents total mass of the exoskeleton arm.

Let the zero-length spring deflections and spring constants be represented by x_i and k_i , respectively. Symbol β denotes the angle between Link OR and the horizontal axis in the counterclockwise direction, while θ denotes the angle between Link OP and the vertical axis in the counterclockwise direction. Due to kinematics of the parallelogram mechanism, Links OR and PS are always parallel to each other. Similarly, Link OP is also always parallel to Link RZ .

Passive gravity balancing is possible when a constant potential energy of overall system is achieved. Omitting the negligible mass of the springs, the potential energy resulting from the gravitational forces on mechanisms can be computed as

$$\begin{aligned}
 V_g = & -m_1gc_1 \cos \theta - m_2g(l_1 \cos \theta + c_2 \sin \beta) \\
 & -m_3gc_3 \sin \beta - m_4g(l_1 \sin \beta + c_4 \cos \theta) \\
 & -m_eg(l_1 \sin \beta + l_4 \cos \theta)
 \end{aligned} \tag{20}$$

where g represents the gravitational acceleration. Similarly, the potential energy stored in the zero-length springs can be formulated as:

$$V_s = \frac{1}{2}k_1x_1^2 + \frac{1}{2}k_2x_2^2 \tag{21}$$

where

$$x_1^2 = (b_1 \sin \theta)^2 + (b_1 \cos \theta + h)^2$$

$$x_2^2 = (b_3 \cos \beta)^2 + (b_3 \sin \beta + h)^2$$

Then, the total potential energy in the system becomes

$$\begin{aligned}
V_t = V_g + V_s = & -m_1 g c_1 \cos \theta \\
& -m_2 g (l_1 \cos \theta + c_2 \sin \beta) - m_3 g c_3 \sin \beta \\
& -m_4 g (l_1 \sin \beta + c_4 \cos \theta) - m_e g (l_1 \sin \beta \\
& + l_4 \cos \theta) + \frac{1}{2} k_1 (h^2 + b_1^2 + 2b_1 h \cos \theta) \\
& + \frac{1}{2} k_2 (h^2 + b_3^2 + 2b_3 h \sin \beta)
\end{aligned} \tag{22}$$

For static balancing, the following condition needs to hold

$$\frac{\partial V_t}{\partial \zeta} = 0 \tag{23}$$

where $\zeta = [\beta; \theta]$ represents the joint variables of the gravity compensator.

Spring constants for constant potential energy can be determined via calculating the partial derivatives of potential energy with respect to joint variables and setting them to zero as

$$k_1 = \frac{m_1 g c_1 + m_2 g l_1 + m_4 g c_4 + m_e g l_4}{b_1 h} \tag{24}$$

$$k_2 = \frac{m_2 g c_2 + m_3 g c_3 + m_4 g l_2 + m_e g l_2}{b_3 h} \tag{25}$$

Note that these spring constants are independent from the location of the gravity center and the joint angles.

Chapter V

5 Implementation of ASSISTON-ARM

In this chapter, implementation details of the ASSISTON-ARM are provided.

5.1 Actuation and Power Transmission

Safety is an imperative criteria for physical human-robot interaction. In order to make human-robot interaction safe, both mechanical design and control method used for interaction should ensure safety. Due to fact that control strategies and performance of robots are closely correlated with the mechanical properties of a robot; mechanical design, actuation and transmission play important roles for achieving a safe human-robot interaction.

Safe robot design can be achieved via several different methods. As intrinsic safety precautions, low weight and inertia of an exoskeleton should be taken into account as a mechanical design criterion to ensure safety [102].

Coupled stability of the controller also plays an important role for a safe physical human-robot interaction. Robots that rely on closed loop force control suffer from fundamental control limitations and are guaranteed to become unstable for large enough controller gains [65,103]. On the other hand, open-loop force control does not utilize force/torque sensors. As a consequence, this approach does not suffer from fundamental limitations of force feedback approaches [104]. Because of this, open loop force and impedance

control methods can easily be designed to ensure coupled stability of interaction through frequency domain passivity approaches. However, in order to achieve good performance through open-loop force and impedance control methods, the device should be designed as mechanically transparent as possible to mitigate effects of parasitic device dynamics.

Mechanical transparency can be achieved by designing the system passively back-driveable, and decreasing weight and inertia of the system as much as possible. Passive back-driveability is a measure of resistance displayed by the device against motion when power is off. In an ideal back-driveable device, users need to apply almost no force to move the device. Consequently, in an ideal passively back-driveable system, friction, damping, gravitational forces need to be kept negligibly small.

One approach to obtain a passively back-driveable design is to utilize precise direct-drive motors to actuate individual joints. However, this option is generally not feasible when large forces are necessary as the actuation size became too large for practical use. Therefore, in order to deliver enough torques to counteract against human torques during physical rehabilitation, some kind of transmission is commonly required for the actuation.

Gear transmissions, such as planetary gears, are widely used in robotic devices in order to amplify torques at output side. However, gear transmissions are susceptible to power losses and it is hard to model friction forces and suffer from precision due to backlash. Depending on the configuration of stages and reduction ratio, gearboxes cannot just hinder but also can completely prevent passive back-driveability.

Another gear transmission that is commonly utilized in robotic devices is the harmonic drive. Harmonic drive employs a compliant inner gear part

that rolls on a rigid outer ring. Harmonic drives have very low internal backlash; hence, they can be used for applications that require high position accuracy. Furthermore, high transmission ratios enabled by harmonic drives enable high torque output capabilities with compact designs. On the other hand, harmonic drives suffer from high friction losses and do not provide passive back-driveability.

Timing belt transmission requires larger space to operate compared to gearbox transmissions. Furthermore, in order to obtain precise operation, proper tensioning of the belt must be ensured. Besides, timing belt transmissions suffer from friction losses and require regular maintenance for safe, long term operation. Along these lines gearboxes, harmonic drives and timing belt transmissions are not preferred for actuation of impedance-type robots, such as ASSISTON-ARM.

In order to achieve a passively back-driveable actuation that can deliver necessary torques for rehabilitation, capstan transmission is preferred for ASSISTON-ARM. Capstan is a cable based transmission method that utilizes high tensile strength low stretch steel cables in order to transmit torque from smaller pinions to larger disks, as depicted in Figure 5.1. The diameter ratio between the actuated pinion and the driven disk defines the transmission ratio of the capstan transmission. Assuming cable stretch is negligible, capstan transmission does not suffer from friction losses, due to pure rolling motion of cable during rotation around pinion and disk. Furthermore, thanks to the continuous cable connection between the pinion and the disk, the capstan transmission does not suffer from backlash.

While implementing a capstan transmission, there are important aspects to be considered, as listed below.

- Cables used for the transmission need to be properly tensioned to deliver forces between the actuated and the driven parts. For this purpose, a tensioning mechanism for the cables should be implemented.
- Cable for the transmission should be selected with a safety factor of at least 10 for dynamic movements, considering the maximum force delivered by the actuation.
- Capstan transmission does not assume unlimited workspace as other transmission methods, such as gears or belt transmissions. Dimensions of disk and pinion need to be designed by considering the workspace of the joint.
- Pinion of the capstan transmission should have large enough diameter to satisfy the minimum turning radius of cables. Improper selection of diameter leads to the loss of cable strength and life.
- The space between the pinion shaft and the disk should be larger than the diameter of the cable and smaller than 2.5 times the diameter of the cable.
- For long life cycle, pinion shaft should be threaded with a pitch that is larger than or equal to the cable diameter, such that the cables travel inside these threads during operation, rather than interacting with each other.
- For long life cycle, two cables are recommended for delivering force to different rotation directions rather than using one cable for the whole operation. In this case, the ends of both cables need to be grounded to the capstan pinion and the disk.

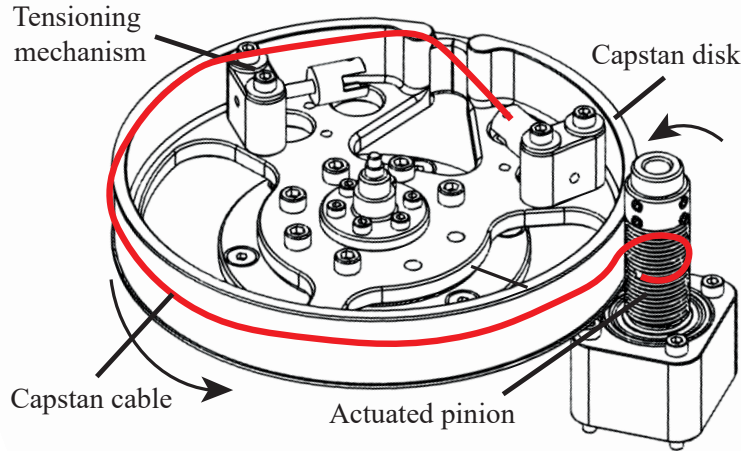


Figure 5.1: Representation of capstan transmission method

All active DoF of ASSISTON-ARM possess a passively back-driveable design, as their actuation and power transmission are implemented via capstan driven direct drive DC motors. In particular, the first revolute joint is responsible for shoulder horizontal abduction/adduction movement possesses a 1:24 capstan transmission, and is powered by a 48 V 250 W brushed DC motor.

3RRP mechanism of ASSISTON-ARM is designed to feature a circular workspace, covering up to 300° rotational and 240 mm translational movements in plane. 3RRP mechanism features dual layer capstan transmission as shown in Figure 5.2. In particular, the first level capstan of transmission provides a 1:5 reduction ratio, while the second layer provides a 1:5.5 reduction ratio. As a result, the dual layer design provides an overall 1:27.5 ratio. To actuate the 3RRP mechanism, three 48 V 200 W brushed DC motors are employed. 3RRP mechanism provides a large torque output without sacrificing passive backdrivability, not only due to the low friction capstan transmission, but also due to the fact that this parallel mechanism acts as a

physical torque summer, superposing the output torque of all three motors at its end-effector. Furthermore, thanks to the parallel kinematics of 3RRP mechanism, the motors are directly attached to the L-shaped link; hence, gravity compensation is not required to counteract their weight.

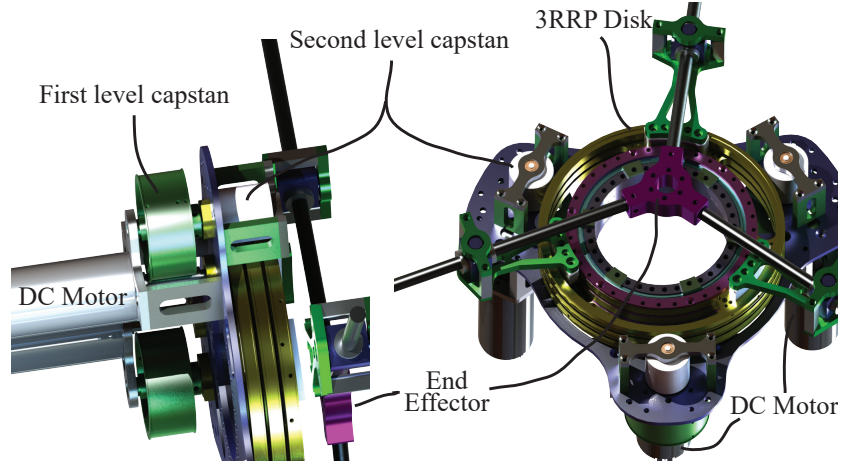


Figure 5.2: Solid model of 3RRP mechanism with dual layered capstan transmission

In order to minimize the mass of actuators and reflected inertia during power transmission while sustaining a high torque output, a single layer capstan transmission is driven by two direct drive motors at the shoulder internal/external joint. In particular, this joint has a 1:25 transmission ratio and is powered with two 48 V 150 W brushed DC motors, as depicted in Figure 5.3.

The elbow rotation features a dual layered capstan transmission with a total of 1:29.5 transmission ratio, powered by a 48 V 260 W brushless DC motor.

Figure 5.4 presents a solid model of ASSISTON-ARM, while the actuation and power transmission details of a prototype are depicted in Figure 5.5.

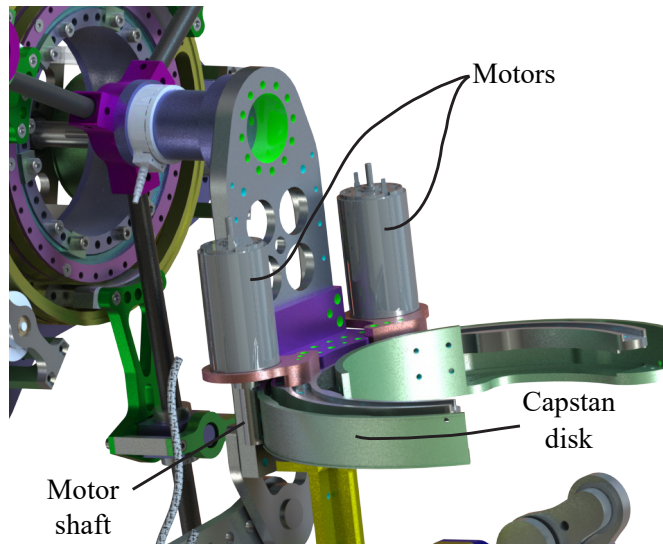


Figure 5.3: Solid model of internal/external joint with a capstan transmission driven by two motors

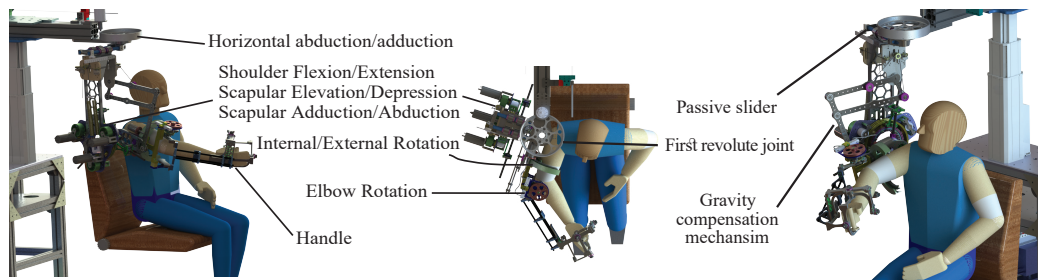


Figure 5.4: Solid model of ASSISTON-ARM

5.2 Power Electronics and Instrumentation

Power electronics of ASSISTON-ARM consists of a 2.5 kW medical grade isolation transformer, multiple medical grade switching power supplies and six 250 W DC motor drivers. The medical grade power supplies are connected in parallel for redundancy. Furthermore, parallel connection allows only the master unit to operate if the total output load is less than a certain threshold, while other power supplies are kept in the standby mode.

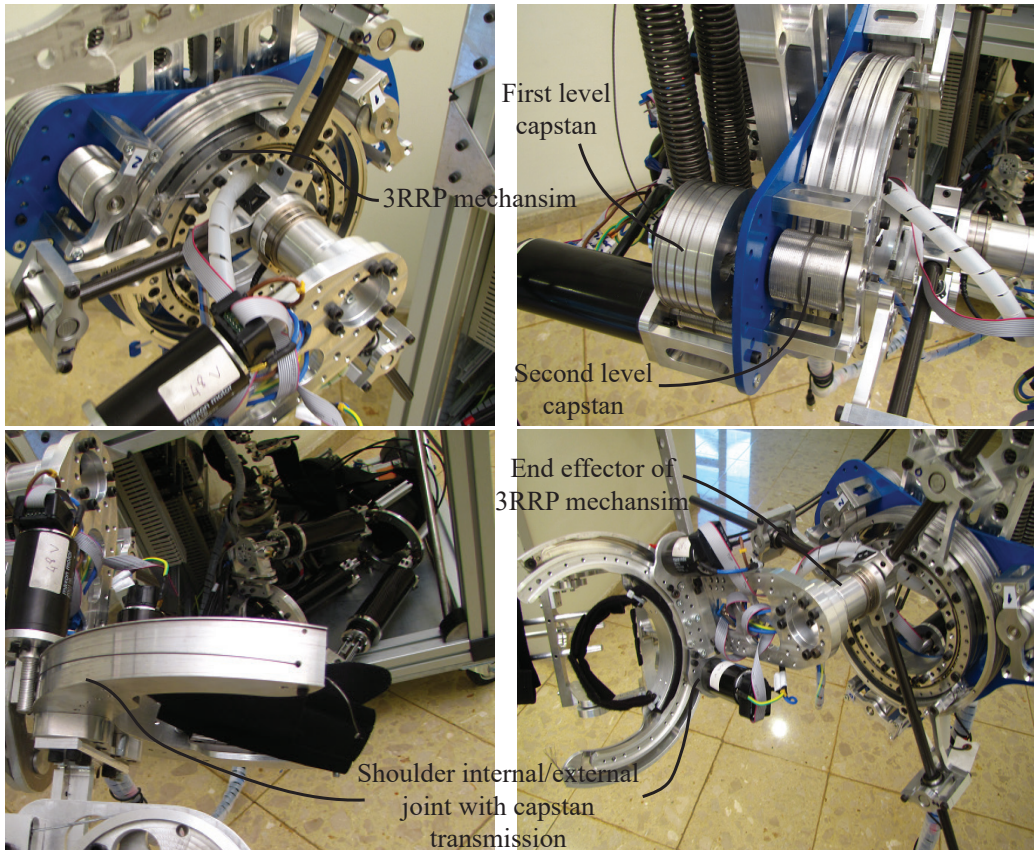


Figure 5.5: Transmission details of ASSISTON-ARM

Each motor is equipped with an optical encoder. In addition to the encoders attached to the driving shaft of the motors, absolute encoders are attached to the driven link at each DoF. These redundant measurements are useful, as they can be used for initialization of the system, as well as for detection of several failure modes. A locking type electromagnetic brake is employed at internal/external joint.

ASSISTON-ARM is equipped with an industrial PC for its real-time control, while an EtherCAT bus is used to ensure real-time communication at 1 kHz sampling rate. Controllers are implemented through rapid prototyping

on a host PC utilizing Matlab/Simulink, while control and data processing take place on a target industrial PC running a real-time operating system (xPC target kernel of Matlab).

5.3 Passive Gravity Compensation

The link lengths of the passive gravity compensation mechanism of ASSISTON-ARM are designed to ensure that the end-effector of this mechanism can track the gravity center of the moving arm of the exoskeleton without any collisions. The spring constants and the strokes of the zero-length springs determine the connection points of springs to the passive gravity compensation mechanism. Due to size limitations, the springs are not attached to links directly, but the spring forces are transmitted via routed cables. The spring settlements and the cable routing of the gravity compensator are depicted in Figure 5.6.

In Figure 5.7, a stand-alone solid model of the gravity compensation mechanism is presented together with its link lengths. The spring forces transmitted through cables are also depicted in this figure. Links are manufactured as custom aluminum parts and joints are supported with ball bearings. The end-effector part of compensator is connected to the upper arm part of the exoskeleton at the calculated center of gravity of the arm module of the exoskeleton.

The center of mass of the arm module of ASSISTON-ARM is located in such a way that, when there is a movement at shoulder module, it translates along a C shaped workspace, as depicted with the red circles in Figure 5.8. The black stars in Figure 5.8 represent the workspace of the passive gravity compensation mechanism. The passive gravity compensation mechanism can track the center of mass of the exoskeleton at almost all configurations.

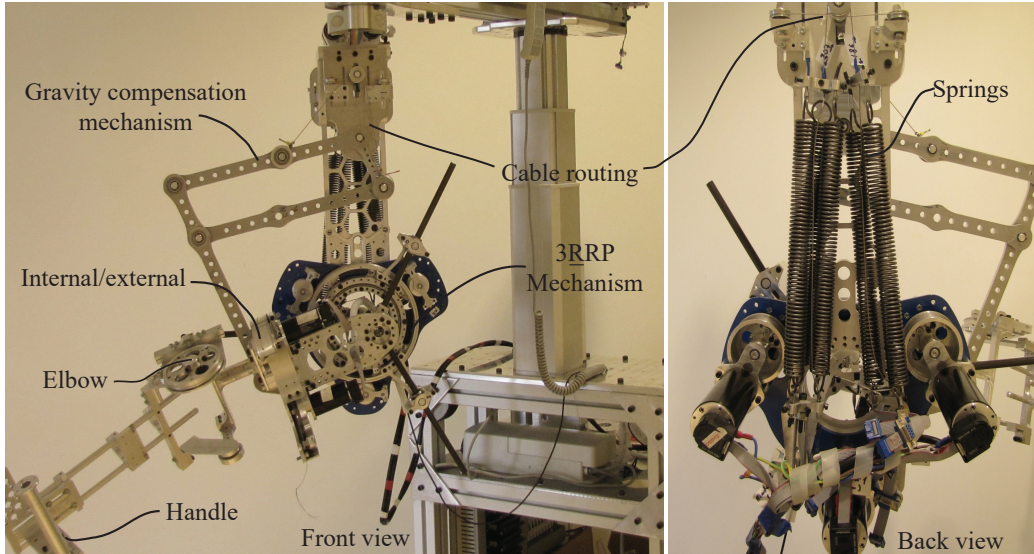


Figure 5.6: ASSISTON-ARM prototype detailing the overall structure and the springs of the passive gravity compensation mechanism located at the back side of shoulder module

Configurations that the gravity compensator cannot reach are already infeasible configurations for the exoskeleton, due to inherent self-collisions of the device.

Considering the weights of the links of the gravity compensator, the moving arm of ASSISTON-ARM, and 3.2 kg of the average human arm weight [105, 106], the spring constants of the gravity compensation mechanism are determined as $k_1 = 3.1$ N/mm and $k_2 = 2.1$ N/mm, respectively.

The motion of the 3RRP mechanism and the rotational motion of shoulder internal/external joint do not change the position of the gravity center with respect to the end-effector of the passive gravity compensation mechanism. However, the rotation of elbow joint or a combined rotation with the shoulder internal/external joint changes the location of the gravity center and affects the performance of the mechanism.

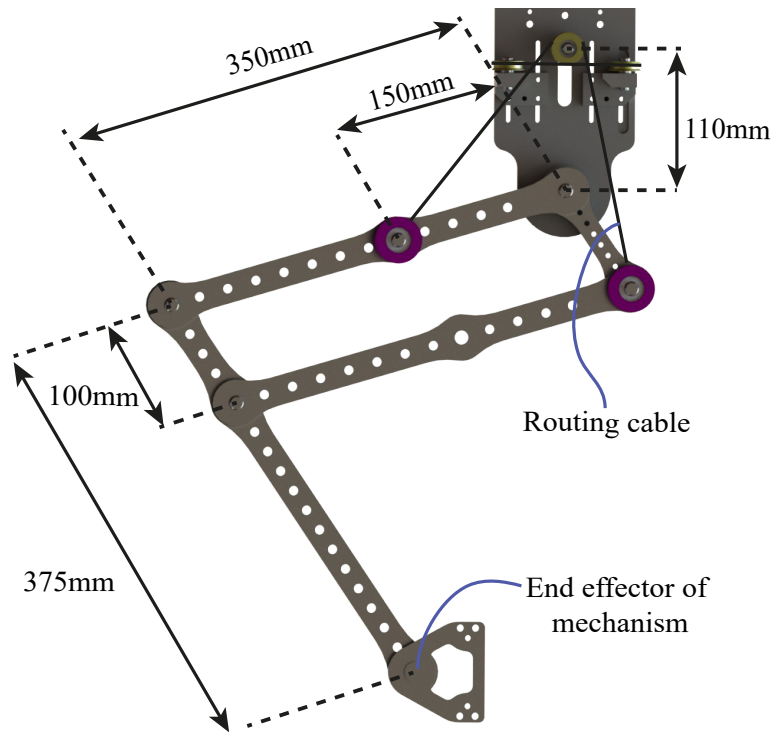


Figure 5.7: Solid model of parallelogram based gravity compensation mechanism

In Figure 5.9, passive gravity compensation performance of ASSISTON-ARM is plotted with respect to elbow flexion angles. In particular, for this analysis, the potential energy stored at the gravity compensation mechanism has been calculated and compared with the gravitational potential energy of the system for various elbow joint configurations. For the majority of ADL that utilize the elbow joint [107, 108], gravity compensation mechanism can passively compensate for more than 70% gravitational forces, including the weight of the patient’s arm and the system. The remaining forces can be compensated actively utilizing the gravity model of the system.

Figure 5.10 presents a prototype of ASSISTON-ARM attached to a healthy volunteer.

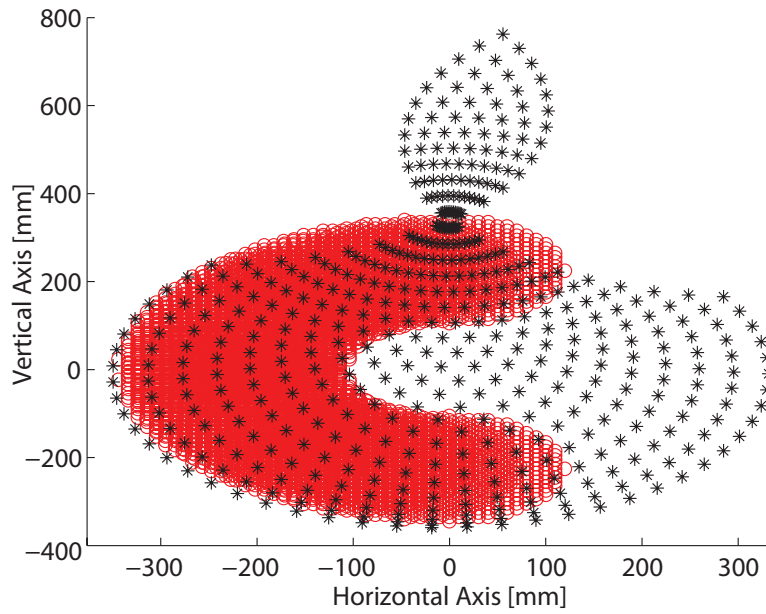


Figure 5.8: Workspace of parallelogram based the gravity compensation mechanism and center of mass of ASSISTON-ARM

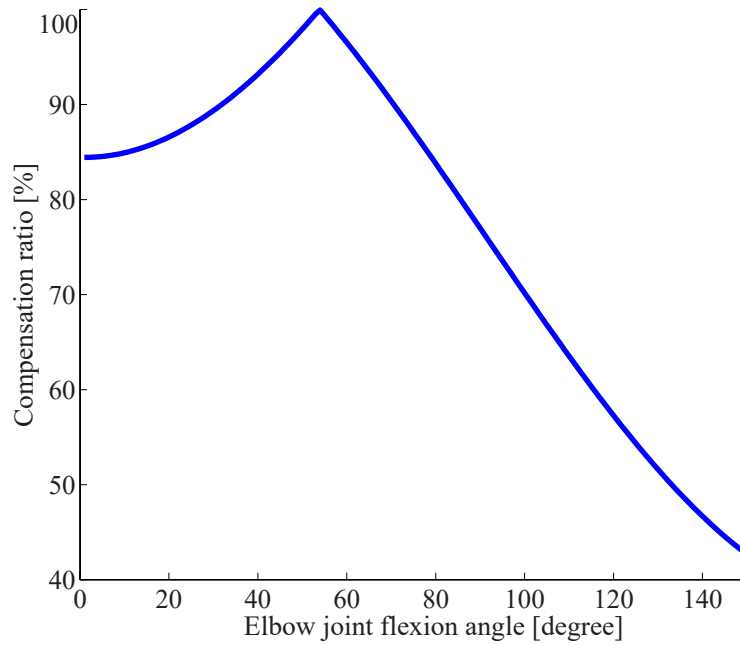


Figure 5.9: Performance characteristics of parallelogram based gravity compensation mechanism with respect to elbow joint motions

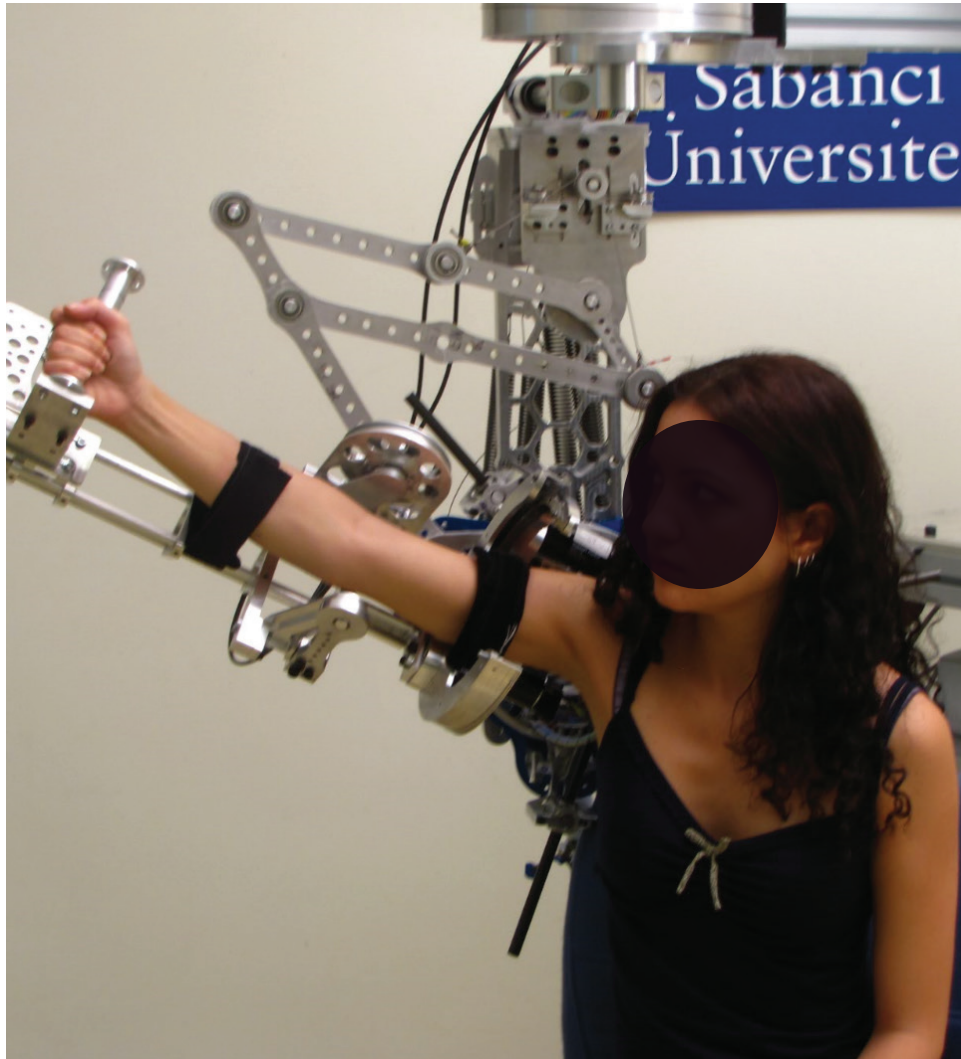


Figure 5.10: A prototype of ASSISTON-ARM

Chapter VI

6 Characterization of ASSISTON-ARM

In this chapter, we evaluate the performance of ASSISTON-ARM through numerical computations and experimental evaluations.

6.1 Manipulability of 3RRP Mechanism

Manipulability measure is a commonly used metric to study performance of manipulators. While a very low value of the manipulability measure indicates presence of a singularity, high manipulability indicates a high kinematic performance of a manipulator. Furthermore, manipulability measure can be used to evaluate isotropy of a mechanism, characterizing the homogenous behaviour of a manipulator over its workspace. In this section we analyze manipulability of the self-aligning 3RRP mechanism, in order to evaluate the isotropy of the mechanism within its workspace, and to study its distance to singularities.

Manipulability measure, calculated using the kinematic Jacobian, is dimensionless. On the other hand, kinematic Jacobian of manipulators that contain different type of joints (prismatic, rotational) and multiple DoF may contain mixed physical units. Along these lines, the kinematic Jacobian needs to be normalized to obtain comparable physical units, before the manipulability measure can be computed. We have adapted a normalization technique

proposed in [109], where the normalized Jacobian matrix is derived as

$$\hat{J} = S_J J_k^T S_T \quad (26)$$

where J_k is the kinematic Jacobian of the manipulator, S_J is the maximum torque/force capabilities of actuators and S_T denotes the maximum desired torques/forces of manipulator at its end-effector.

After the normalized Jacobian matrix is obtained, the manipulability measure u of system is derived through the equation

$$u = \sqrt{\hat{J} \hat{J}^T}. \quad (27)$$

Manipulability of the 3RRP mechanism is plotted in Figure 6.1 as a contour plot, when the end-effector rotation is kept at $\theta = 0^\circ$. The manipulability values are normalized by dividing them with the largest manipulability within the whole translational workspace.

Figure 6.1 shows that the manipulability measure is bounded away from singularities and its variation stays within 25% of its maximum value, indicating a highly uniform behaviour of 3RRP mechanism within its workspace.

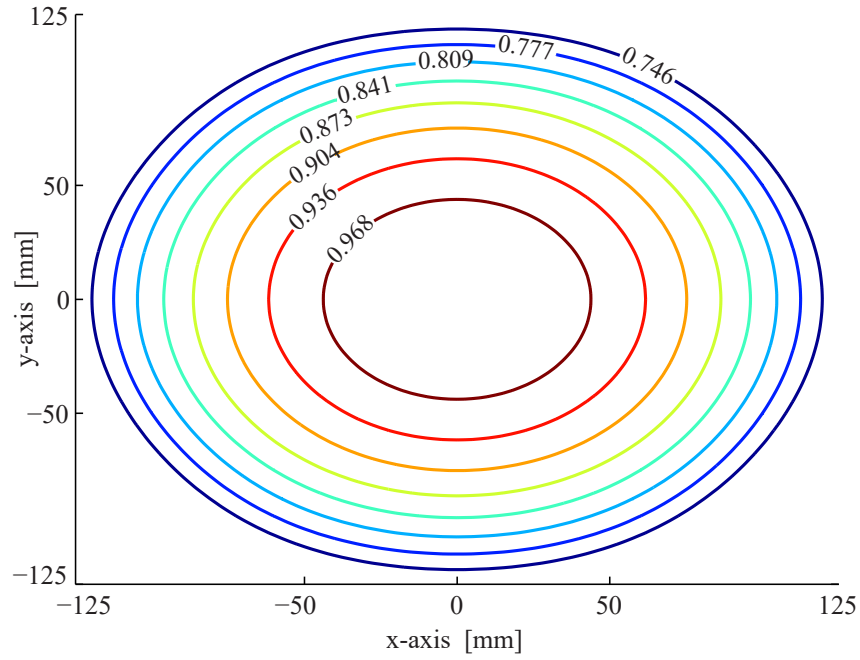


Figure 6.1: Normalized manipulability of 3RRP mechanism at $\theta = 0^\circ$

Figure 6.2 presents the manipulability of the mechanisms when the end-effector is rotated from $\theta = 0^\circ$ to $\theta = 120^\circ$ with 30° intervals. Note that rotations above $\theta = 120^\circ$ need not be plotted due to the symmetric construction of the mechanism. According to Figure 6.2, 3RRP mechanism preserves its isotropic nature even under rotations of its end-effector.

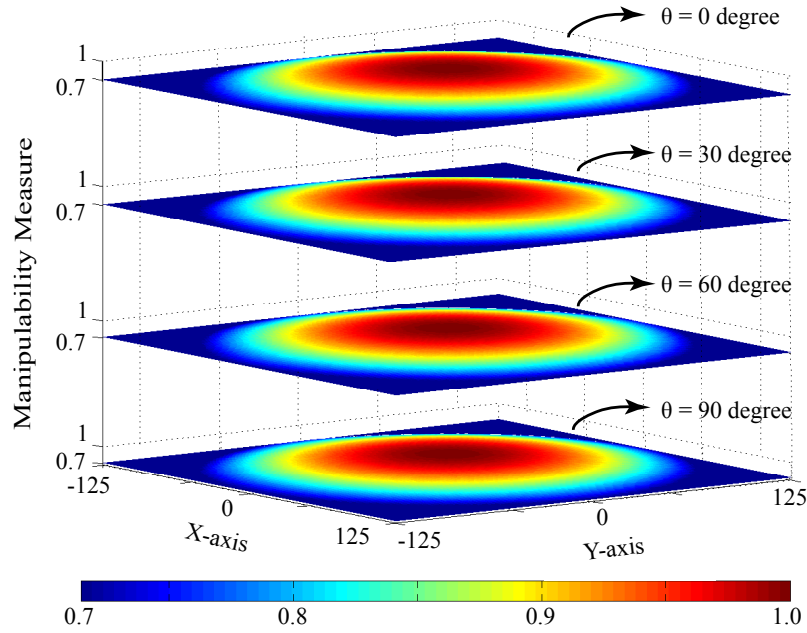


Figure 6.2: Manipulability of 3RRP mechanism for at various orientations of its end-effector

6.2 Performance Characterization of ASSISTON-ARM

Transmission ratios and actuators of ASSISTON-ARM are determined by considering the human force/torque limits. The first revolute joint responsible for shoulder horizontal abduction/adduction movement can deliver 12 Nm continuous torque through a $1 : 24$ transmission ratio. The 3RRP mechanism can deliver up to 135 N force and 36.5 Nm torque continuously along its translational and rotational DoF, respectively, thanks to its dual layered capstan transmission with an effective transmission ratio of $1 : 27.5$. Internal/external rotation of shoulder joint of the exoskeleton has a $1 : 25$ capstan ratio and is actuated by two motors to exert 9.5 Nm continuous

torque. Elbow module can deliver 30 Nm continuous torque, with its 1 : 29.5 transmission ratio. Peak torques at each joint are limited by the continuous current that can be supplied by the drivers. Peak torques can be delivered for periods exceeding 60 s without any active cooling requirements for the motors. Table 6.1 provides a summary of force/torque output capabilities of ASSISTON-ARM, together with its actuation details.

Table 6.2 presents the experimentally verified actuation characterization of the standalone $\underline{3RRP}$ mechanism, together with its encoder resolution. The table also includes experimentally characterized passive backdrivability of the $\underline{3RRP}$ mechanism, reporting the minimum force/torque levels to be exerted to the system in order to move it when all actuators are off. Passive backdrivability characterization of this mechanism indicates that the end-effector of $\underline{3RRP}$ mechanism can be moved with less than 4.5 N along the translational directions, while less than 0.95 Nm torque is required for its rotation, when the mechanism is not attached to ASSISTON-ARM.

Table 6.1: Actuation characteristics of ASSISTON-ARM

	Exoskeleton Continuous	Exoskeleton Peak	Actuator Type	Transmission Type and Transmission Ratio
Horizontal Abduction/Adduction Rotation	12 Nm	45 Nm	250 W Brushed DC	Capstan 1:24
Shoulder Flexion/Extension Rotation	36.5 Nm	120 Nm	3RRP	Dual-layer capstan
Scapular Elevation/Depression	135 N	440 N	3 units of	1:27.5
Scapular Adduction/Abduction	135 N	440 N	200 W Brushed DC	
Shoulder Internal/External Rotation	9.5 Nm	45 Nm	150 W Brushed DC 2 units	Capstan 1:25
Elbow Rotation	30 Nm	100 Nm	260 W Brushless DC	Dual-layer capstan 1:29.5

Table 6.2: Experimental characterization results for the prototype of 3RRP mechanism

Criteria	z_s	y_s	θ
Instantaneous Peak Force/Torque	440 N	440 N	120 Nm
Maximum Continuous Force/Torque	135 N	135 N	36.5 Nm
End-effector Resolution	0.021 mm	0.038 mm	0.0001 rad
Back-driveability	4.3 N	3.4 N	0.92 Nm

Table 6.3 presents the experimental characterization of the passive back-drivability of ASSISTON-ARM. This experimental characterization is performed when all modules of the exoskeleton, including the 3RRP mechanism, shoulder internal/external rotation, elbow rotation and passive gravity compensation mechanism are attached to the exoskeleton. Passive backdrivability experiments indicate that the first revolute joint can be moved with about 1.6 Nm torque. The end-effector of 3RRP mechanism can be moved with 10 N force along the translational directions, while a torque of about 2.6 Nm is required for shoulder flexion/extension rotation. Moreover, the shoulder internal/external joint can be moved with 1.4 Nm, while backdriving the elbow joint requires about 1.6 Nm torque.

Table 6.3: Experimental back-driveability characterization results of realized assembly

Criteria	Back-driveability
Horizontal abduction/adduction	1.56 Nm
Horizontal DoF of 3RRP	10.67 N
Vertical DoF of 3RRP	10.02 N
Rotational DoF of 3RRP	2.56 Nm
Shoulder internal/external joint	1.33 Nm
Elbow joint	1.58 Nm

ASSISTON-ARM is attached to its users via three interaction points located at the upper arm, the lower arm, and its handle. It is intuitive to map the backdrivability levels listed in Table 6.3 to forces that need to be applied at the handle of the exoskeleton. Along these lines, 2.6 N is required to be applied at the handle for initiating passive movements of the

shoulder horizontal abduction/adduction, 4.2 N is required for the shoulder flexion/extension, and 2.6 N is required for the elbow rotation. These values verify that a high level of passive backdrivability has been achieved with the implementation of ASSISTON-ARM as an impedance type device.

The workspace of ASSISTON-ARM has also been experimentally verified. Videos demonstrating the workspace, passive backdrivability, and self-alignment of the device are also available at https://www.dropbox.com/s/t23b8e0mvrspawb/tech_ASSISTON_ARM.wmv?dl=0.

Chapter VII

7 Interaction Control And Operation Modes of ASSISTON-ARM

Control methods used to implement rehabilitation exercises with ASSISTON-ARM can be loosely categorized into two: interaction control and path tracking control. To ensure safety of interactions, impedance characteristics of the robot at the interaction port needs to be controlled precisely [68]. For interaction control, the impedance control approach is utilized. For some operation modes under interaction control, velocity and force control approaches are also employed. Path control methods are essential to induce desired movements while ensuring coordination and synchronization among various degrees of freedom. Path control decouples the speed of movement from the coordination aspects of the exercise, enabling task speed to be independently controlled to match requirements of the patient. Path control can be used to impose exercises at the preferred pace of the patient, to break undesired synergy patterns and to assists patients as needed.

7.1 Interaction Control of ASSISTON-ARM

Safe and natural physical human-robot interactions form the basis of successful applications in rehabilitation robotics. Along these lines, many robot

designs and impedance control schemes [110] have been proposed.

Most of the exoskeletons rely on closed-loop force control to compensate for parasitic forces originating from their mechanical design. Unfortunately, the performance of all causal force feedback controllers suffer from a fundamental limitation imposed by the inherent non-collocation of sensors and actuators. In particular, the inevitable compliance between the actuators and the force sensor results in a fundamental performance limitation for interaction controllers, by introducing an upper bound on the loop gain of the closed-loop force-controlled system. Above this limit, the closed-loop system becomes unstable [65, 103]. Hence, proper adjustment the controller gains becomes a safety critical task with force feedback.

Guaranteeing safety of interactions when the exoskeleton is coupled to a human user is an imperative design requirement that dominates the whole mechatronic system design process. The safety of interaction requires study of the coupled stability of the controlled exoskeleton together with the human operator. The presence of a human operator in the loop significantly complicates the stability analysis, since a comprehensive model for human dynamics is, in general, not available. Contact interactions with the environment pose similar challenges.

The coupled stability analysis of physical human-robot-interaction systems in the absence of human and environment models is commonly conducted using the frequency domain passivity framework [104, 111, 112]. In this approach, it is assumed that the human operator does not intentionally try to destabilize the system, that is, the intentional part of human inputs is state independent. Under this assumption, the human can be treated as a passive network element in the closed-loop analysis, and coupled stability can

be concluded through frequency domain passivity arguments [104]. A passivity based design approach is advantageous as it provides robust stability for a large range of realistic human and environment models.

ASSISTON-ARM has been designed as a mechanically transparent impedance type robot such that robust and high-fidelity interaction control can be achieved in an open-loop fashion. In particular, the motor torques/impedances of ASSISTON-ARM are directly mapped to the end-effector forces/impedance at high control bandwidths. Avoiding the use of force sensors, ASSISTON-ARM does not suffer from the fundamental the limitation of force-feedback controllers imposed by the non-collocation. More importantly, ensuring coupled stability of interactions through the frequency domain passivity framework is trivial for open-loop controllers [104].

Due to its open-loop control architecture, the control performance of ASSISTON-ARM relies on the transparency of its mechanical design. In particular, high stiffness, low inertia, and highly passively back-driveable design minimizes parasitic forces, ensuring high interaction control performance of ASSISTON-ARM.

Figure 7.2 presents the open-loop impedance control scheme used to control ASSISTON-ARM. In Figure 7.2, q and \dot{q} represent the joint positions and velocities, \dot{x} indicate the task space velocities of ASSISTON-ARM. Mapping from the joint space to the task space is realized with the kinematic Jacobian J_k . The desired impedance is set to Z_d during open loop impedance control. F_d represents the reference force/torque trajectories at the task space of the robot. Symbols τ_d , τ_{ff} , τ_g and τ represent the desired, the active feed-forward gravity compensation, the passive gravity compensation and the motor torques at the joint space, respectively. M denotes the inertia

matrix, C is the Coriolis matrix and G indicates the gravity matrix of the exoskeleton. P signifies the gravity matrix that models the passive gravity compensation mechanism. The symbol $(\hat{\cdot})$ denotes estimates of the actual system parameters. Thick lines represent physical forces.

Figure 7.1 presents sample experimental results collected during the joint space impedance control of the first joint of ASSISTON-ARM, which is responsible for shoulder horizontal abduction/adduction movement. A sinusoidal reference trajectory with a 50° amplitude and 0.4 Hz frequency is imposed to joint. The controller stiffness of the joint space impedance controller is set to 600 Nm/rad. RMS error for this trajectory tracking experiment is calculated as 1.05%.

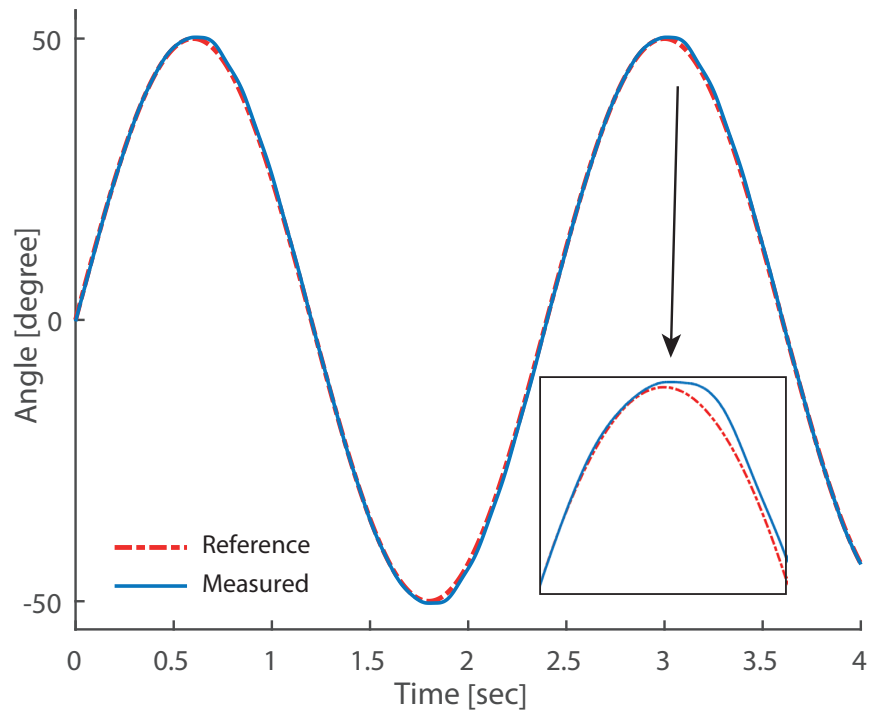


Figure 7.1: Reference and experimentally measured trajectories during the joint space impedance control of the first revolute joint

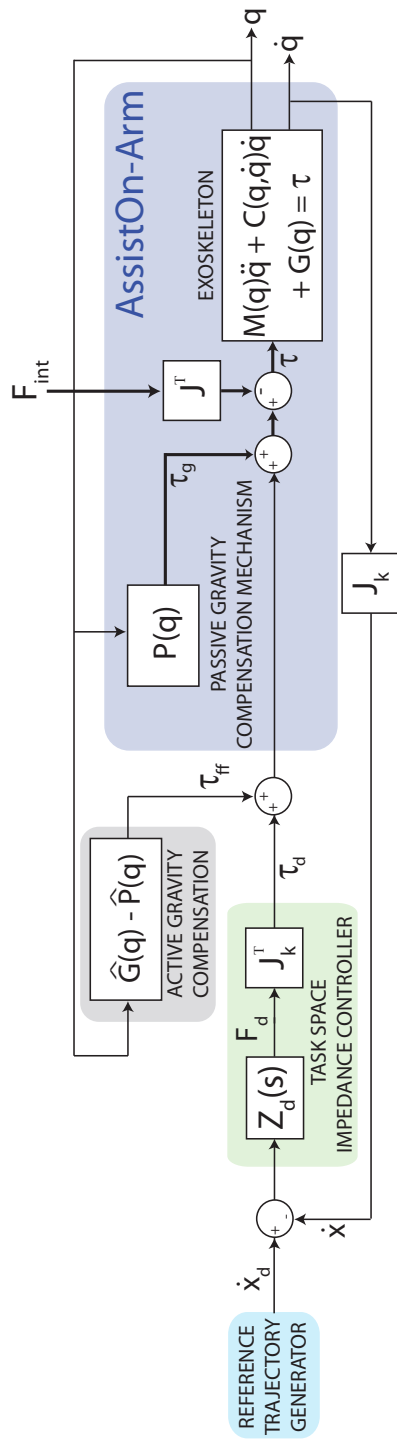


Figure 7.2: Open loop impedance control block diagram

Figure 7.3 depicts sample experimental results collected during the task space impedance control of the $3\underline{R}R\underline{P}$ mechanism of ASSISTON-ARM. During this experiment, the translational DoF of $3\underline{R}R\underline{P}$ are set to stay constant at the center of their workspace, while the rotational DoF of $3\underline{R}R\underline{P}$ is desired to follow a sinusoidal reference trajectory with 57.3° (1 rad) amplitude and 0.6 Hz frequency. The controller stiffness of the joint space impedance controller is set to 200 Nm/rad. RMS error for this trajectory tracking experiment is calculated as 1.03% .

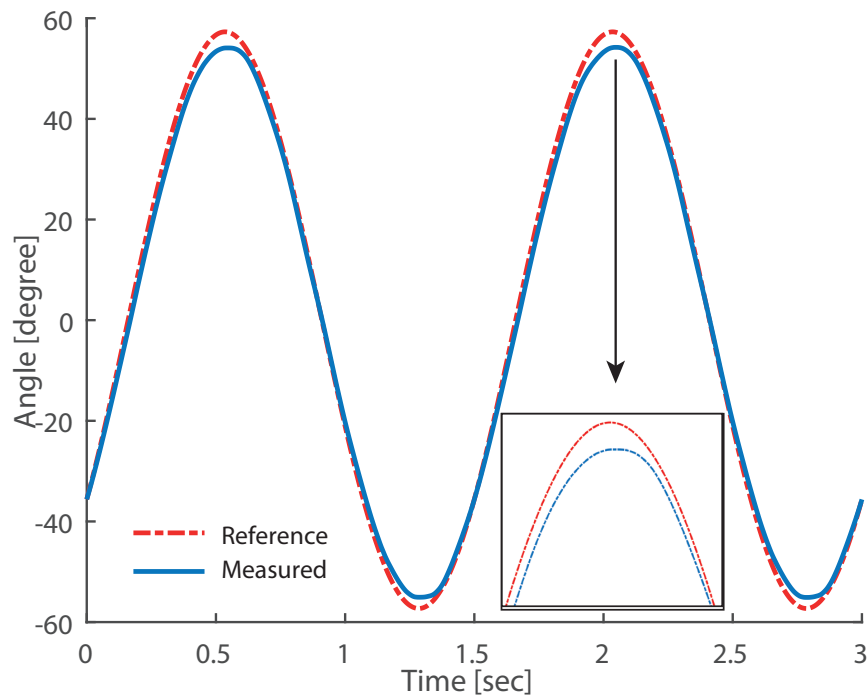


Figure 7.3: Reference and experimentally measured trajectories during the task space impedance control of the rotational DoF of the $3\underline{R}R\underline{P}$ mechanism

Figure 7.4 depicts sample experimental results collected during the task space impedance control of the translational DoF of $3\underline{R}R\underline{P}$ mechanism of ASSISTON-ARM. During this experiment, a circular reference trajectory with

150 mm diameter is imposed to end-effector of 3RRP, while the orientation of 3RRP mechanism is commanded to stay constant. The frequency of the circular movement is set as 0.5 Hz. The controller stiffness of the task space impedance controller is set to 33 N/mm along the translational DoF. RMS error for this task space trajectory tracking experiment is calculated as 1.4%.

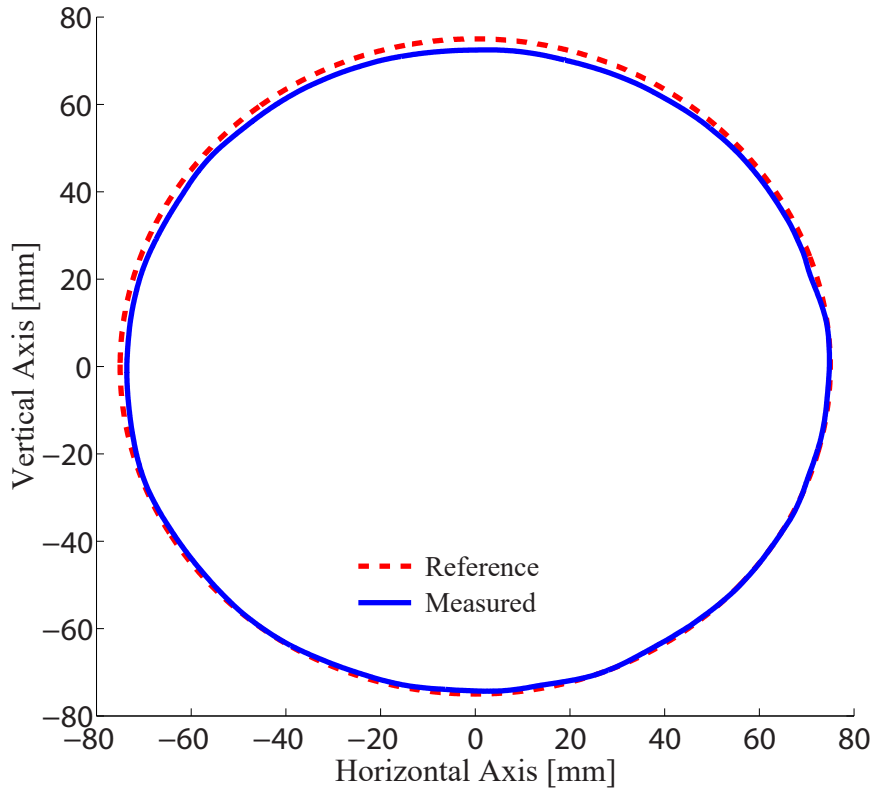


Figure 7.4: Reference and experimentally measured trajectories during the task space impedance control of the translational DoF of the 3RRP mechanism

Figure 7.5 presents sample experimental results collected during the joint space impedance control of the shoulder internal/external rotation of ASSISTON-ARM. A sinusoidal reference trajectory with a 28.64° (0.5 rad) amplitude and 0.66 Hz frequency is imposed to the joint. The controller stiffness of the

joint space impedance is set to 100 Nm/rad. RMS error for this joint space trajectory tracking experiment is calculated as 3%.

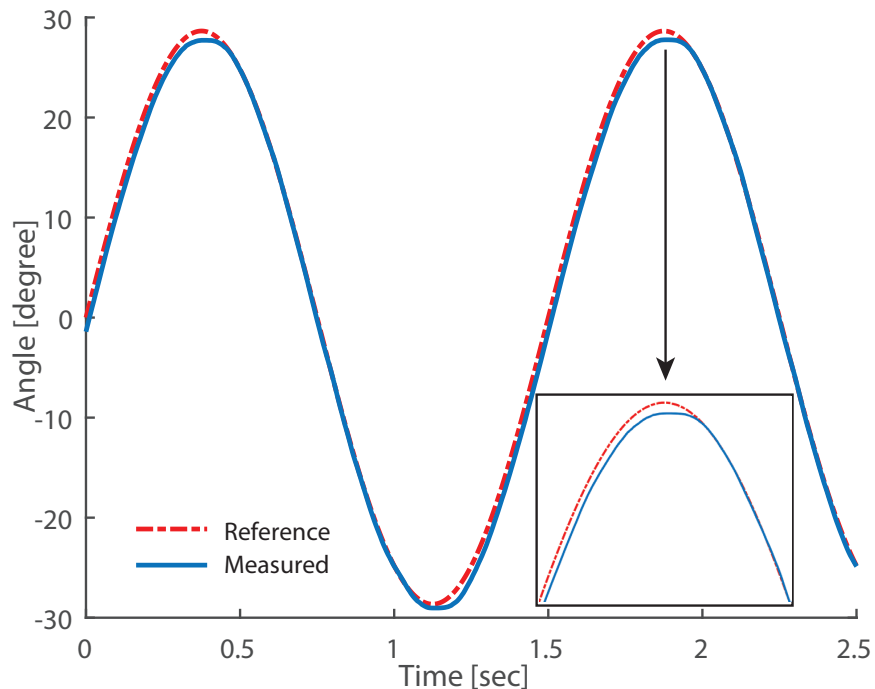


Figure 7.5: Reference and experimentally measured trajectories during the joint space impedance control of the internal/external rotation

Figure 7.6 depicts sample experimental results collected during the joint space impedance control of the elbow joint of ASSISTON-ARM. A sinusoidal reference trajectory with 28.64° (0.5 rad) amplitude and 0.66 Hz frequency is imposed to the joint. The controller stiffness of the joint space impedance control is set to 200 Nm/rad. RMS error for this joint space trajectory tracking experiment is calculated as 0.8%.

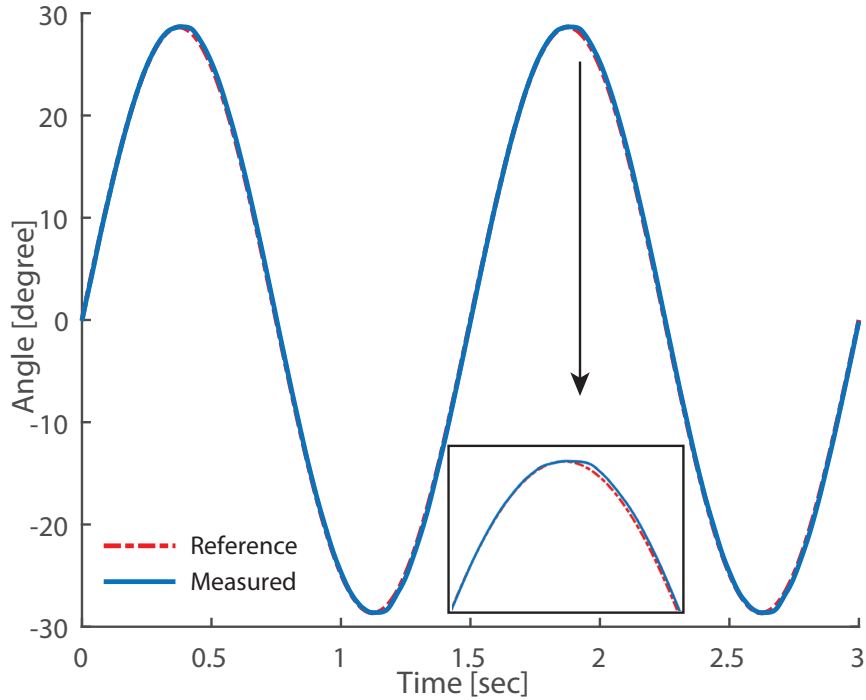


Figure 7.6: Reference and experimentally measured trajectories during the joint space impedance control of the elbow joint

In addition to trajectory tracking, in order to observe the impedance rendering performance of the system, a stiffness rendering experiment is realized for the self aligning 3RRP mechanism located at the shoulder. During the experiments, a virtual stiffness is rendered through open-loop impedance control. Various loads ranging from 425 g to 5000 g are hanged to the end-effector of the 3RRP mechanism and the deflections of the end-effector are measured. A force sensor located at the end-effector is also used to verify the loads.

Figure 7.7 depicts sample experimental results collected during the stiffness rendering experiment under open-loop impedance control, where the virtual stiffness is set to 5 N/mm. In the figure, diamonds represent the

experimentally determined stiffness values, while the blue line is the best line fit to the data computed in the least square sense. The slope of this line is computed as 5.06 N/mm, which serves a good estimate of the stiffness level experienced during the rendering experiment. RMS error for this stiffness rendering experiment is 1.2%. This experiments not only shows the impedance rendering performance, but also verifies the mechanical transparency of ASSISTON-ARM as the rendering experiments are performed with an open-loop impedance controller.

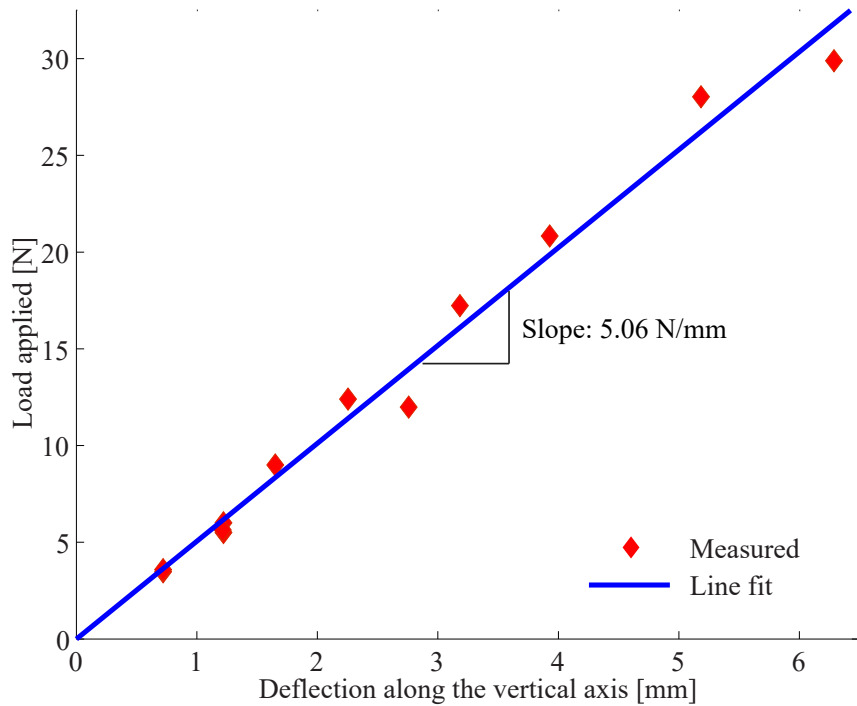


Figure 7.7: Rendering virtual stiffness of 5 N/mm under open-loop impedance control

The rest of interaction control section describes various modes of operation of ASSISTON-ARM that rely on impedance control. With the help of a user-interface, a therapist can select the desired mode of operation as well as the targeted DoF, stiffness of the interaction, and the number of repetitions.

7.1.1 Isometric Mode

During isometric exercises, the length of the muscle does not change and the joint that muscles work around does not move. Pushing a steady wall with your limb can be considered as an instance of this exercise. Isometric exercises can be applied at the early stages of rehabilitation process in order to minimize muscle atrophy [113].

Isometric exercises are one the basic methods in rehabilitation that can be applied by therapists or patients themselves. Isometric exercises help specific muscles to be strengthened, improve joint flexibility and improve neuromuscular recruitment just after surgery or injury [114].

ASSISTON-ARM can deliver isometric exercises to the shoulder complex and elbow under impedance control by implementing stiff virtual constraints. The exoskeleton does not allow for motion around specified constraints. The torques applied during the exercise are provided to the patient as visual feedback and can be reported to the therapists for evaluation.

7.1.2 Isotonic Mode

Isotonic exercise is defined as the dynamic muscular work against a constant force or torque [115]. During isotonic exercises, muscle fibers shorten and return their original length, dynamically. For instance, push-up exercises, stair climbs or dumbbell exercises are considered as isotonic exercises. Iso-

tonic exercises are not only beneficial for fitness, but can also be used for rehabilitation. In particular isotonic exercises increase the range of motion of joints, help to add muscle mass and power and improve joint strength.

ASSISTON-ARM can deliver isotonic exercises to all revolute joints by implementing a force controller. In this particular exercise, the exoskeleton permits motion of the DoF while giving a constant torque to the specified DoF. During isotonic exercises, the direction and intensity of the joint resistance can be adjusted as required.

7.1.3 Isokinetic Mode

Isokinetic exercises are realized with a constant speed while matching the muscle forces [116]. To implement isokinetic exercises, a device should change and match the resistance against the limb, as the user applies force to the device. Swimming can be considered as the closest example to an isokinetic exercise. Isokinetic exercises are advanced exercises, applied at the later phases of rehabilitation or with the healthy subjects for the purpose of training and gaining athletic performance. Isokinetic exercises help to gain muscle mass, endurance and strength, enable tracking of the development of joint or muscle group and offer concentric-concentric, concentric-eccentric, or eccentric-eccentric actions at various velocities [117].

In the isokinetic mode, patients are expected to exert as much torque to the selected rotational joints as possible. During this rehabilitation mode, exoskeleton resists the applied force/torque with same amount, such that the exoskeleton starts motion and follow a sinusoidal trajectory while ensuring that the desired velocity is realized under a velocity control.

7.2 Path Following Control of ASSISTON-ARM

In many daily tasks, such as reaching and exercising, individuals need to complete tasks, decoupled from the timing. In particular, the shape of the contour, capturing the coordination and synchronization of the limb movements are the important factors during motion in order to achieve the task. To achieve natural movement ability of the limb after stroke, physical therapy is mainly focused on specific coordination movements of human limbs while exact timing of the exercise is left to the patient. In order to administer such exercises, path following control can be used.

Another important consideration for the control of rehabilitation robots is radial reduction. During trajectory based control methods, if external forces constrain the motion of the robot, the reference position will keep on advancing as the time progresses. Under these controllers when the external forces are removed, the robot trajectory may significantly deviate from the desired contour. Hence, during trajectory control, sharp and sudden movements of the controller may injure the patients. Radial reduction can be prevented, and smooth motion can be obtained with path following control methods.

7.2.1 Record and Play

A general rehabilitation timeline spans from the day after the stroke, to months and even to years. During the first stage of post-stroke, patients generally cannot move limbs of the affected area. In order to prevent abnormal muscle co-activation, loss of inter-joint coordination, and loss of muscle tone and power, rehabilitation process should start as soon as possible. On the other hand, during the acute phase, the limb of patient is unresponsive [118] and patient is in passive state; hereby, rehabilitation exercises should be

given to the patient in a mode where the patient is passive. Since movements can be administered by the robot with Record and Play mode, this mode can be used in all phases of rehabilitation including the acute phase. As name suggests, in this mode movements are recorded and delivered using the exoskeleton.

During the recording phase, in order to provide back-driveability and easy-of-use for the therapist, active gravity compensation is applied to cancel any remaining gravitational forces effecting the exoskeleton.

After the therapist introduces the desired movement to the patient, a continuous path is fitted to the desired movement. The generated path is independent of the time; hence, any preferred velocity can induced along the generated path. Next, a virtual tunnel around the desired path is implemented to introduce a workspace limit and to avoid access to undesired regions. In the virtual tunnel, users can move freely, but cannot violate the limits of the virtual wall. This feature of the wall ensure variation inside the wall. As a consequence, repetitive tasks without repeating the same motion can be obtained.

Virtual tunnel for robotic devices can be generated in two ways: in joint space or task space. A joint level virtual tunnel is simply defines a two dimensional envelope around the movement path of the joint. For reaching exercises, utilizing a virtual tunnel around movement of the end-effector may be more meaningful. Considering the Cartesian movement of the end-effector, a virtual tunnel on the end-effector movement can be visualized as a circle that sweeps along the path, as illustrated in Figure 7.8.

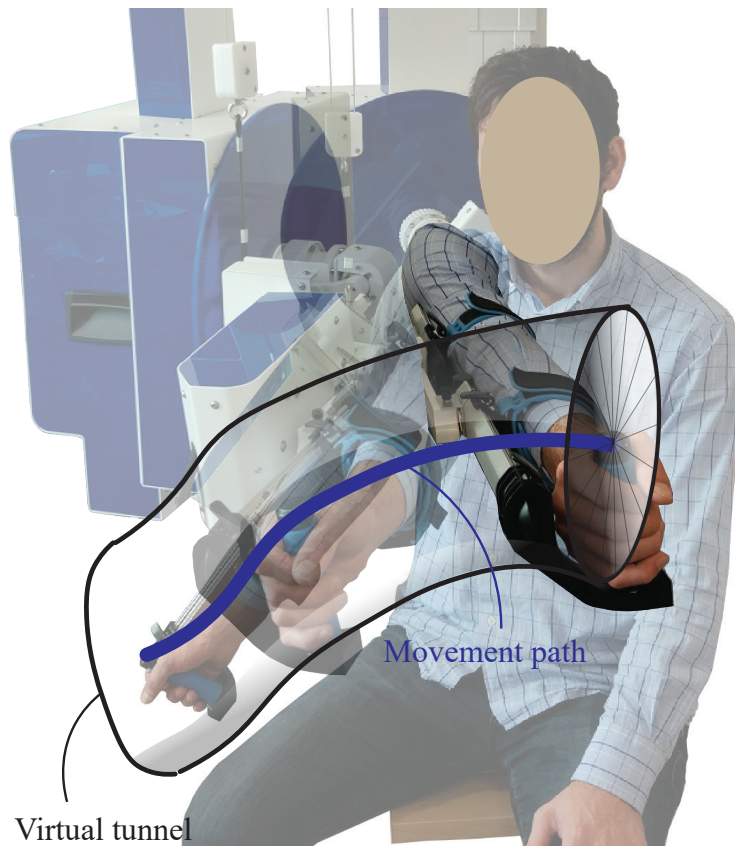


Figure 7.8: A virtual tunnel around the path during a Record-and-Play exercise

Parameters of the virtual tunnel can be modified in order to make the task more challenging, or the virtual tunnel can be generated close to the desired path in order to ensure that the user follows the desired path in a precise manner.

A force field perpendicular to the path, known as *corrective control*, is generated to guide the user towards the desired path. The strength of the corrective control force is proportional to the distance between the measured position and the desired path. The parameters for the corrective controller can be adjusted to provide strict or loose control towards the path.

A tangential force field along the path, known as *assistive control*, is also

applied to the users in order to assist the movement. This force field can be adjusted in order to control the speed of the task.

After the patient starts to take initiative and move limbs, then more advanced control modes, such as *Assist-As-Needed* mode, can be utilized. Since *Assist-As-Needed* mode promotes users to move limbs and actively participate to the exercises.

7.2.2 Assist-As-Needed

Assist-As-Needed (AAN) control method is an adaptive control approach [119] that adjusts the level of assistance during rehabilitation exercises. AAN control method has been widely utilized in the literature for rehabilitation in order to induce active participation of users to the rehabilitation process [120–127].

Apart from the adaptation of the assistive force field, AAN control mode and *Record-and-Play* mode are implemented similarly. Generation and modification of assistive force field help AAN controller to exert proper level of assistance to the patient to ensure task completion, while maximizing the engagement of the patient.

Assistance level with the AAN controller can be determined by evaluating the performance of the patient during the exercise. Velocity of the movement of the patient can be used as a simple and meaningful metric for determining the performance of the task. Along these lines, a threshold velocity can be specified, and if the user is moving slower than the threshold velocity, than AAN control can modify the assistance force field accordingly.

In order to be able to claim coupled stability during exercises through the frequency domain passivity, the force fields may be implemented in a

feedforward manner, such that they are independent from the states of the system. To ensure state independence, assistance level may be adapted in an offline manner; after each movement of the user is completed. This way, the updated force field of AAN controller is delivered to each new movement.

During implementation, as the first step of the adaptation of the assistance force field of AAN controller, the generated path is divided into subsections. The movement pattern of user is observed for every subsection of the path. If the median velocity of user movement is slower than the threshold velocity of ϵ_v within these subsections, then the assistive force field is updated with F^{\parallel} to provide larger assistive forces for the next repetition of movement for that specific subsection. In particular, the force F^{\parallel} along tangential direction of the path can be calculated as

$$F^{\parallel} = \rho \left(\frac{1}{1 + e^{\delta(v - \frac{\epsilon_v}{2})}} \right) \quad (28)$$

where ρ defines the maximum amount of assistance and is determined based on the needs of the patient. In order to ensure smooth assistance to the user, the additional force field is generated based on a sigmoid function. The symbol v denotes the measured mean velocity of the user during an individual subsection, while δ adjusts the steepness of the sigmoid force curve. The default value of δ is taken as 2 for the AAN controller implemented in ASSISTON-ARM. Assistance level is decreased in a similar manner.

During the modes that utilizes the path following control, such as *Record and Play* and *Assist-As-Needed*, the parameters that determine the properties of the virtual tunnel and the force fields can also be adjusted in order to make the exercises more (or less) challenging for the users. For instance,

the diameter of the virtual tunnel can be modified in order to allow free movements around the path, or the normal force field can be reversed in a such a way that it pushes the user away from the desired path to provide disturbances. In these situations, the user needs to spend more effort to realize the desired movement. Therapist, as the main decision maker, can determine the parameters of each mode and develop personalized exercises for each patient.

Most of the stroke patients cannot move their limbs in the first phases of post-stroke period. At the first phase of post-stroke, modes based on path following control method can be used to deliver movements to patients, in order to realize reaching exercises and increase their range of motion. On the other hand, for the operation modes and exercises based on interaction control such as *isometric*, *isotonic*, *isokinetic* modes, active participation of the user is required. In this sense, these operation modes can not only be utilized for stroke patients in the late phases of the rehabilitation, but also for patients that have orthopedic problems and require exercises. In particular, these modes can be used for muscle strengthening, improving joint flexibility and muscle tones of even healthy users, such as athletes.

Chapter VIII

8 User Studies with ASSISTON-ARM

We have verified the ergonomic movement, workspace, range of motion and useability of ASSISTON-ARM through a set of human subject experiments as follows.

8.1 Participants

Five volunteers (4 males and 1 female) with ages between 20 to 30 participated in the experiment. None of the participants had any sensory-motor impairments. All participants signed an informed consent approved by IRB of Sabanci University.

8.2 Experimental Setup

The experimental setup consisted of an ASSISTON-ARM prototype as shown in Figure 8.1. This prototype featured custom 3D printed covers to ensure that moving parts and cables were not exposed to the volunteer. Volunteers, therapists and researchers who supervise the experiments were equipped with emergency stop buttons to terminate the trials, if necessary. When the emergency stop button is pressed, the exoskeleton floats in space thanks to its passively back-driveable design with spring-based gravity compensation.

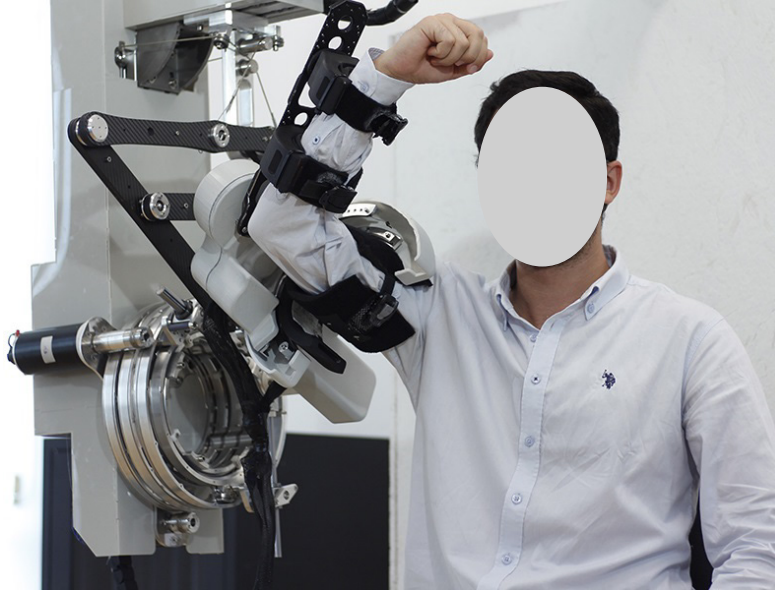


Figure 8.1: ASSISTON-ARM prototype used during the human subject experiments

8.3 Experimental Procedure

Before the experiment, volunteers were introduced to ASSISTON-ARM, informed about the purpose of the study, trained about the safety features of the device, and asked to utilize the emergency stop button anytime whenever they felt uncomfortable.

The setup time required to attach volunteers to the exoskeleton took less than a minute, thanks to the self-aligning nature of ASSISTON-ARM. Following the explanations, the volunteers went through an unrecorded session for 300 s in order to familiarize themselves with ASSISTON-ARM.

Two experimental conditions, *patient active* and *patient passive*, were tested for flexion/extension movements in the sagittal plane and abduction/adduction movements in the frontal plane. The conditions were pre-

sented to the volunteers in a randomized order. Each condition was tested with five consecutive trials and data was recorded using ASSISTON-ARM.

For the patient active condition, volunteers moved the exoskeleton to perform the instructed movement, while ASSISTON-ARM provided no assistance other than compensation of its weight. In particular, to perform flexion/extension movements, the volunteers were instructed to start at a configuration when their arm was oriented vertically down and their palm was facing toward their body. Then, they were asked to raise their arm with a constant speed movement in the sagittal plane, until it was oriented vertically up. They were also instructed to keep their elbow locked during the motion. Next, they were asked to reverse the movement such that they reached their initial pose. A short break was scheduled before the volunteers started the next trial.

Similarly, to perform abduction/adduction movements, the volunteers were instructed to start at a configuration when their arm was oriented vertically down and their palm facing forward. Then, they were asked to raise their arm with a constant speed movement in the frontal plane, until it was oriented vertically up. They were also instructed to keep their elbow kept locked during the motion. Next, they were asked to reverse the movement. A short break was scheduled between consecutive trials.

For the patient passive condition, first a therapist moved the volunteer with the exoskeleton to record flexion/extension movements in the sagittal plane and abduction/adduction movements in the frontal plane, as instructed in the patient active condition. Then, these recorded trajectories were played back to the user through the impedance controller. An impedance controller with 33 N/mm stiffness along translational directions, 280 Nm/rad stiffness

about the rotational DoF of the 3RRP were utilized during the patient passive trials.

8.4 Performance Measurement

Range of motion during flexion/extension and abduction/adduction movements were used to evaluate the ergonomic fitness and workspace of ASSISTON-ARM with volunteers.

Repeatability of the therapist recorded movements in the patient passive condition, when users were attached to the device, was used to evaluate the trajectory tracking performance of ASSISTON-ARM. Repeatability is used for indicating the precision of robots. It represents how well a robot will return the same position, or track the same trajectory in a repeated manner.

Smoothness analysis during rehabilitation has been used for evaluating movement capabilities and progress of neurologically impaired patients. During rehabilitation, as the recovery takes place, movements of patients become less fragmented and more coordinated [128]. Furthermore, maximizing smoothness has been shown to be competent mathematical model of coordination. For the patients that are in the late phases of rehabilitation or for healthy individuals smooth movements can be observed.

Apart from observing recovery and movement coordination of patients, smoothness analysis also can be utilized for evaluating the transparency of a wearable mechanism. When a healthy user delivers movement with an ideally back-driveable and mechanically transparent exoskeleton, a smooth and natural movement is expected to be observed.

The time required to attach the volunteers to ASSISTON-ARM and start administering required movements was recorded to evaluate useability of

the device. Furthermore, qualitative feedback from both the therapists and the volunteers were collected to evaluate the user-friendliness and perceived safety of the device.

8.5 Results and Discussion

8.5.1 Range of Motion

Figures 8.2 and 8.3 present data collected when volunteers performed flexion/extension movements in the sagittal plane and abduction/adduction movements in the frontal plane, during the patient active condition, respectively. In particular, movement of each volunteer is depicted with a solid line representing the average movement pattern and an enveloping shaded area representing deviations from the mean during 5 consecutive trials performed by the volunteer. The horizontal green dashed lines mark the joint limits of ASSISTON-ARM.

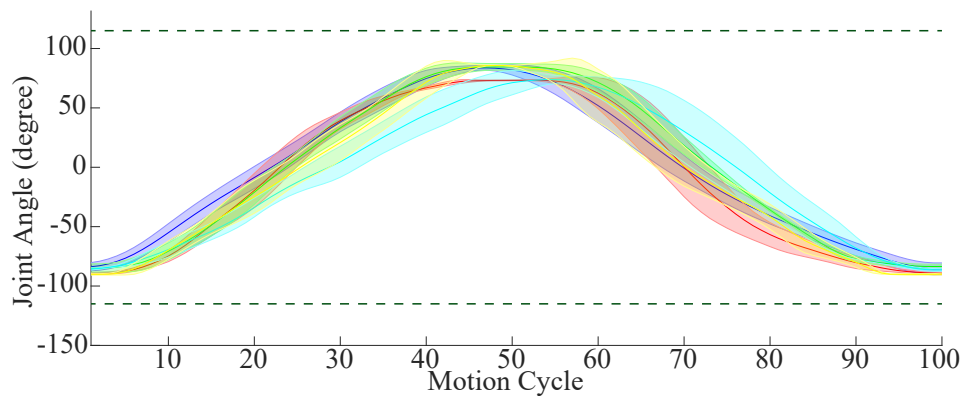


Figure 8.2: Data recorded during flexion/extension movements in the sagittal plane during patient active trials

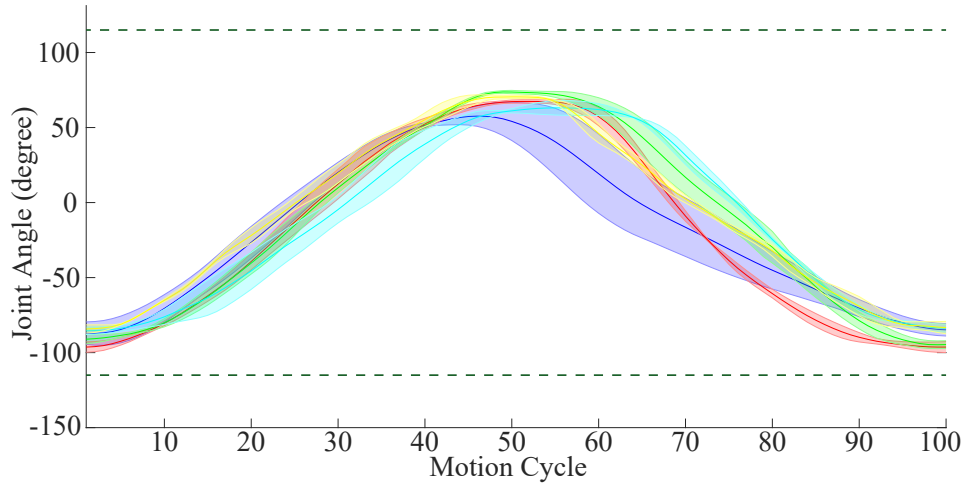


Figure 8.3: Data recorded during abduction/adduction movements in the horizontal plane during patient active trials

Figure 8.4 presents the motion of humerus head in the sagittal plane during flexion/extension of the shoulder complex from a sample trial of a volunteer. In this figure, blue lines represent the actual movement of humerus head, while numbers inside circles depict the flexion amount. The dexterous workspace of the 3RRP mechanism is marked with green dashed lines. Similarly, Figure 8.5 presents the motion of humerus head in the sagittal plane of five volunteers during consecutive flexion/extension of the shoulder complex.

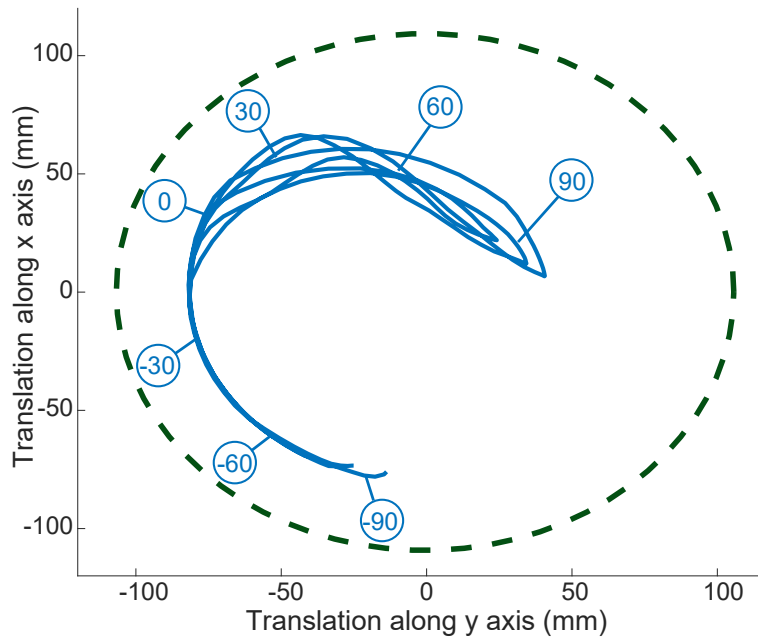


Figure 8.4: Translations of the humerus head in the sagittal plane of a volunteer during flexion/extension of the shoulder complex during a patient active trial

Figures 8.2 and 8.3 provide evidence that ASSISTON-ARM does not limit the movements of volunteers as they were able to perform smooth natural movements within their range of motion. They also indicate that the workspace of device is large enough to accommodate flexion/extension and abduction/adduction movements of shoulder complex of a variety of users. In particular, volunteers were able to reach to their natural joint limits by rotating their shoulder in a range that extended to vertically up and down postures during both of these movements.

Figures 8.4 and 8.5 indicate that ASSISTON-ARM can accommodate a wide variety of scapulohumeral movements. In particular, one can observe from

these figures that humerus head follows a distinct closed loop trajectory during flexion/extension movements, which is unique to each volunteer based on the individual characteristics of their bones, ligaments, muscle structures, as well as how the volunteer is attached to the device. Furthermore, these results provide evidence that the workspace of the device is sufficient to accommodate SH rhythms of a variety of users.

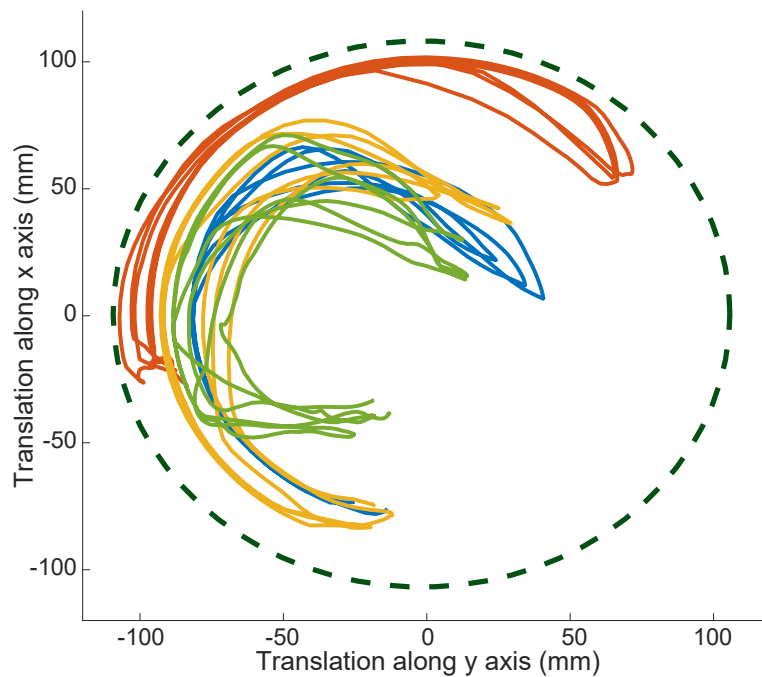


Figure 8.5: Translations of the humerus head in the sagittal plane of five volunteers during flexion/extension of the shoulder complex during patient active trials

8.5.2 Repeatability

Figures 8.6 and 8.7 present data collected when therapist recorded flexion/extension movements in the sagittal plane and abduction/adduction movements in the frontal plane were imposed to volunteers during the patient

passive condition, respectively. Movements of each volunteer are depicted with a solid line for five consecutive trials performed. The horizontal green dashed lines mark the joint limits of ASSISTON-ARM.

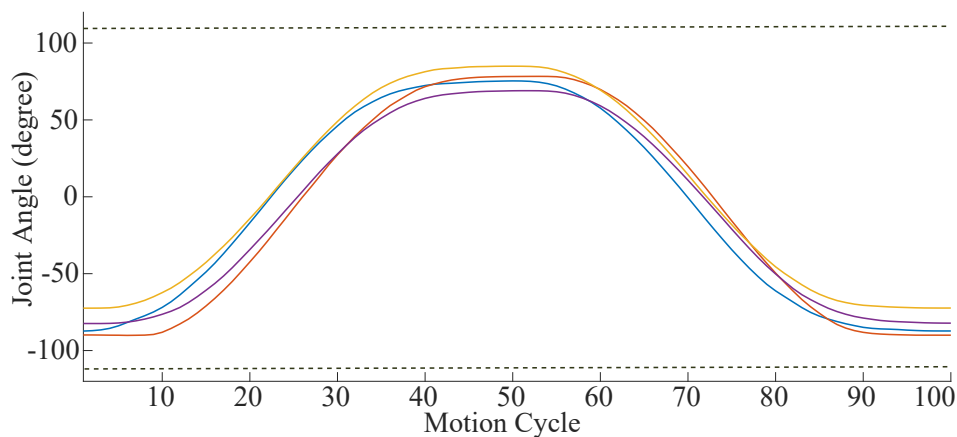


Figure 8.6: Data recorded during flexion/extension movements in the sagittal plane during patient passive trials

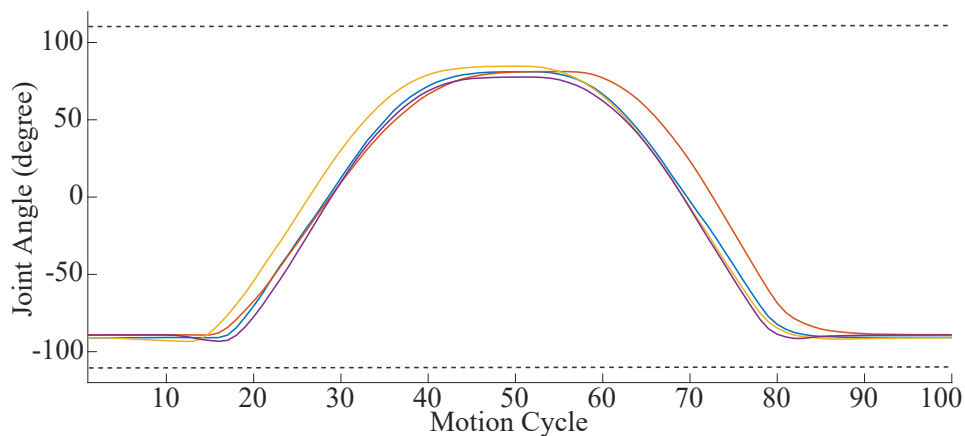


Figure 8.7: Data recorded during abduction/adduction movements in the frontal plane during patient passive trials

Figures 8.8 and 8.9 present the motion of humerus head in the sagittal plane and frontal plane of five volunteers during consecutive flexion/extension

and abduction/adduction movements of the shoulder complex during patient passive trials, respectively. The dexterous workspace of the 3RRP mechanism is marked with green dashed lines.

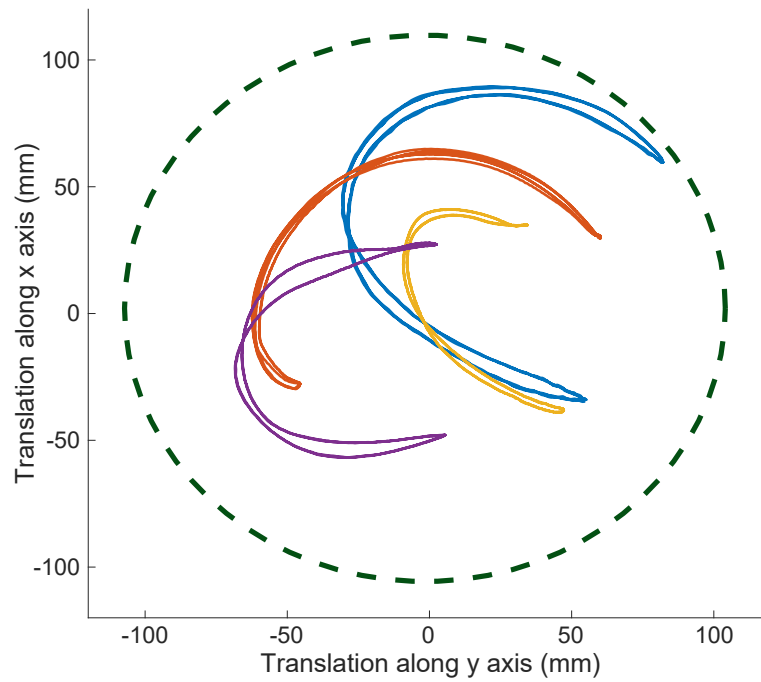


Figure 8.8: Translations of the humerus head in the sagittal plane of five volunteers during flexion/extension of the shoulder complex during patient passive trials

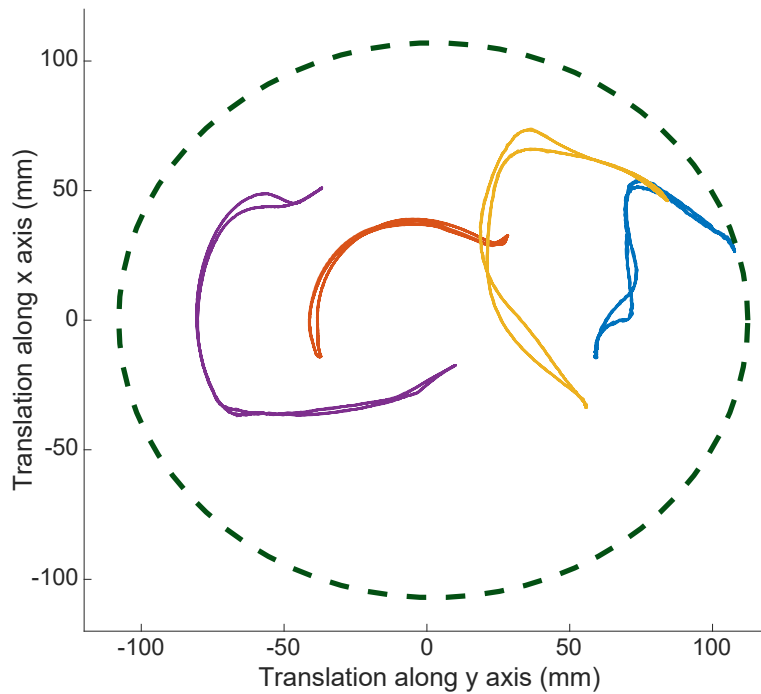


Figure 8.9: Translations of the humerus head in the frontal plane of four volunteers during abduction/adduction of the shoulder complex during patient passive trials

Figures 8.6 and 8.7 provide evidence that impedance controller of ASSISTON-ARM can impose the desired movements to volunteers with high repeatability, as the RMS error for trajectory tracking is less than 1% for all trials. Figures 8.8 and 8.9 indicate that ASSISTON-ARM can accommodate individual SH rhythms of volunteers in the sagittal and the frontal planes to impose the desired flexion/extension and abduction/adduction movements in an ergonomic manner.

8.5.3 Smoothness

In the literature, there are different metrics that are used for quantifying smoothness and coordination of movement. Most studies uses jerk, time derivative of acceleration, for determining the smoothness. A normalized and dimensionless squared jerk metric is commonly used in order to measure smoothness of movements [128–130]. Dimensionless squared jerk metric measure increases as the magnitude of speed fluctuations increase. Furthermore, this measure increases monotonically with the temporal separation between submovements. Hence, it properly captures common departures from smoothness, including multiple speed peaks and periods of arrest.

Dimensionless squared jerk metric is preferable as it is insensitive to movement amplitude and duration, while capturing and quantifying common deviations from smooth and coordinated movement. Dimensionless normalized squared jerk metric μ_{nj} is calculated as

$$\mu_{nj} = \left(\int_{t_1}^{t_2} \ddot{x}(t)^2 dt \right) \frac{D^3}{v_{max}^2} \quad (29)$$

where $x(t)$ is the configuration level movement and D equals to $t_2 - t_1$. Symbols t_2 and t_1 represents the final and the initial times of the movement, respectively. Symbol v_{max} is the peak velocity that can be achieved during the movement. According to this definition, a minimum jerk trajectory can be modeled as

$$x(t) = x_i + (x_f - x_i) \left(10\left(\frac{t}{d}\right)^3 - 15\left(\frac{t}{d}\right)^4 + 6\left(\frac{t}{d}\right)^5 \right) \quad (30)$$

where x_i and x_f are the initial and the final positions of the movement,

respectively. Here, t represents time and d represents the final time when the movement is terminated.

In order to analyze the smoothness of the movement with ASSISTON-ARM, shoulder flexion movements actively delivered by five participants are compared with the same movement delivered by the exoskeleton. When participants are actively executing these movements, the exoskeleton is used only for recording the flexion movements. Later, each recorded movement is fitted with a minimum jerk path, in order to generate a smooth movement to be delivered by the exoskeleton. Then, these movements are actively delivered to the users by the exoskeleton, where users are instructed passive. Lastly, dimensionless jerk metric analysis for both user active and user passive movements are performed.

In Figure 8.10, the dimensionless jerk metric analysis results of shoulder flexion movements are depicted. According to dimensionless jerk analysis, smaller values of jerk metric indicate smoother movements than higher values. The result for dimensionless jerk metric analysis for user passive movements are depicted with dotted curves, while user active ones are presented with continuous curves. Since there is no multiple speed peaks, periods of arrests or sudden movement changes due to parasitic device dynamics, dimensionless squared jerk analysis results of all active and passive flexion movements are accumulated at the top of the figure, indicating smooth movements.

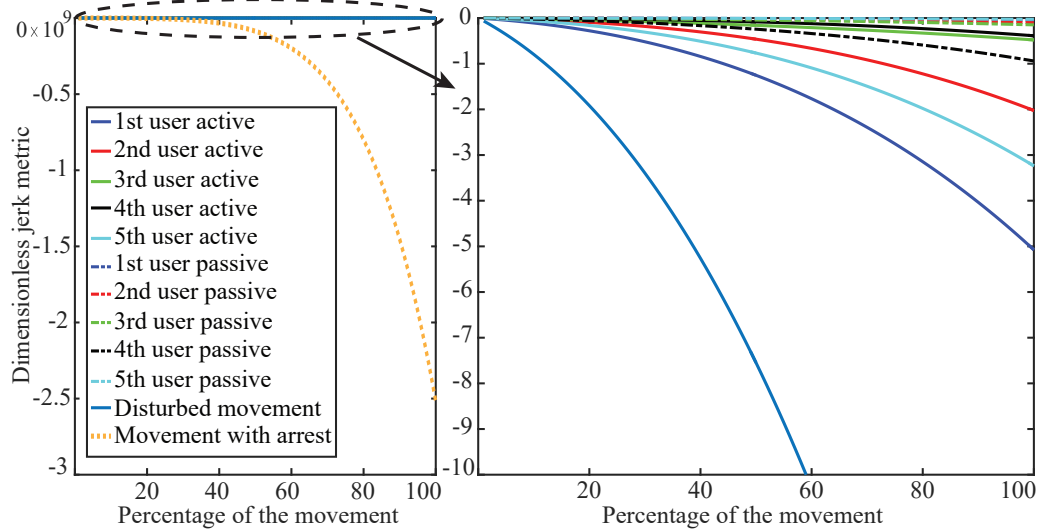


Figure 8.10: Dimensionless jerk metric analysis of user active and passive shoulder flexion movements

In order to better evaluate the smoothness of these movements, a slightly disturbed movement and a movement with arrest, depicted in Figure 8.11, are generated. In Figure 8.11, also the difference between user active and user passive movements can be observed. Even though the disturbed movement path does not include periods of arrest or sudden changes, the dimensionless jerk metric increases very quickly as expected. On the other hand, hand movement with arrest change the dimensionless jerk measure dramatically, indicating deteriorated smoothness. The user active and user passive movements have much smaller dimensionless jerk measures indicating their smoothness. Furthermore, there seems no significant difference between user active and user passive movements, verify the transparent operation of ASSISTON-ARM.

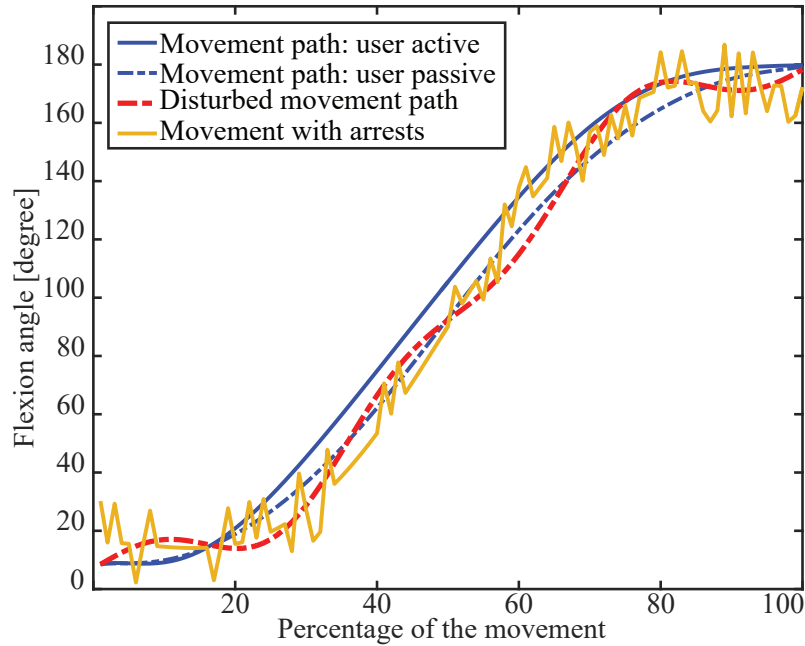


Figure 8.11: User active and user passive shoulder flexion movement together with a generated disturbed movement path

8.5.4 Quantitative Evaluation

During the post trial interviews, all of the therapists who used the device indicated that they found the device safe and easy-to-use. They evaluated the self-aligning property as an indispensable feature for achieving the desired RoM, while the passive back-driveability was perceived as an important safety feature. Furthermore, they indicated that the easy setup of the device significantly improved its useability.

During the post trial interviews, all of the volunteers indicated that they felt comfortable and safe while moving their arms attached to ASSISTON-ARM. They also indicated that the device was ergonomic and gentle, while it imposed the therapist determined trajectories during the patient passive condition. The volunteers were satisfied with the workspace of the device

and evaluated it as sufficiently large to perform most ADL.

Overall, the qualitative feedback provided by the therapists and volunteers were positive, providing evidence for the user-friendliness and the perceived safety of the device. The quantitative measurements also supported the ergonomic nature of movements with and sufficiency of the RoM of ASSISTON-ARM.

Chapter XI

9 Conclusion and Future Works

We have presented the design, control, characterization and user evaluations of ASSISTON-ARM, a novel arm exoskeleton for robot-assisted rehabilitation that enables mobilization of the shoulder girdle along with all shoulder rotations. We have derived kinematics and singularity-free workspace of ASSISTON-ARM and implemented an impedance controller with feed-forward gravity compensation. We have verified the passive back-driveability and control performance of the device with and without volunteers attached to it.

Through user studies, we have verified the ease-of-use of the device and showed that the workspace of ASSISTON-ARM covers most of the reachable workspace of human arm and its passively back-driveable shoulder module permits shoulder mobilization during exercises, enabling natural movements within the human RoM in an ergonomic manner.

9.1 Design Improvements for ASSISTON-ARM

Design of the exoskeleton should, not only ensure mechanical transparency for good force control performance, but also be safe and convenient for clinical use. Possible collisions of the device with its user, the use of the device for both right and left handed subjects are important design considerations for

the usability of the device. Along these lines, several modifications have been implemented to improve the real-life useability of ASSISTON-ARM. Note that while these changes improve the useability, they do not change the underlying kinematics or controller of the system.

To implement internal/external rotation of the shoulder, a remote center of rotation mechanism consisting of a C-shaped guide rail has been used in the original design. However, in this implementation C-shaped guide may come very close to human trunk during shoulder horizontal abduction/adduction movements. While, collisions may be avoided with software limits, the user experience and the workspace of the device are detrimentally effected. By this guide, to resolve this problem, an alternative mechanism is used in the modified design to implement the *remote center of rotation* (RCoR) of this joint. The improved implementation of the shoulder internal/external rotation, depicted in Figure 9.1, ensures a clean separation between the device and the user.

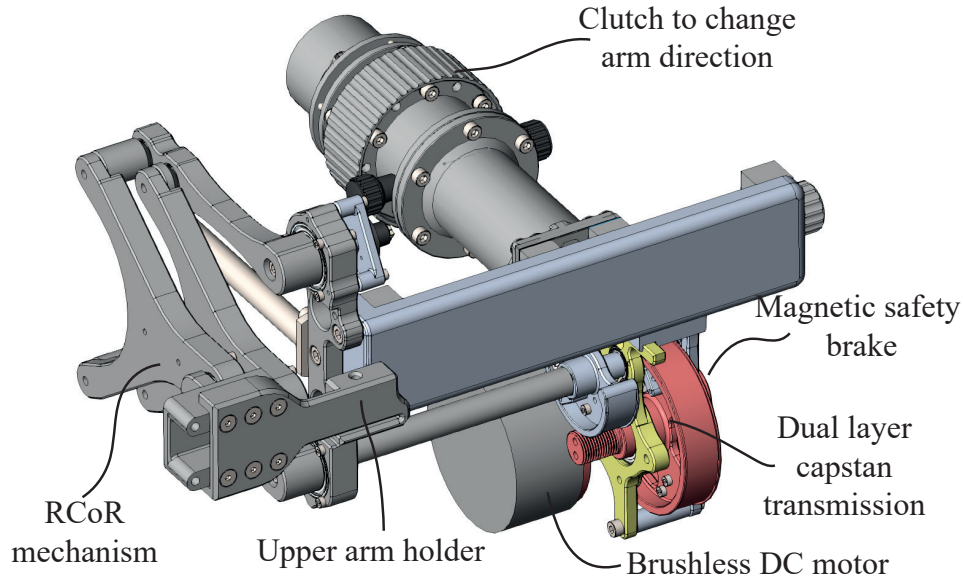


Figure 9.1: Implementation of remote center of rotation mechanism for improving perceived safety and useability of the device

Figure 9.3 depicts the kinematics of the RCoR mechanism. This mechanism consists of two inter connected parallelogram mechanisms providing a rotation axis for the shoulder internal/external rotation around the arm.

The mechanism is implemented to connect lower arm Body H to upper arm Body U. Bodies U, B, C and F construct the first parallelogram between Points Δ , Φ , Ψ and Σ . Similarly, Bodies U, B, C and D construct the second parallelogram between Points Δ , K, M and Σ . The double parallelogram system is connected to each other in such a way that a virtual parallelogram spanning Points $\Phi K M \Psi$ is constructed. With this assembly, one can verify that Bodies D and F stay always parallel to \vec{u}_1 . The end-effector of RCoR is indicated by Body L. After Bodies D and F are connected to the end-effector Body L via Points W and Y, a virtual revolute joint with rotation center Point X is obtained. Parallelogram structure ensures that Bodies B and L

rotate the same amount with respect to \vec{u}_1 .

One can arrange the radius γ_3 and the position of revolute center Point X with via changing the link lengths γ_1 and γ_2 . RCoR based shoulder internal/external rotation of ASSISTON-ARM has a symmetrical workspace of 83° along both directions.

A second modification to original design is due to introduction of a clutch mechanism that enables configuration of ASSISTON-ARM for both right hand and left hand usage. Figure 9.2 presents ASSISTON-ARM on both arm configuration. In order to change the direction of arm, the clutch is released, rotated clockwise for 180° and re-locked. Then, the orthosis is replaced with the proper arm. Finally, joint limit of the elbow joint is reconfigured.

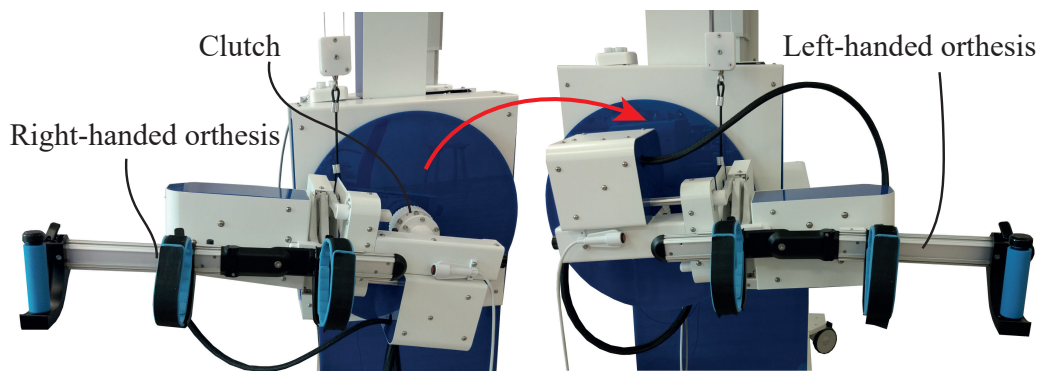


Figure 9.2: Configuration of ASSISTON-ARM for right/left arm use

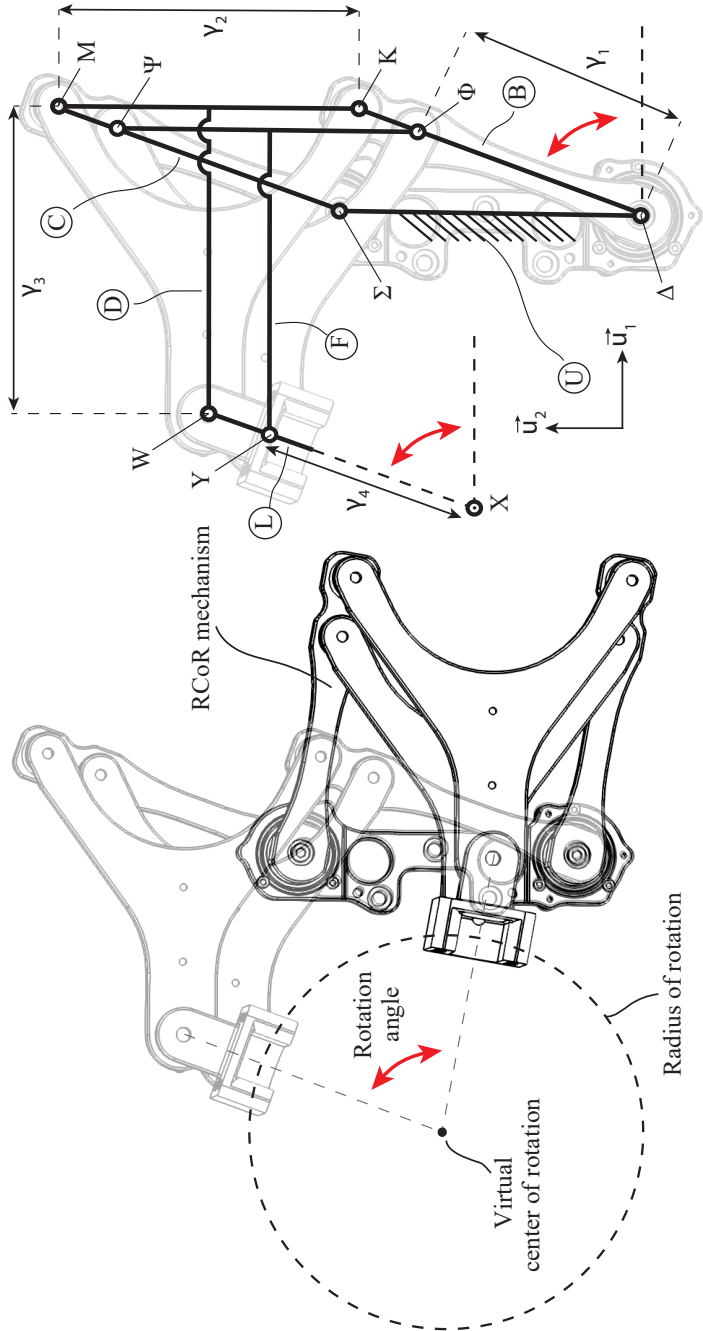


Figure 9.3: CAD details and schematics of RCoR mechanism: at left side overall CAD and motion capabilities of RCoR are showed, at right side kinematic schematics of RCoR mechanism is represented

Passive gravity compensation mechanism developed for ASSISTON-ARM is explained in Section 4.8. As depicted in Figure 9.4 (a), this mechanism has a parallelogram based kinematic structure to balance a load M_g at Point L_a .

In order to employ the passive gravity compensation mechanism for both left and right handed subjects, the workspace of the compensator device need to be approximately doubled. For this purpose, symmetric parallelogram-type of gravity compensation mechanism, illustrated with Figure 9.4 (b), is designed. In order to prevent collision of the links of gravity compensation mechanism and arm module of the exoskeleton, an auxiliary link between Points K_b and L_b is introduced. Additional parallelogram linkages are added to the design in order to ensure that link K_bL_b is vertical at all the times, so that the vertical and horizontal movements of the compensation mechanism do not affect each other. Spring forces F_{1a} and F_{2a} are exerted to Points A_a and B_a via pulleys and cables.

Both parallelogram designs feature passive, spring based compensation of the arm weight. On the other hand, springs required for these designs need long strokes and exert high forces. Forces reaching up to $550N$ introduce friction on routing pulleys and bearings, hindering passive back-driveability of the system. Higher stroked springs with lower spring forces are not ideal for integration to ASSISTON-ARM due to dimension constraints.

Due to workspace limitations, additional complexity and high friction problems of spring based gravity compensation mechanism, a counter-weight based gravity compensation mechanism has been introduced to ASSISTON-ARM, as shown at Figure 9.4 (c). Experimental results show that counter-weight based gravity compensation mechanism is more mechanically trans-

parent and back-driveable with respect to spring-based counterparts. Presented in the schematic representation at Figure 9.4 (d), counter-weight based compensator design has a pulley at Point C_f that halves the required force for the gravity compensation, while doubling the required stroke for motion of the counter weight. In order to achieve the desired stroke for the counter-weight and situate the counter-weight at the base of ASSISTON-ARM, routing pulleys have been introduced to the design.

The workspace of ASSISTON-ARM after these improvements is demonstrated in Figure 9.5.

The cover design of the system is realized by an industrial design company, DESIGNOBIS, and has been implemented on ASSISTON-ARM.

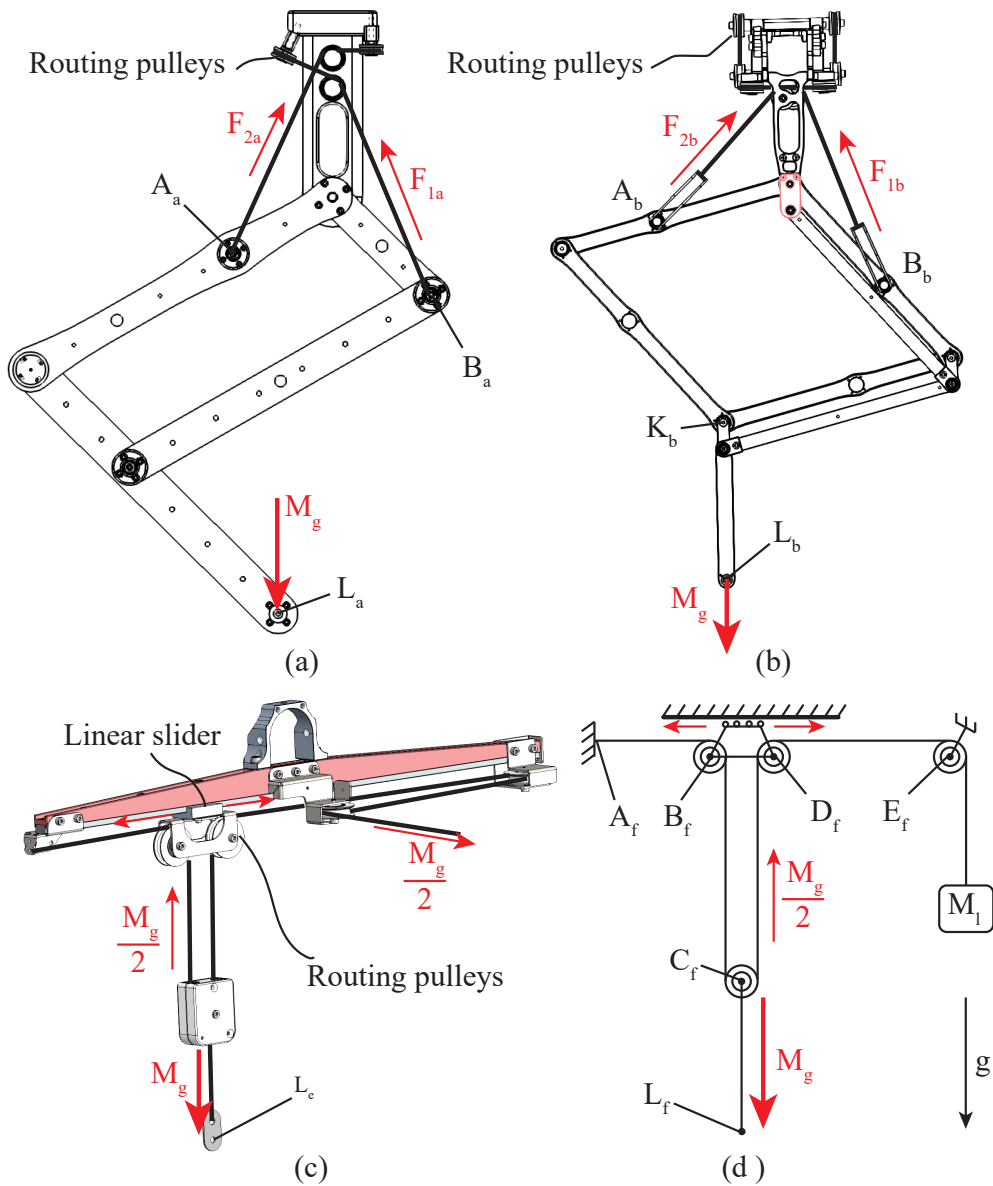


Figure 9.4: Representation of the gravity compensation mechanism options for ASSISTON-ARM: (a) spring-based mechanism for right handed use, (b) spring-based mechanism developed for both right and left handed use, (c) counter-weight based mechanism, and (d) schematics of the gravity compensation mechanism based on the counter-weight.

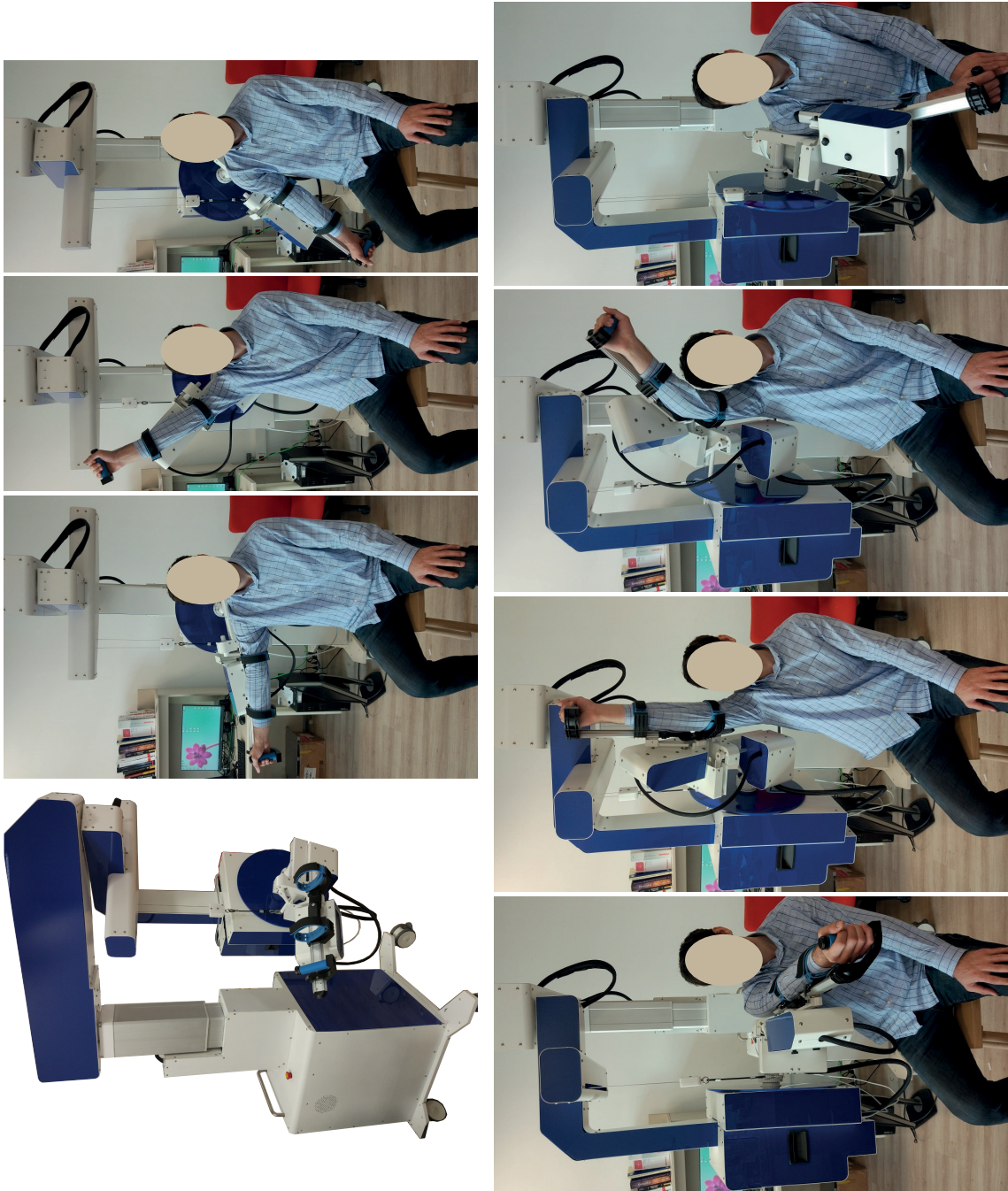


Figure 9.5: ASSISTON-ARM with a healthy volunteer shown at various arm poses

9.2 Future Works

With the first human subject experiments ergonomic movement, workspace, range of motion and useability of ASSISTON-ARM have been verified. Effectiveness of the modes of operation and benefits of rehabilitation protocols of ASSISTON-ARM will be studied with further clinical studies in the future. Along these lines, our ongoing work includes clinical trial with a larger population of volunteers to support the results from the initial user studies with more conclusive statistical analysis.

References

- [1] M. Katan and A. Luft. Global burden of stroke. *Seminars in Neurology*, 38(2):208–211, 2018.
- [2] C. Butefisch, H. Hummelsheim, P. Denzler, and K. H. Mauritz. Repetitive training of isolated movements improves the outcome of motor rehabilitation of the centrally paretic hand. *Journal of The Neurological Sciences*, 130(1):59–68, 1995.
- [3] G. Kwakkel, R.C. Wagenaar, J.W. Twisk, G.J. Lankhorst, and J.C. Koetsier. Intensity of leg and arm training after primary middle-cerebral-artery stroke: A randomised trial. *The Lancet*, 354(9174):191–196, 1999.
- [4] Nestor A. Bayona, Jamie Bitensky, Katherine Salter, and Robert Teasell. The role of task-specific training in rehabilitation therapies. *Topics in Stroke Rehabilitation*, 12(3):58–65, 2005.
- [5] A. Sunderland, D. J. Tinson, E. L. Bradley, D. Fletcher, H. R. Langton, and D. T. Wade. Enhanced physical therapy improves recovery of arm function after stroke. A randomised controlled trial. *Journal of Neurology, Neurosurgery and Psychiatry*, 55(7):530–535, 1992.
- [6] B. T. Volpe, H. I. Krebs, and N. Hogan. Is robot-aided sensorimotor training in stroke rehabilitation a realistic option ? *Current Opinion in Neurology*, 14(6):745–752, 2001.
- [7] J. H. Van der Lee, I. A. Snels, H. Beckerman, G. J. Lankhorst, R. C. Wagenaar, and L. M Bouter. Exercise therapy for arm function in

- stroke patients: A systematic review of randomized controlled trials. *Clinical Rehabilitation*, 15(1):20–31, 2001.
- [8] T. Platz. Evidence-based arm rehabilitation - A systematic review of the literature. *Der Nervenarzt*, 74(10):841–849, 2003.
- [9] G. B. Prange, M. J. Jannink, C. G. Groothuis-Oudshoorn, H. J. Hermens, and M. J. Ijzerman. Systematic review of the effect of robot-aided therapy on recovery of the hemiparetic arm after stroke. *Journal of rehabilitation research and development*, 43(2):171–184, 2006.
- [10] G. Kwakkel, B. J. Kollen, and H. I. Krebs. Effects of robot-assisted therapy on upper limb recovery after stroke: A systematic review. *Neurorehabilitation and Neural Repair*, 22(2):111–121, 2008.
- [11] J. Mehrholz, M. Pohl, T. Platz, J. Kugler, and B. Elsner. Electromechanical and robot-assisted arm training for improving activities of daily living, arm function, and arm muscle strength after stroke. *Cochrane database of systematic reviews (Online)*, 11, 2015.
- [12] R. Bertani, C. Melegari, De Cola M.C., Bramanti A., Bramanti P., and R.S. Calabro. Effects of robot-assisted upper limb rehabilitation in stroke patients: a systematic review with meta-analysis. *Neurological Sciences*, 38(9):1561–1569, 2017.
- [13] C. Zhang, C.W. Li-Tsang, and R.K. Au. Robotic approaches for the rehabilitation of upper limb recovery after stroke: A systematic review and meta-analysis. *International Journal of Rehabilitation Research*, 40(1):19–28, 2017.

- [14] N. Hogan, H.I. Krebs, J. Charnnarong, P. Srikrishna, and A. Sharon. MIT-MANUS: A workstation for manual therapy and training. i. In *IEEE International Workshop on Robot and Human Communication*, pages 161–165, 1992.
- [15] A. A. Carlo, N. Satler, G. Cappiello, A. Scoglio, E. Ruffaldi, and M. Bergamasco. MOTORE: A mobile haptic interface for neuro-rehabilitation. In *IEEE International Symposium on Robot and Human Interactive Communication*, pages 383–388, 2011.
- [16] M. Sarac, M. A. Ergin, and V. Patoglu. AssistOn-Mobile: A series elastic holonomic mobile platform for upper extremity rehabilitation. In *World Haptics Conference*, pages 283–288, 2013.
- [17] T. Sukal, M. Ellis, and J. Dewald. Shoulder abduction induced reductions in reaching work area following hemiparetic stroke: Neuroscientific implications. *Experimental Brain Research*, 183(2):215–223, 2007.
- [18] A. Frisoli, F. Rocchi, S. Marcheschi, A. Dettori, F. Salsedo, and M. Bergamasco. A new force-feedback arm exoskeleton for haptic interaction in virtual environments. In *Eurohaptics Conference and Symposium on Haptic Interfaces for Virtual Environment and Teleoperator Systems, World Haptics*, pages 195–201, 2005.
- [19] T. Nef, M. Mihelj, G. Kiefer, C. Perndl, R. Muller, and R. Riener. ARMin - Exoskeleton for arm therapy in stroke patients. In *IEEE International Conference on Rehabilitation Robotics*, pages 68–74, 2007.

- [20] J.C. Perry, J. Rosen, and S. Burns. Upper-limb powered exoskeleton design. *IEEE/ASME Transactions on Mechatronics*, 12(4):408–417, 2007.
- [21] M.A. Ergin and V. Patoglu. AssistOn-SE: A self-aligning shoulder-elbow exoskeleton. In *IEEE International Conference on Robotics and Automation*, pages 2479–2485, 2012.
- [22] T. Sakurada, T. Kawase, K. Takano, T. Komatsu, and K. Kansaku. A BMI-based occupational therapy assist suit: asynchronous control by SSVEP. *Front Neuroscience*, 7(172):2479–2485, 2013.
- [23] E. Pirondini, M. Coscia, S. Marcheschi, G. Roas, F. Salsedo, A. Frisoli, M. Bergamasco, and S. Micera. Evaluation of the effects of the arm light exoskeleton on movement execution and muscle activities: A pilot study on healthy subjects. *Journal of NeuroEngineering and Rehabilitation*, 13(1):1–9, 2016.
- [24] B. Kim and AD. Deshpande. An upper-body rehabilitation exoskeleton Harmony with an anatomical shoulder mechanism: Design, modeling, control, and performance evaluation. *The International Journal of Robotics Research*, 34(4):414–425, 2017.
- [25] D.J. Reinkensmeyer, L.E. Kahn, M. Averbuch, A. McKenna-Cole, B.D. Schmit, and W.Z. Rymer. Understanding and treating arm movement impairment after chronic brain injury: progress with the ARM guide. *Journal of Rehabilitation Research and Development*, 37(6):653–662, 2000.

- [26] P.S. Lum, C.G. Burgar, P.C. Shor, M. Majmundar, and M. Van der Loos. Robot-assisted movement training compared with conventional therapy techniques for the rehabilitation of upper limb motor function following stroke. *Archives Physical Medical Rehabilitation*, 83(7):952–959, 2002.
- [27] S. Coote, E. K. Stokes, B. T. Murphy, and W. Harwin. GENTLE/s Robot mediated therapy on upper extremity function poststroke. In *International Conference on Rehabilitation Robotics*, pages 21–26, 2003.
- [28] A. Schiele and F.C.T. Van der Helm. Kinematic design to improve ergonomics in human machine interaction. *IEEE Transactions on Neural Systems and Rehabilitation Engineering*, 14(4):456–469, 2006.
- [29] A.H.A. Stienen, E.E.G. Hekman, F.C.T. Van der Helm, and H. Van der Kooij. Self-aligning exoskeleton axes through decoupling of joint rotations and translations. *IEEE Transactions on Robotics*, 25(3):628–633, 2009.
- [30] P.S. Lum, S. Mulroy, R.L. Amdur, P. Requejo, B.I. Prilutsky, and A.W. Dromerick. Gains in upper extremity function after stroke via recovery or compensation: Potential differential effects on amount of real-world limb use. *Topics in Stroke Rehabilitation*, 16(4):237–253, 2009.
- [31] D.P. Romilly, C. Anglin, R.G. Gosine, C. Hershler, and S.U. Raschke. A functional task analysis and motion simulation for the development of a powered upper-limb orthosis. *IEEE Transactions on Rehabilitation Engineering*, 2(3):119–129, 1994.

- [32] G. Wu, F.C. Van der Helm, H.E. Veeger, M. Makhsous, P. Van Roy, C. Anglin, J. Nagels, A.R. Karduna, K. McQuade, X. Wang, F.W. Werner, and B Buchholz. ISB recommendation on definitions of joint coordinate systems of various joints for the reporting of human joint motion - Part II: Shoulder, elbow, wrist and hand. *Journal of Biomechanics*, 38(5):981–992, 2005.
- [33] J. Lenarcic and M. Stanisic. A humanoid shoulder complex and the humeral pointing kinematics. *IEEE Transactions on Robotics and Automation*, 19(3):499–506, 2003.
- [34] H. Moskowitz, C.R. Goodman, E. Smith, E. Balthazar, and H.Z. Mellins. Hemiplegic shoulder. *NY State Journal of Medicine*, 69(4):548–550, 1969.
- [35] R.D. Zorowitz, M.B. Hughes, D. Idank, T. Ikai, and M.V. Johnston. Shoulder pain and subluxation after stroke: Correlation of coincidence? *American Journal of Occupational Therapy*, 50(3):194–201, 1996.
- [36] H.C. Hanger, P. Whitewood, G. Brown, M.C. Ball, J. Harper, R. Cox, and R.A. Sainbury. A randomized controlled trial of strapping to prevent post-stroke shoulder pain. *Clinical Rehabilitation*, 14(4):370–380, 2000.
- [37] E. Dursun, N. Dursun, C.E. Ural, and A. Cakci. Glenohumeral joint subluxation and reflex symathetic dystrophy in hemiplegic patients. *Archives of Physical Medicine and Rehabilitation*, 81(7):944–946, 2000.

- [38] K. Kiguchi, M.H. Rahman, M. Sasaki, and K. Teramoto. Development of a 3DOF mobile exoskeleton robot for human upper-limb motion assist. *Robotics and Autonomous Systems*, 56(8):678–691, 2008.
- [39] P. Letier, M. Avraam, S. Veillerette, M. Horodinca, M. De Bartolomei, A. Schiele, and A. Preumont. SAM: A 7-DoF portable arm exoskeleton with local joint control. In *IEEE/RSJ International Conference on Intelligent Robots and Systems*, pages 3501–3506, 2008.
- [40] H. Shing Lo and S.S.Q. Xie. An upper limb exoskeleton with an optimized 4R spherical wrist mechanism for the shoulder joint. In *IEEE/ASME International Conference on Advanced Intelligent Mechatronics*, pages 269–274, 2014.
- [41] A. Frisoli, M. Bergamasco, M.C. Carboncini, and B. Rossi. Robotic assisted rehabilitation in virtual reality with the L-EXOS. *Studies in Health Technology and Informatics*, 145:40–54, 2009.
- [42] D.G. Caldwell, C. Favede, and N. Tsagarakis. Dextrous exploration of a virtual world for improved prototyping. In *IEEE International Conference on Robotics and Automation*, volume 1, pages 298–303, 1998.
- [43] A. Schiele and G. Visentin. The ESA human arm exoskeleton for space robotics telepresence. In *International Symposium on Artificial Intelligence, Robotics and Automation in Space*, 2003.
- [44] C. Carignan, M. Liszka, and S. Roderick. Design of an arm exoskeleton with scapula motion for shoulder rehabilitation. In *International Conference on Advanced Robotics*, pages 524–531, 2005.

- [45] T. Rahman, W. Sample, R. Seliktar, M. Alexander, and M. Scavina. A body-powered functional upper limb orthosis. *Journal of Rehabilitation Research and Development*, 37(6):675–680, 2000.
- [46] R.J. Sanchez, Jiayin L., S. Rao, P. Shah, R. Smith, T. Rahman, S.C. Cramer, J.E. Bobrow, and D.J. Reinkensmeyer. Automating arm movement training following severe stroke: Functional exercises with quantitative feedback in a gravity-reduced environment. *IEEE Transactions on Neural Systems and Rehabilitation Engineering*, 14(3):378–389, 2006.
- [47] R.J.Jr. Sanchez, E. Wolbrecht, R. Smith, J. Liu, S. Rao, S. Cramer, T. Rahman, J.E. Bobrow, and D.J. Reinkensmeyer. A pneumatic robot for re-training arm movement after stroke: Rationale and mechanical design. In *International Conference on Rehabilitation Robotics*, pages 500–504, 2005.
- [48] T.G. Sugar, H. Jiping, E.J. Koeneman, J.B. Koeneman, R. Herman, H. Huang, R.S. Schultz, D.E. Herring, J. Wanberg, S. Balasubramanian, P. Swenson, and J. A. Ward. Design and control of RUPERT: A device for robotic upper extremity repetitive therapy. *IEEE Transactions on Neural Systems and Rehabilitation Engineering*, 15(3):336–346, 2007.
- [49] S. Nahema, B. Vincent, C. Frederic, and D. Philippe. Ergonomic contribution of ABLE exoskeleton in automotive industry. *International Journal of Industrial Ergonomics*, 3(8):475–481, 2014.

- [50] F. Molteni, G. Gasperini, M. Colombo, C. Giovanzana, C. Lorenzon, N. Farina, G. Cannaviello, S. Scarano, D. Proserpio, D. Liberali, and E. Guazioli. Wearable robotic exoskeleton for over-ground gait training in sub-acute and chronic hemiparetic stroke patients: Preliminary results. *European Journal of Physical and Rehabilitation Medicine*, 53(5):676–684, 2017.
- [51] T. Nef, M. Mihelj, and R. Riener. Armin: a robot for patient-cooperative arm therapy. *Medical And Biological Engineering And Computing*, 45(9):887–900, 2007.
- [52] M. Mihelj, T. Nef, and R. Riener. ARMin II 7 DoF rehabilitation robot: mechanics and kinematics. In *IEEE International Conference on Robotics and Automation*, pages 4120–4125, 2007.
- [53] T. Nef, M. Guidali, and R. Riener. ARMin III - Arm therapy exoskeleton with an ergonomic shoulder actuation. 2(6):127–142, 2009.
- [54] M. Guidali, A. Duschau-Wicke, S. Broggi, V. Klamroth-Marganska, T. Nef, and R. Riener. A robotic system to train activities of daily living in a virtual environment. *Medical and Biological Engineering & Computing*, 49(10):1213–1223, 2011.
- [55] A.H.A. Stienen, E.E.G. Hekman, F.C.T. Van der Helm, G.B. Prange, M.J.A. Jannink, A.M.M. Aalsma, and H. Van der Kooij. Dampace: Dynamic force-coordination trainer for the upper extremities. In *International Conference on Rehabilitation Robotics*, pages 820–826, 2007.
- [56] A.H.A. Stienen, E.E.G. Hekman, H. Ter Braak, A.M.M. Aalsma, F.C.T. Van der Helm, and H. Van der Kooij. Design of a rotational

- hydroelastic actuator for a powered exoskeleton for upper limb rehabilitation. *IEEE Transactions on Biomedical Engineering*, 57(3):728–735, 2010.
- [57] B. Dehez and J. Sapin. ShouldeRO An alignment-free two-dof rehabilitation robot for the shoulder complex. In *IEEE International Conference on Rehabilitation Robotics*, pages 1–8, 2011.
- [58] H.S. Park, Y. Ren, and L.Q. Zhang. IntelliArm: An exoskeleton for diagnosis and treatment of patients with neurological impairments. In *IEEE/RAS-EMBS International Conference on Biomedical Robotics and Biomechatronics*, pages 109–114, 2008.
- [59] S. Ball, I. Brown, and S. Scott. MEDARM: A rehabilitation robot with 5DoF at the shoulder complex. In *IEEE/ASME International Conference on Advanced Intelligent Mechatronics*, pages 1–6, 2007.
- [60] D. Koo, P.H. Chang, M.K. Sohn, and J. Shin. Shoulder mechanism design of an exoskeleton robot for stroke patient rehabilitation. In *IEEE International Conference on Rehabilitation Robotics*, pages 1–6, 2011.
- [61] B. Kim and AD. Deshpande. Mechanical design of a wearable robot for upper body rehabilitation. *International Workshop on Wearable Robotics*, 2014.
- [62] V. Inman, J. Saunders, and L. Abbott. Observations of function of the shoulder joint. *Clinical Orthopedics and Related Research*, 330(1):3–12, 1996.

- [63] M. B. Naf, K. Junius, M. Rossini, C. Rodriguez-Guerrero, B. Vanderborght, and D. Lefeber. Misalignment compensation for full human-exoskeleton kinematic compatibility: state of the art and evaluation. *ASME Applied Mechanics Reviews*, 70(5):050802–050802–19, 2018.
- [64] R. J. Adams and B. Hannaford. Stable haptic interaction with virtual environments. *IEEE Transactions on Robotics and Automation*, 15:465–474, 1999.
- [65] S.D. Eppinger and W.P. Seering. Understanding bandwidth limitations in robot force control. In *IEEE International Conference on Robotics and Automation*, volume 4, pages 904–909, 1987.
- [66] W.S. Newman. Stability and performance limits of interaction controllers. *ASME Transactions of The Journal of Dynamic Systems Measurement and Control*, 114(4):563–570, 12 1992.
- [67] J.S. Hart and G. Niemeyer. Absolutely stable model-based 2-port force controller for telerobotic applications. *International Journal of Robotics Research*, 33(6):847–865, 2014.
- [68] J.E. Colgate. *The control of dynamically interacting systems*. PhD thesis, Massachusetts Institute of Technology, 1988.
- [69] T.B. Moeslund. Modelling the human arm. Technical report, Aalborg University, 2002.
- [70] S.J. Ball. *Novel robotic mechanisms for upper-limb rehabilitation and assessment*. PhD thesis, Queen’s University, Ontario, Canada, 2008.

- [71] T.B. Moeslund, C.B. Madsen, and E. Granum. Modelling the 3D pose of a human arm and the shoulder complex utilising only two parameters. *Integrated Computer-Aided Engineering*, 12(2):159–175, 2005.
- [72] C.C. Norkin and D.J. White. *Measurement of Joint Motion, A Guide to Goniometry*. F. A. Davis Company, 4th edition edition, 2009.
- [73] M. Bottlang, S.M. Madey, C.M. Steyers, J.L. Marsh, and T.D. Brown. Assessment of elbow joint kinematics in passive motion by electromagnetic motion tracking. *Journal of Orthopaedic Research*, 18(2):195–202, 2000.
- [74] Jungeun Park and Alfinio Flores. Fermat’s point from five perspectives. *International Journal of Mathematical Education in Science and Technology*, 46(3):425–441, 2015.
- [75] R. A. Johnson. *Modern Geometry: An Elementary Treatise on the Geometry of the Triangle and the Circle*. Houghton Mifflin, Boston, MA, 1929. pp. 221-222.
- [76] I.A. Bonev, A. Yu, and P. Zsombor-Murray. Xy-theta positioning table with parallel kinematics and unlimited theta rotation. In *IEEE International Symposium on Industrial Electronics*, pages 3113–3117, 2006.
- [77] I.H. Ertas and V. Patoglu. A multi-functional rehabilitation device to assist forearm/wrist and grasp therapies. In *EuroHaptics 2010: Haptics: Generating and Perceiving Tangible Sensations*, pages 283–290, 2010.

- [78] Bruno Siciliano, Lorenzo Sciavicco, Luigi Villani, and Giuseppe Oriolo. *Robotics – Modelling, Planning and Control*. Springer-Verlag London, 2009.
- [79] T.R. Kane and D.A. Levinson. The use of Kane’s dynamical equations in robotics. *International Journal of Robotics Research*, 2(3):3–21, 1983.
- [80] I.H. Ertas. Design and implementation of robotic devices for physical therapy of distal upper extremity. Master’s thesis, Sabanci University, Istanbul, Turkey, 2010.
- [81] Oriol Bohigas, Montserrat Manubens, , and Lluís Ros. A complete method for workspace boundary determination on general structure manipulators. *IEEE Transactions On Robotics*, 28(5):993–1006, 2012.
- [82] Pyung H. Chang. A dexterity measure for the kinematic control of robot manipulator with redundancy. Technical report, Massachusetts Institute of Technologys, Cambridge, MA, USA, 1988.
- [83] Bertrand Tondou. A theorem on the manipulability of redundant serial kinematic chains. *Engineering Letters*, 15(2):362–369, 2007.
- [84] Muhammad J. Mirza, Muhammad W. Tahir, and Nadeem Anjum. On singularities computation and classification of redundant robots. In *International Conference on Computing, Communication and Control Engineering*, pages 113–117, 2015.
- [85] B. Loverna, L.A. Strouda, N.A. Ferranb, S.L. Evansa, R.O. Evansb, and C.A. Holta. Motion analysis of the glenohumeral joint during activ-

- ities of daily living. *Computer Methods in Biomechanics and Biomedical Engineering*, 13(6):803–809, 2010.
- [86] A.A. Amis. *Operative Elbow Surgery Expert Consult: Online and Print*. Churchill Livingstone, China, 2012.
- [87] J. Ryu, W. Cooney, L. Askew, An K., and Chao E. Computer methods in biomechanics and biomedical engineering. *The Journal of Hand Surgery*, 16(3):409–419, 1991.
- [88] A. Agrawal and S.K. Agrawal. Design of gravity balancing leg orthosis using non-zero free length springs. *Mechanism and Machine Theory*, 40(6):693–709, 2005.
- [89] S.K. Banala, S.K. Agrawal, A. Fattah, V. Krishnamoorthy, W. Hsu, J. Scholz, and K. Rudolph. Gravity balancing leg orthosis and its performance evaluation. *IEEE Transactions on Robotics*, 22(6):1228–1239, 2006.
- [90] N.P. Chironis, editor. *Spring Mechanisms - Point Balancing and Continuous Balancing*. McGraw-Hill, New York, 1961.
- [91] R.M. Nathan. Perfect spring equilibrators for rotatable bodies. *ASME Journal of Mechanisms, Transmissions, and Automation in Design*, 107(4):508–512, 1989.
- [92] D.A. Streit and B.J. Gilmore. Perfect spring equilibrators for rotatable bodies. *Journal of Mechanisms, Transmissions and Automation in Design*, 111(4):451–458, 1989.

- [93] D.A. Streit and E. Shin. Equilibrators for planar linkages. *Journal of Mechanical Design*, 115(3):604–611, 1993.
- [94] T. Rahman, R. Ramanathan, R. Seliktar, and W. Harwin. A simple technique to passively gravity-balance articulated mechanisms. *ASME Journal of Mechanical Design*, 117(4):655–658, 1995.
- [95] W.D. Van Dorsser, J.L. Herder, B.M. Wisse, and R. Barents. Balancing device. US Patent, 2008. US 0,210,842-A1.
- [96] A.H.A. Stienen, E.E.G. Hekman, F.C.T. Van der Helm, and H. Von der Kooij. Freebal: Dedicated gravity compensation for the upper extremities. In *IEEE International Conference on Rehabilitation Robotics*, pages 804–808, 2007.
- [97] L.C. Hsu, W.W. Wang, G.D. Lee, Y.W. Liao, L.C. Fu, and J.S. Lai. A gravity compensation-based upper limb rehabilitation robot. In *2012 American Control Conference (ACC)*, pages 4819–4824, 2012.
- [98] R. Altenburger, D. Scherly, and K.S. Stadler. Design of a passive, iso-elastic upper limb exoskeleton for gravity compensation. *Robomech*, 3(12):1–12, 2016.
- [99] P.Y. Lin, W.B. Shieh, and Chen D.Z. Design of a gravity-balanced general spatial serial-type manipulator. *Journal of Mechanisms and Robotics*, 2(8):1003–1010, 2010.
- [100] P Pracht, P Minotti, and M Dahan. Synthesis and balancing of cam-modulated linkages. *American Society of Mechanical Engineers, Design Engineering Division (Publication) DE*, 10(2):221–226, 01 1987.

- [101] C. Baradat, V. Arakelian, S. Briot, and S. Guegan. Design and prototyping of a new balancing mechanism for spatial parallel manipulators. *Journal of Mechanical Design*, 130(7):2305–2313, 2008.
- [102] R. Alami, A. Albu-Schaeffer, A. Bicchi, R. Bischoff, R. Chatila, A. De Luca, A. De Santis, G. Giralt, J. Guiochet, G. Hirzinger, F. Ingrand, V. Lippiello, R. Mattone, D. Powell, S. Sen, B. Siciliano, G. Tonietti, and L. Villani. Safe and dependable physical human-robot interaction in anthropic domains: State of the art and challenges. 2016.
- [103] Chae H. An and J.M. Hollerbach. Dynamic stability issues in force control of manipulators. In *American Control Conference*, pages 821–827, 1987.
- [104] J. E. Colgate and N. Hogan. Robust control of dynamically interacting systems. *International Journal of Control*, 48(1):65–88, 1988.
- [105] T. Aydin. *Human Body Dynamics Classical Mechanics and Human Movement*, pages 1–3. Springer, New York, 2000.
- [106] D.G Steele and C.A. Bramblett. *The Anatomy and Biology of the Human Skeleton*, pages 153–172. Texas A and M University Press, United States of America, 2007.
- [107] M. Sardelli, R.Z. Tashjian, and B.A. MacWilliams. Functional elbow range of motion for contemporary tasks. *The Journal of Bone And Joint Surgery*, 93(5):471–477, 2011.
- [108] A.M. Oosterwijk, M.K. Nieuwenhuis, C.P. Van der Schans, and L.J. Mouton. Shoulder and elbow range of motion for the performance of

- activities of daily living: A systematic review. *Physiotherapy Theory and Practice*, 34(7):505–528, 2018.
- [109] L.J. Stocco. *Robot Design Optimization with Haptic Interface Applications*. PhD thesis, The University of British Columbia, 1999.
- [110] Neville Hogan. Impedance control: An approach to manipulation: Part i—theory. *Journal of Dynamic Systems, Measurement, and Control*, 107(1):1–7, 1985.
- [111] S.S. Haykin. *Active Network Theory*. Addison-Wesley, 1970.
- [112] J. Edward Colgate and Gerd G. Schenkel. Passivity of a class of sampled-data systems: Application to haptic interfaces. *Journal of Robotic Systems*, 14(1):37–47, 1997.
- [113] C. Cooper. *Fundamentals of Hand Therapy Clinical Reasoning and Treatment Guidelines for Common Diagnoses of the Upper Extremity*. Elsevier Health Sciences, 2014.
- [114] B. Sears. Isometric exercise in physical therapy. <https://www.verywellhealth.com/isometric-exercise-in-physical-therapy-2696510>, 2019.
- [115] W. R. Frontera, S. A. Herring, L. J. Micheli, J. K. Silver, and T. P. Young. *Clinical Sports Medicine Medical Management and Rehabilitation*. Elsevier Inc., 2007.
- [116] J. R. Andrews, G. L. Harrelson, and K. E. Wilk. *Physical Rehabilitation of the Injured Athlete*. Elsevier Inc., 2012.

- [117] E. Quinn. Benefits of isokinetic muscle contraction specialized training for sports performance and rehabilitation. <https://www.verywellfit.com/isokinetic-definition-3120353>, 2019.
- [118] T. Proietti, V. Crocher, A. Roby-Brami, and N. Jarrasse. Upper-limb robot exoskeletons for neurorehabilitation: a review on control strategies. *IEEE Reviews in Biomedical Engineering*, 10, 2016.
- [119] S. Hussain. *Design and Assist-as-Needed Control of an Intrinsically Compliant Robotic Orthosis for Gait Rehabilitation*. PhD thesis, The University of Auckland, 2012.
- [120] H. I. Krebs, B. T. Volpe, M. L. Aisen, W. Hening, S. Adamovich, H. Poizner, K. Subrahmanyam, and N. Hogan. Robotic applications in neuromotor rehabilitation. *Robotica*, 21:3–11, 2003.
- [121] R. Riener, L. Lunenburger, S. Jezernik, M. Anderschitz, G. Colombo, and V. Dietz. Patient-cooperative strategies for robot-aided treadmill training: first experimental results. *IEEE Transactions on Neural Systems and Rehabilitation Engineering*, 13(3):380–394, 2005.
- [122] J. Emken, J. Bobrow, and D. Reinkensmeyer. Robotic movement training as an optimization problem: Designing a controller that assists only as needed. In *IEEE International Conference on Rehabilitation Robotics*, 2005.
- [123] C. Carignan, J. Tang, and S. Roderick. Development of an exoskeleton haptic interface for virtual task training. In *IEEE/RJS International Conference on Intelligent robots and systems*, 2019.

- [124] A. Gupta and M. OMalley. Design of a haptic arm exoskeleton for training and rehabilitation. *TMECH*, 11:181–186, 2006.
- [125] A. Kousidou, N. G. Tsagarakis, C. Smith, and D. G. Caldwell. Task-oriented biofeedback system for the rehabilitation of the upper limb. In *IEEE International Conference on Rehabilitation Robotics*, 2007.
- [126] P. Culmer, A. Jackson, S. Makower, R. Richardson, J. Cozens, M. Levesley, and B. Bhakta. A control strategy for upper limb robotic rehabilitation with a dual robot system. *TMECH*, 15:575–585, 2010.
- [127] A.Erdogan and V. Patoglu. Slacking prevention during assistive contour following tasks with guaranteed coupled stability. In *IEEE/RJS International Conference on Intelligent robots and systems*, 2012.
- [128] B. Rohrer, S. Fasoli, H.I. Krebs, B. Hughes, B. Volpe, W.R. Frontera, J. Stein, and N. Hogan. Movement smoothness changes during stroke recovery. *The Journal of Neuroscience*, 22(18):8297–8304, 2002.
- [129] T. Flash and N. Hogan. The coordination of arm movements: An experimentally confirmed mathematical model. *The Journal of Neuroscience*, 5(7):1688–1702, 1985.
- [130] N. Hogan and D. Sternad. Sensitivity of smoothness measures to movement duration, amplitude and arrest. *Journal of Motor Behavior*, 41(6):529–534, 2009.

APPENDICES

Appendix I

Given the $3\underline{R}RP$ mechanism is singularity free, a simplified kinematic model can be employed to study the singular configurations of ASSISTON-ARM. In particular, the end effector motion of $3\underline{R}RP$ mechanism can be modelled with a revolute joint serially connected to two perpendicularly connected prismatic joints in series, as depicted in Figure 9.6, to result in an equivalent serial $\underline{R}\overline{P}\underline{P}\underline{P}\underline{R}\underline{R}\underline{R}$ kinematic chain.

While kinematic singularities for shoulder orientations are unavoidable for the underlying kinematics that utilize only three rotations, the singular configurations of ASSISTON-ARM can be relocated to more favorable configurations within the workspace of the device, through introduction of oblique rigid connections between the rotating bodies. To implement for such a connection, Figure 9.6 introduces two design parameters β and γ that define the tilting angles around unit directions of \vec{u}_2 and \vec{u}_3 , respectively. With this oblique connection member in place, the determinant of the kinematic Jacobian for the upper-arm can be expressed as

$$\det[J_u] = -\cos(\gamma)\cos(\theta) - \sin(\beta)\sin(\gamma)\sin(\theta). \quad (31)$$

which indicates that the singular configurations of the Jacobian depend on the design parameters β and γ .

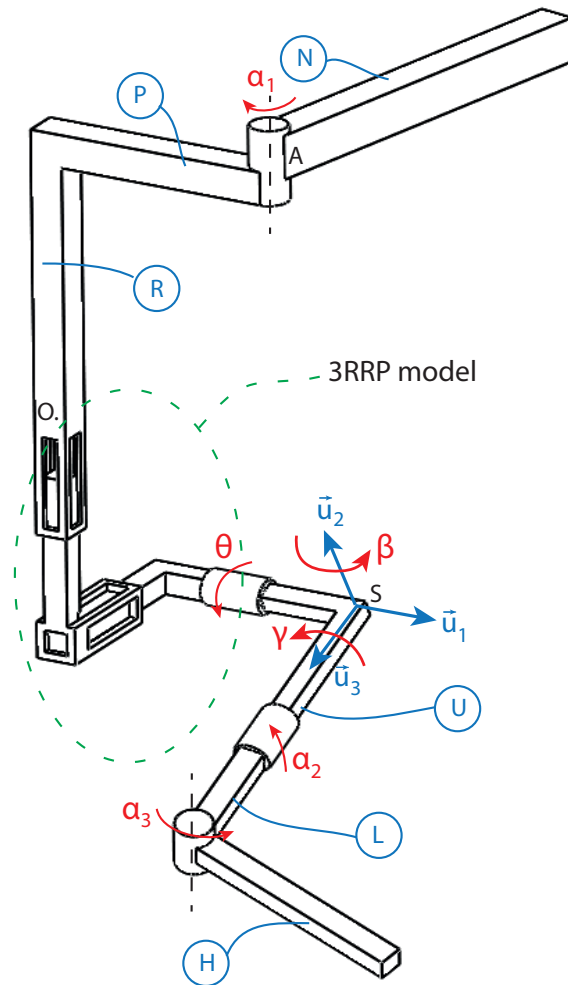


Figure 9.6: Schematic representation of simplified kinematics of ASSISTON-ARM used for singularity analysis

Vertically down arm posture may be useful during rehabilitation. In order to shift the singular configuration away from the vertically down arm posture without introducing large orientation changes between connecting parts, we solve for the minimum tilting angles, such that the kinematic singularity is relocated to $\theta = 92^\circ$. Figure 9.7 depicts the numerical solution of Eqn. (31)

when $\theta = 92^\circ$. From this plot, the minimum tilting angles to relocate the singular configuration can be determined as $\beta = 8.5^\circ$ and $\gamma = 11.45^\circ$.

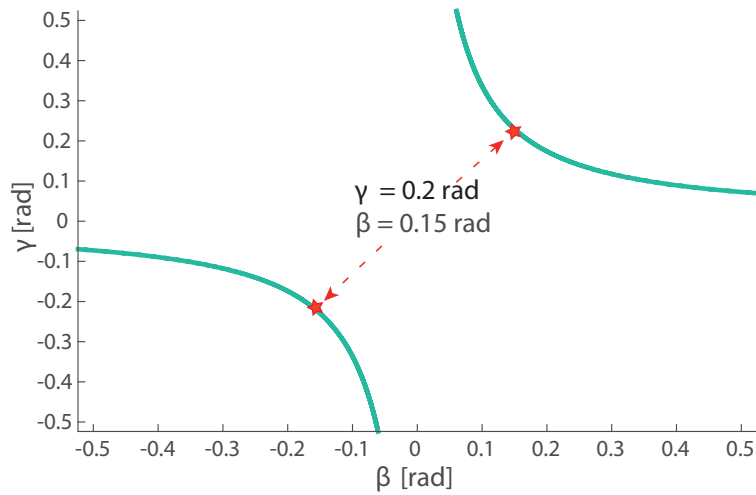


Figure 9.7: Representation of tilting angles β and γ , after introducing them in order to extent usable range of motion without singularities, when $\theta = 92^\circ$ and determinant of J_u is equal to zero